Regulation of human Argonaute proteins and its implications in disease

DISSERTATION

zur Erlangung des Doktorgrades der Naturwissenschaften (Dr. rer. nat.)

der Fakultät für Biologie und Vorklinische Medizin

der Universität Regensburg

vorgelegt von Daniela Zeitler

aus Regensburg

im Jahr 2019

Das Promotionsgesuch wurde eingereicht am: 11.01.2019

Die Arbeit wurde angeleitet von Prof. Dr. Gunter Meister

Daniela Zeitler

Meiner Familie

Not everything that counts can be counted,

and not everything that can be counted counts.

Albert Einstein

Contents

Abstract

Argonaute (Ago) proteins are key components of small RNA-guided gene silencing pathways. They interact with small non-coding RNAs, which guide them to specific RNA targets and are therefore referred as guide RNA. Some Ago proteins cleave RNA targets, which are perfect complementary to the bound guide RNA. In case of partial complementarity between guide and target RNA, Ago proteins recruit additional factors to mediate translational repression and mRNA degradation.

With such an important role in small RNA-guided gene silencing, it is necessary to understand the regulation of Ago proteins. Post-translational modifications, in particular phosphorylations, are an essential tool for protein regulation. Therefore, phosphorylations of Ago proteins from different species were analyzed using mass spectrometry. Here, multiple endogenous and highly conserved phosphorylation sites were identified. Moreover, five of them were organized in a phosphorylation cluster. This phosphorylation cluster was analyzed further regarding functionality and modifying enzymes. It turned out that this phosphorylation cluster is required for efficient target release and it is essential for early development *C. elegans*. By analyzing mass spectrometry data, one phosphatase was identified to be involved in the de-phosphorylation of this phosphorylation cluster.

Mis-regulated Ago expression levels or mutations of Ago proteins are known to result in various diseases or cancer. A collaboration partner found different heterozygous Ago2 mutations in patients showing the same neurological phenotype. In the second part of this thesis, all these detected mutations were characterized and checked regarding similarities. Here, a common mis-regulation in target release was revealed and sheds light on the unexpected finding that heterozygous Ago2 mutations lead to neurodevelopmental disease.

Zusammenfassung

Argonaut (Ago)-Proteine zählen zu den Schlüsselkomponenten der kleinen RNS-gesteuerten Genstilllegung. Diese Proteine interagieren mit kleinen-nicht kodierenden RNS, die sie zu spezifischen Ziel-RNS leiten und deshalb als Führungs-RNS bezeichnet werden. Einige Ago Proteine sind in der Lage Ziel-RNAs zu spalten, die zu den Führungs-RNS perfekt komplementär sind. Im Falle einer nur teilweisen Komplementarität zwischen Führungs-RNS und Ziel-RNS, rekrutieren Ago Proteine zusätzliche Faktoren, um die Translationsrepression und den mRNS-Abbau zu vermitteln.

Mit dieser wichtigen Rolle bei der Genstilllegung mittels kleinen RNAs ist es notwendig, die Regulation von Ago Proteinen zu verstehen. Posttranslationale Modifikationen, insbesondere Phosphorylierungen, sind ein wesentliches Instrument für die Proteinregulierung. Daher wurden Phosphorylierungen von Ago Proteinen aus verschiedenen Spezies unter Verwendung von Massenspektrometrie analysiert. Hier konnten mehrere endogene und hochkonservierte Phosphorylierungsstellen identifiziert werden. Darüber hinaus waren fünf von diesen Phosphorylierungen in Phosphorylierungsclustern organisiert. Dieses wurde weiter auf Funktionalität und modifizierende Enzyme hin untersucht. Es stellte sich heraus, dass dieses Phosphorylierungscluster für eine effiziente Freisetzung der Ziel-RNS erforderlich ist und dass dieses auch für die frühe Entwicklung in *C. elegans* unerlässlich ist. Bei der Analyse der Daten generiert durch Massenspektrometrie wurde eine Phosphatase identifiziert, die an der Dephosphorylierung von diesem Phosphorylierungscluster beteiligt ist.

Es ist bekannt, dass falsch regulierte Expressionsniveaus von Ago Proteinen oder deren Mutationen zu verschiedenen Erkrankungen oder Krebs führen können. Ein Kooperationspartner fand bei Patienten, die einen ähnlichen neurologischen Phänotypen aufweisen, verschiedene heterozygote Mutationen in Ago2. Im zweiten Teil dieser Arbeit wurden all diese nachgewiesenen Mutationen charakterisiert und auf Ähnlichkeiten überprüft. Hier konnte eine Fehlregulierung bei der Freigabe der Ziel-RNS aufgedeckt werden und Licht auf die unerwartete Feststellung werfen, dass heterozygote Ago2 Mutationen zu einer neurologischen Erkrankung führen.

Publications and Presentations

Parts of this thesis were published in the following article:

Huberdeau M. Q.*, Zeitler D. M.*, Hauptmann J., Bruckmann A., Fressigne L., Danner J., Piquet S., Strieder N., Engelmann J. C., Jannot G., Deutzmann R., Simard M. J., Meister G. Phosphorylation of Argonaute proteins affects mRNA binding and is essential for microRNA-guided gene silencing in vivo. *EMBO J.* **36,** 2088–2106 (2017) **These authors contributed equally*

Lessel D, Zeitler D. M., Kazantsev A., Ignatova Z., Meister G., Kreienkamp H. J. Heterozygous mutations in Ago2 result in neurodevelopmental disorders. *Manuscript in preparation.*

Additionally, I contributed to the following article:

Gust A., Jakob L., Zeitler D. M., Bruckmann A., Kramm K., Willkomm S., Tinnefeld P., Meister G., Grohmann D. Site-Specific Labelling of Native Mammalian Proteins for Single-Molecule FRET Measurements. *Chembiochem.*;**19**(8):780-783 (2018)

Parts of this thesis have been presented at international conferences:

Danner J., Hauptmann J., Zeitler D. M., Bruckmann A., Kremmer E., Deutzmann R., Meister G. Exploiting peptide and antibody purification strategies to analyze post-translational modifications of endogenous Argonaute and TNRC6 proteins. Poster presentation, 11th Microsymposium on Small RNA Biology, 2016, Vienna, Austria.

Zeitler D. M., Huberdeau M. Q., Hauptmann J., Bruckmann A., Fressigne L., Danner J., Piquet S., Strieder N., Engelmann J. C., Jannot G., Deutzmann R., Simard M. J., Meister G. Hyper-Phosphorylation of Argonaute Proteins Affects mRNA Binding and is Essential for microRNA-guided Gene Silencing *in vivo*. Oral presentation, 2nd International Symposium on Frontiers in Molecular Science Non-Coding RNAs and Epigenetics in Cancer, 2017, Basel, Switzerland.

Zeitler D. M., Huberdeau M. Q., Hauptmann J., Bruckmann A., Fressigne L., Danner J., Piquet S., Strieder N., Engelmann J. C., Jannot G., Deutzmann R., Simard M. J., Meister G. Phosphorylation of Argonaute Proteins Affects mRNA Binding and is Essential for microRNA-guided Gene Silencing. Poster presentation, SFB960-Symposium, The Biology of RNA-Protein Complexes, 2017, Regensburg, Germany.

1 Introduction

In 1998, Andrew Fire and Craig Mello discovered RNAi in *C. elegans* and 8 years later they received the Nobel Price for their groundbreaking discovery[1]. It was shown that the injection of double stranded (ds) RNA molecules can lead to silencing of complementary genes much better than single stranded (ss) RNA molecules[1]. Since then, key insights of the role of small, non-coding RNAs in different cellular processes have been unraveled.

1.1 Small RNA classes and their biogenesis

Small, non-coding RNAs that play roles in regulation of gene expression can be divided in three main classes based on the structure of the precursors, biogenesis, appearance, and mode of action. The classes are named microRNAs (miRNAs), small interfering RNAs (siRNAs) and the PIWI-interacting RNAs (piRNAs). They have their length of 20-35 nucleotides (nt) in common and that they are all loaded into a member of the Argonaute protein family. Loaded in Argonaute proteins (Ago), small RNAs guide the repression of gene expression in various organisms[2–4]. miRNAs are mainly transcribed by polymerase II or III and form a stem-loop structure, called primary-miRNA (pri-miRNA)[5–7]. The primary transcript is processed in the nucleus by the RNase III enzyme Drosha and cofactor DiGeorge syndrome critical region gene 8 (DGCR8)[8–11]. The stem-loop structure is recognized by DGCR8 and Drosha crops the pri-miRNA to generate precursor-miRNA (pre-miRNA)[8–16]. After the first processing step, pre-miRNAs are exported by Exportin5 from the nucleus into the cytoplasm[17–20]. In the cytoplasm, a second processing step occurs mediated by the RNase III enzyme Dicer and its cofactors PACT (protein activator of the interferon-induced protein kinase) and TRBP (TAR RNA binding protein)[21–28]. PACT and TRBP recognize dsRNA and promote the substrate interaction[29–33]. The loop of the pre-miRNA is cut off and a small RNA duplex with a length of about 22 nt with 5' phosphates and 2 nt 3' overhangs is generated[9,21,22,34–38]. One strand (guide strand) is bound by Ago (see chapter 1.2.1). The other strand of this intermediate miRNA structure, often referred to as miRNA*, is removed from Ago and degraded in most cases[2,39–42] (Figure 1). Dicer, TRBP and Ago form a stable complex, which is referred to as loading complex of the RNA-induced silencing complex (RISC loading complex, RLC). This complex allows pre-miRNA processing and Ago-loading[21,23–25].

siRNAs are independent of Drosha cleavage and are processed by the RNase III enzyme Dicer from long, dsRNAs to about 21 nt long RNA duplexes. Their sources can be exogenous (exo-siRNAs) or endogenous (endo-siRNAs). Exo-siRNAs can be generated by the cleavage of viral RNAs. Endo-siRNAs derive for example from transposable elements, natural antisense transcripts or hairpin RNAs[43–46]. The duplexes are composed of a guide strand, which is perfectly complementary to its target (antisense strand), and the complementary passenger strand (sense strand)[3]. Like miRNAs, siRNA duplexes are separated and the guide is incorporated into the RISC (Figure 1). This strand guides the complex to perfect complementary targets, which are cleaved by sequence-specifically RISC. The passenger strand is unstable and degraded after unwinding[2–4]. In contrast to the biogenesis of miRNAs or siRNAs, piRNAs originate from ssRNA precursors[47]. They are transcribed from large piRNA clusters, which also represent a pool of transposon sequences[4,47]. piRNAs are associated with a member of the PIWI clade of the Argonaute protein family and are exclusively expressed in the germline where they silence transposons[48,49].

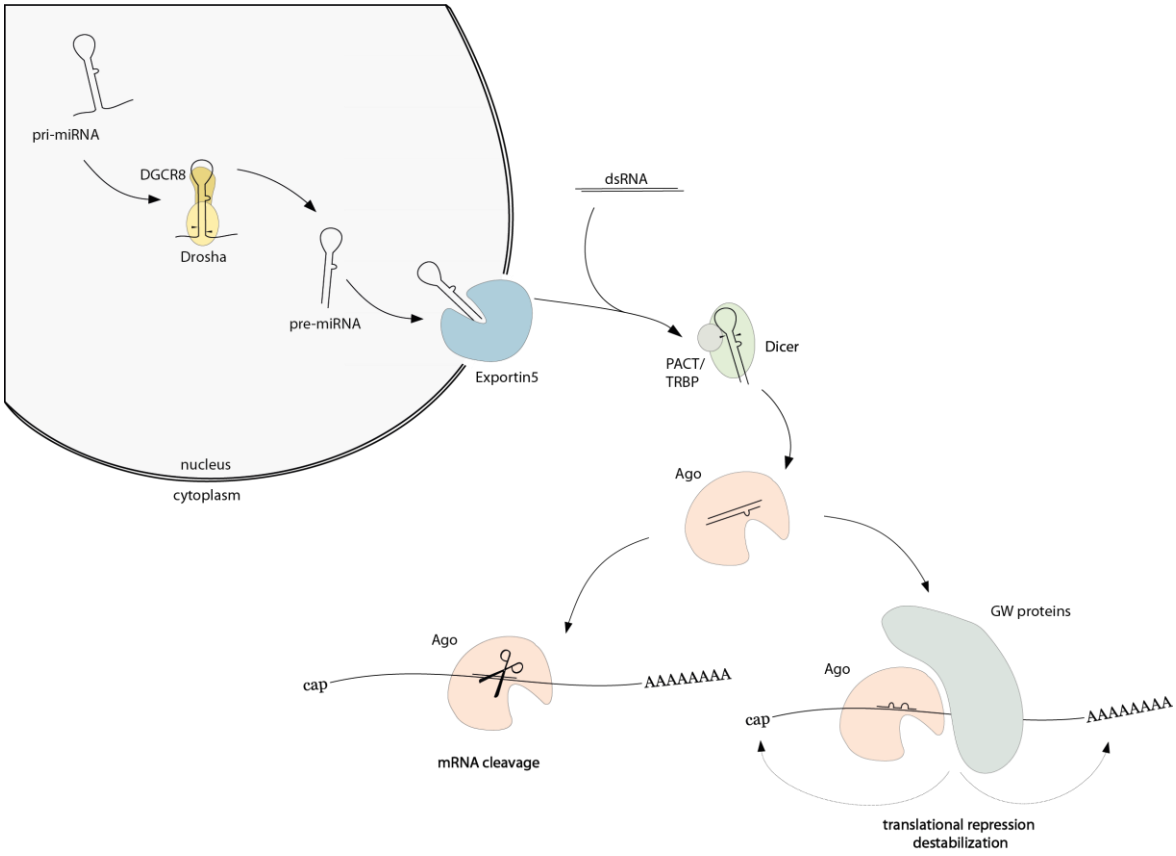

Figure 1 miRNA/siRNA biogenesis pathway. miRNAs are transcribed by RNA polymerase II or III to form stem-loop structures, called pri-miRNA. In the nucleus, a first processing step to pre-miRNA takes place, which is performed by Drosha and its cofactor DGCR8 (cleavage sites are marked by arrowheads). After export into the cytoplasm by Exportin5, the precursor is processed a second time. Dicer and its cofactor TRBP cut off the loop (cleavage sites are marked by arrowheads). siRNAs derived from exogenous or endogenous sources are also

processed by Dicer. One strand of the duplex is then incorporated into Ago proteins. In case of perfect complementarity, Ago2 in humans can cleave the mRNA. In case of partial complementarity between guide RNA and target RNA, GW182 proteins are recruited. These proteins serve as binding platforms for other proteins or complexes which lead to translational repression and destabilization[8,9,50–52].

1.2 Argonaute proteins

Argonaute proteins play an essential role in small RNA-guided gene silencing. They are specialists in binding small RNAs, which guide them to the targets. Argonaute proteins are named after the characteristic phenotype of an Ago-knockout in *Arabidopsis thaliana* that looks like the octopus *Argonauta argo*[53]. Argonaute proteins can be found in various organism but differ in their number. For example, there are twenty-six Ago proteins present in *Caenorhabditis elegans* (*C. elegans*), ten in *Arabidopsis thaliana*, eight in mammalia, five in *Drosophila melanogaster* and one in *Schizosaccharomyces pombe*[2]. The Argonaute protein family can be classified in three clades: The Ago proteins, referred after Ago1 of *Arabidopsis thaliana*, the PIWI proteins, named after PIWI of *Drosophila melanogaster*, and the worm-specific WAGO proteins[54–56]. Four of the eight mammalian Ago proteins are part of the PIWI subfamily, called HIWI1-3 and HILI, the remaining four Ago proteins belong to the Ago clade, and are termed Ago1-4[4]. PIWI proteins are mainly expressed in the germline and interact with piRNAs to protect the genome from mobile genetic elements via transcriptional silencing processes[47,57,58]. The members of the Ago protein clade are ubiquitously expressed and key players of the small RNA-guided gene silencing pathway. Some of them are able to silence targets or to mediate target repression by endonucleolytic cleavage (see chapter 1.2.1). Another way to achieve silencing is the recruitment of other factors that destabilize the target RNA[59,60] (see chapter 1.4). In addition, Argonaute proteins are present in archaea and bacteria. Bacterial and archaeal Ago proteins show a domain organization, which similar to the eukaryotic Ago proteins[61–64]. Of note, all characterized Ago proteins in prokaryotes target DNA, indicating that they are involved in DNA silencing[61–63,65–68]. Some studies hypothesized that prokaryotic Ago proteins are involved in protection against invasive genetic elements[63,67,69].

1.2.1 Functional domains of Ago proteins

Ago proteins are two-lobe proteins, which comprise four different domains: the (N)-terminal domain, the Piwi-Argonaute-Zwille (PAZ) domain, the middle (MID) domain and the P-element-induced wimpy testes (PIWI) domain (Figure 2). Two linkers (L1 and L2) link the N-terminal with the PAZ and the MID with the PIWI domain. The 3' nucleotide of the small RNA is bound by the PAZ domain, its 5' end anchors in the MID and PIWI domain[68,70–72].

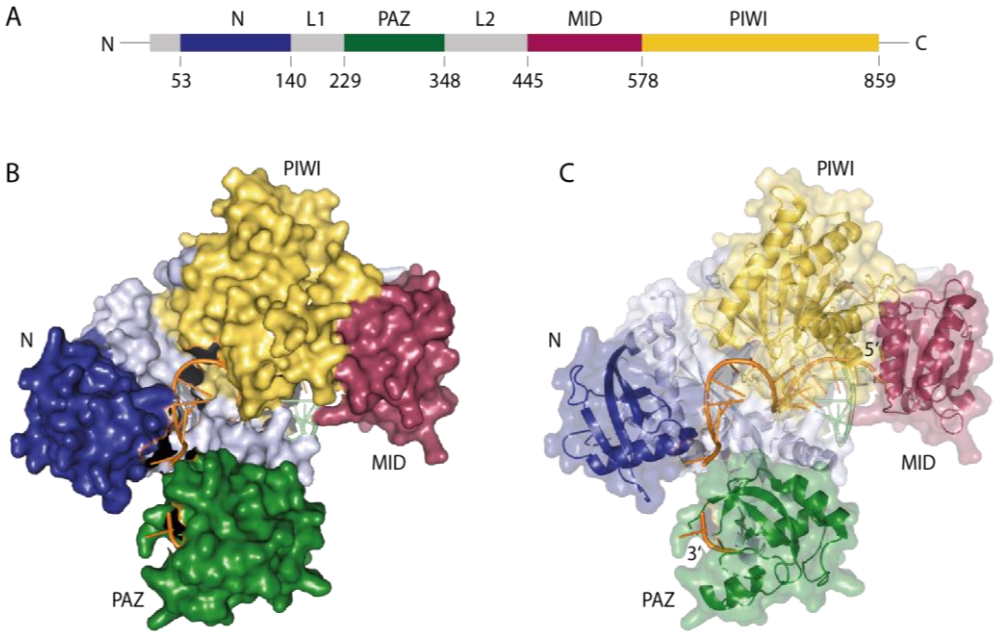

Figure 2 Crystal structure of human Ago2. (A) Domain organization of human Ago2. Color code: N domain – blue, PAZ – dark green, MID – magenta, PIWI – yellow, linker domains - grey (B)/(C) Crystal structure of human Ago2 with co-crystalized miRNA (orange) and parts of mRNA (light green). The domains are indicated like (A). The 5' end of the miRNA anchors in the MID domain, its 3' end is bound to the PAZ domain. The structure is based on the model 4W5O[73].

Ago proteins associate with one strand of the miRNA duplex. In consequence, there must be a mechanism to unwind the duplex and to decide, which strand is bound by Ago. It is suggested that the N-terminal domain functions as the initiator for duplex unwinding of the miRNA during RISC assembly[74]. But the detailed mechanism of duplex-unwinding is not completely clear. The stability of the miRNA ends is one important determinant for strand selection, which is called 'asymmetry rule'. The strand with the less thermodynamically stable 5'-terminus is preferentially loaded into Ago [75,76].

The PIWI domain contains an RNase-H like fold that catalyzes cleavage of complementary RNA targets endonucleolytically, a process often referred to as 'slicing'[56]. This slicing ability is based on a catalytic center, which contains a tetrade of Asp-Glu-Asp-His[70]. Only human Ago2 is able to cleave targets in case of fully complementarity between guide and target RNA[77,78]. In addition to its slicing function, the PIWI domain contains two binding pockets, which allow for binding to a member of the glycine-tryptophan protein of 182 kDa (GW182) protein family[50,71].

1.2.2 Binding of guide and target RNA

Small RNAs are bound by Ago proteins via their phosphate-sugar backbone. This is the basis for guide target interaction, because the bases of the guide RNA protrude into the binding channel for target RNA[68,71]. Experiments of the DNA-binding Ago protein of *Thermus thermophilus* showed that base pairing of the guide strand at positions 4-16 is necessary for DNA cleavage. Only mismatches between position 2-8 reduced cleavage activity and mismatches at the cleavage site abolished slicing function because the catalytic center is not reached[79].

The position 2-8 is referred to as seed sequence and its complementarity is the main criterion for target-site prediction in the miRNA pathway[72,80–83]. Overall, miRNA target sites are located in the 3' UTR of mRNAs[83]. Structural investigations revealed that the strongest canonical target sites with seed complementarity contain an adenine opposite the first nucleotide of the guide. This adenine is recognized by a specific binding pocket within Ago proteins[73,81,84]. Target recognition occurs in two steps: first, the seed nucleotides 2-6 are pre-organized by MID and PIWI domains, resulting in a stacked and helical conformation with exposed nucleotides 2-4[71]. This enables a fast and primary binding but it only leads to stable target binding, when the sites are complementary to the full miRNA seed[85]. With no full complementary seed, Ago either laterally diffuses along the mRNA to scan for potential targets or dissociate completely[85]. Crosslinking of Ago and its targets revealed also non-canonical targets, which do not have a full seed match[86–89]. Additionally to seed interaction, the guide's 3' end is also able to contribute to target recognition. Here, in particular the nucleotides 13-16 are involved[81,90]. Recent publications have shown that also the 3' half of the guide can direct the miRNA family members with the same seed to different target sites in *C. elegans*[91] and mouse brain[86].

1.3 GW182 proteins and their interaction with Ago proteins

In mammals, only a minor part of miRNA-guided gene silencing is based on endonucleolytic cleavage of target RNAs. The main part depends on Ago-miRNA binding to 3' UTR and gene silencing through translational repression and mRNA decay of partially complementary target RNAs[92,93]. To fulfill these duties, Ago proteins recruit GW182 proteins[24,94–96]. GW182 proteins are large and unstructured proteins, which in humans are referred to as trinucleotide repeat-containing protein 6 A, B, C (TNRC6A-C). They serve as binding platforms for other effector complexes that are required for repression[24,97] (see chapter 1.4, Figure 3). Of note, GW182 proteins can repress a reporter gene without Ago, when artificially tethered to a target by recruiting effector complexes, which are responsible for deadenylation and decapping of the target RNA, indicating that this step is independent of Ago[98]. It is assumed that translational repression and/or storage is performed in structured protein networks of various size called processing bodies (p-bodies)[94,99–101].

1.3.1 Molecular basis of Ago-GW182 binding

The three human GW182 paralogs are structurally similar. They consist of two main regions, an unstructured N-terminal Ago binging domain and the C-terminal silencing domain. The silencing domain mediates the recruitment of mRNA deadenylation machinery like CCR4-NOT or PAN2-PAN3[102–104] (see chapter 1.4). As their name suggests, GW182 proteins contain many glycine-tryptophan (GW)-repeats, distributed over the whole protein[50,92,102,105]. Deadenylase complexes CCR4-NOT and PAN2-PAN3 are bound by tryptophans of GW182 proteins[103,104,106]. In addition, Ago proteins interact also with tryptophans of GW182 proteins. Several binding sites for Ago could be identified in TNRC6, but only two Ws in the region comprising residues 599-683 in TNRC6B might be important for binding[50,107]. In contrast, a recent study reported three Ago proteins that are interacting with TNRC6A at the same time at three different motifs with high affinity[108]. Notably, all four human Ago proteins can be bound in the same fashion[107,109–112]. It is suggested that the Ws need 10 specific amino acids, which serve as spacers between the two Ws, for efficient Ago binding[50,107].

1.4 Mechanism of GW182-mediated repression

GW182 proteins interact with polyadenylate-binding protein (PABP) and thereby recruit the poly(A)-nuclease deadenylation complex subunit 2 (PAN2)-PAN3 and the carbon catabolite repressor protein 4 (CCR4)-NOT complexes (Figure 3)[98,102–104,113]. These recruitments catalyze deadenylation of the mRNA. Deadenylation is followed by decapping by mRNA-decapping enzyme subunit 1 (DCP1)-DCP2 complex[113]. The loss of the cap enables rapid degradation by the 5'-3' exoribonuclease 1 (XRN1)[114]. In addition, the recruitment of the CCR4-NOT complex also leads to translational repression. The CCR4-NOT complex recruits probable ATP-dependent RNA helicase (DDX6), which inhibits translation (Figure 3)[92,115].

In addition, translational repression occurs through inhibition of translation initiation. The eukaryotic initiation factor 4A (eIF4A) is an RNA helicase that is needed for unwinding of secondary structures within the 5' UTR of mRNAs[116]. This process is necessary for the ribosomal scanning, wherein the small ribosomal subunit attaches to the 5'-end of the target RNA and then searches for the start codon[116,117]. There are discrepancies about the mechanisms of the interference with eIF4AI/II but the consensus suggest that miRNA indicate the dissociation of these factors from the mRNA[72,92,118–120]. This might lead to blocking of the ribosomal scanning process and the assembly to eIF4F complex, which is composed of the eIF4A (eIF4AI/II), the eukaryotic initiation factor 4G (eIF4G) and the eukaryotic initiation factor 4E (eIF4E)[72,92,118–120]. In Drosophila, translational repression was also reported to be independent of GW182 proteins[118]. This underlines that the detailed molecular mechanisms of miRNA-guided gene silencing are still not fully understood.

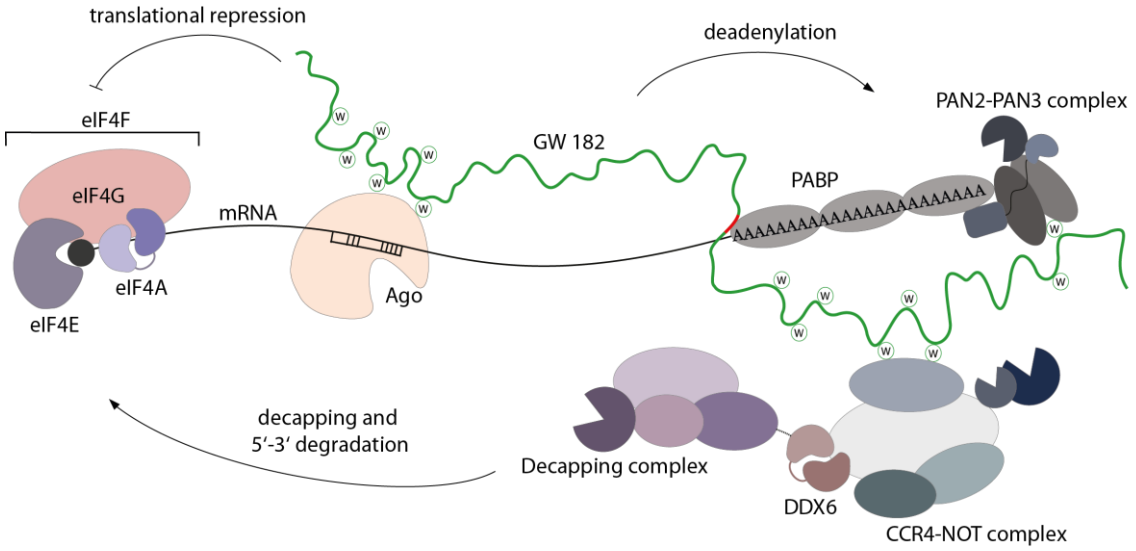

Figure 3 Schematic model of miRNA-mediated gene silencing in animals. Ago proteins are guided by miRNA to their target mRNAs and GW182 proteins are recruited, which bind via two tryptophans to the binding pockets of Ago. GW182 proteins interact with PABP, the cytoplasmic deadenylase complexes PAN2-PAN3 and CCR4-NOT. These complexes promote deadenylation of the mRNA. After deadenylation, decapping and degradation occurs. Additionally, translation is repressed. Therefore, miRNAs block translational initiation by interfering with the activity of eukaryotic initiation factor 4F (eIF4F) complex. The cap structure is shown as a black circle. PABP-interacting motif is depicted in red. (modified from [92])

1.5 Post-translational modifications of Ago proteins

It is known that Ago proteins are post-translationally modified at multiple sites and in many ways, e.g. by ubiquitination, hydroxylation, SUMOylation, PARylation and phosphorylation.

Ubiquitinations of Ago proteins leads to destabilization by the ubiquitin-proteasome pathway and were detected in mouse embryonic stem cells and also in *Drosophila* Ago1[121,122]. One reported E3 ubiquitin ligase interacting with Ago is mLin41 (Trim71) and is involved in the regulation of Ago2 turnover[122]. Empty *Drosophila* Ago1 is selectively ubiquitinated by the RING-type E3 ubiquitin ligase Iruka (Iru) to trigger its degradation and to ensure correct Ago function[121]. The reduction of the abundance of *Drosophila* Ago1 and mouse Ago2 is regulated by the ubiquitin-proteasome system[123]. Additionally, Ago1 and Ago2 are reported to be downregulated during T cell activation by ubiquitination and proteasomal degradation[124]. In addition, SUMOylations are known to regulate Ago proteins. Here, a member of the SUMO (small ubiquitin-like modifier) family is attached to lysines of specific proteins[125]. SUMOylation at position L402 of Ago2, has been reported by two labs but with contrary effects: on the one hand it is suggested that SUMOylation leads to destabilization of Ago2[126], on the other hand it might be required for full Ago2 siRNA-mediated activity[127](Figure 4). In

contrast, an increase of Ago2 stability in mouse and human cells has been observed with a hydroxylation at proline (P) 700[128]. This hydroxyl group is attached to Ago2 by the type I collagen prolyl-4 hydroxylase[128]. Both, mutation of P700 to A and depletion of the hydroxylase result in destabilization of Ago2, indicating a link between hydroxylation and protein stability[128]. Because the P700 position is located close to a W-binding pocket in Ago2 that ensures an interaction with TNRC6 proteins[71,108], it remains speculative if the hydroxylation at this position affect miRISC assembly[72] (Figure 4). In human cells, all Ago proteins undergo poly (ADP-ribosylation) (PARylation)[129]. Poly(ADP-ribose) (PAR) is an important regulatory molecule in the nucleus and regulates transcription, chromosome structure and DNA damage repair. This macromolecule is also reported to be added to Asp (D), Glu (E) and Lys (K) residues of Ago proteins. PARylation is involved in stress regulation, especially in the formation of cytoplasmic stress granules and therefore regulates mRNA translation and stability [129,130]. It has been published that PARylation of Ago proteins reduced translational repression and slicer activity, which might come from an impeded target accessibility[129]. In addition, downregulated RNAi activity was monitored shortly after viral infection via PARylation of the RISC[131] (Figure 4).

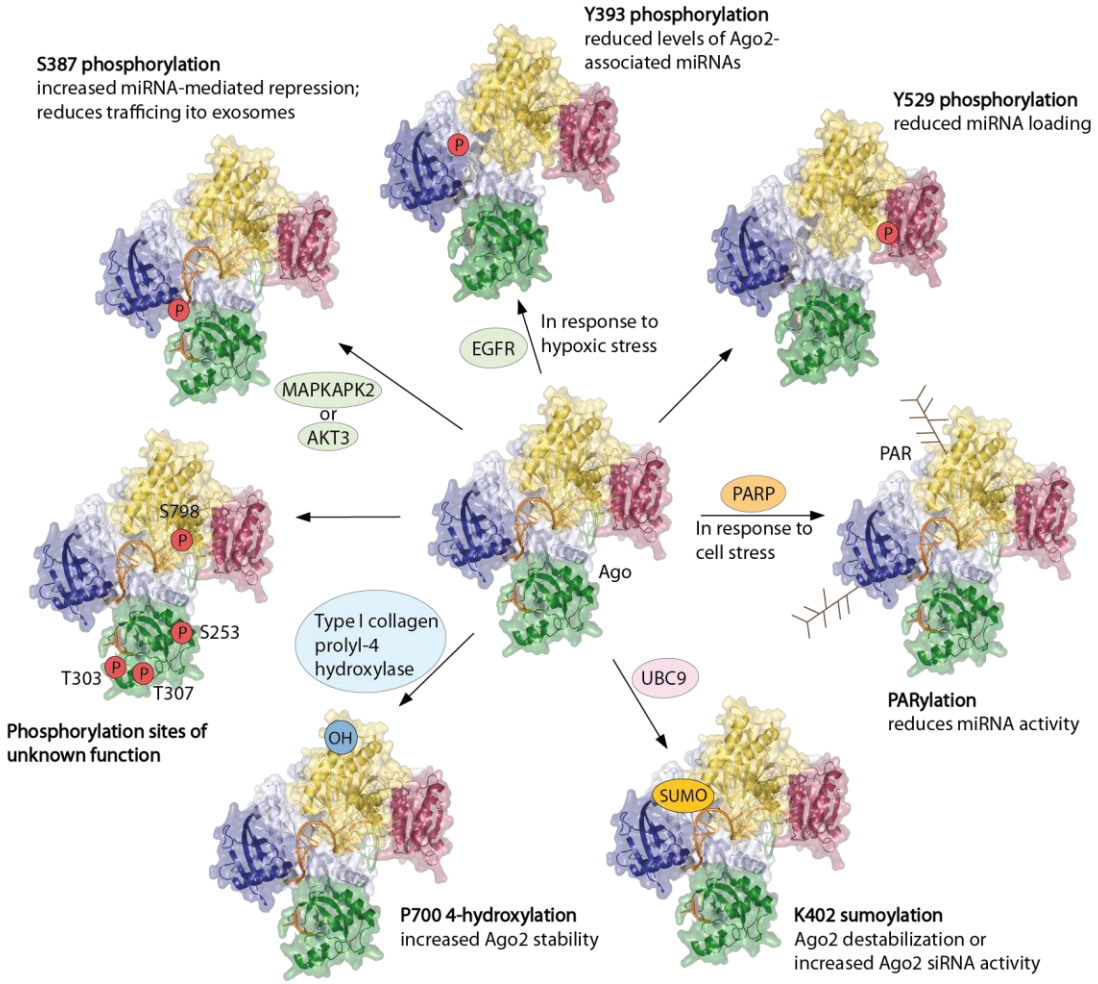

Figure 4 Post-translational modifications of Ago2. Phosphorylation of Y529, which is located near the 5' binding pocket of the miRNA in the MID domain, prevent the miRNA loading[132]. Phosphorylation of Y393 is located in the linker 2 region and reduces the levels of Ago2 associated miRNAs[133,134]. The neighboring phosphorylation of S387was published to be mediated by MAPKAPK2[135] or AKT3[136] *in vitro*. This phosphorylation is responsible for increased miRNA activity by stimulating the assembly of RISC. In addition, it leads to the translocation of Ago2 to multivesicular endosomes and secretion of exosomes[137]. Some other phosphorylations (S253, T303, T307 and S798) were identified but the function of these have not been assigned yet[132]. Additionally, modifications like hydroxylation at P700 were measured. This hydroxylation increases the Ago2 stability[128]. SUMOylation at K402 was described either to destabilize Ago2[126] or to be necessary for siRNA activity[127]. Also poly (ADP-ribosylation) (PARylation) was found, which blocks miRNA activity by decreasing target accessibility[129,131]. EGFR: epidermal growth factor receptor; OH: hydroxyl group; P: phosphate; PAR: poly (ADP-ribose); PARP: poly (ADP-ribose) polymerase; SUMO: small ubiquitin-like modifier; UBC9: ubiquitin carrier protein 9. Modified from [72].

1.5.1 Phosphorylation of Ago proteins

Phosphorylations are probably among the best-investigated post-translational modifications. This might be due to its important role in various signaling pathways. Several phosphorylated sites were also found in Ago proteins.

Some studies detected a phosphorylation at S387, which is located in the L2 region of Ago2[132,135,136] (Figure 4). *In vitro* studies discovered MAP kinase-activated protein kinase 2 (MAPKAPK2) in the p38 MAPK pathway-mediated stress response[135] and the proto-oncogene RACγ serine/threonine-protein kinase (AKT3)[136] to phosphorylate S387 in Ago2. Different results of localization within the cell are reported with the mutation of S387 into A in Ago2, which resembles a phospho-lacking mutant, indicating a not fully clear function of the phosphorylation in localization[135,136,138]. Phosphorylation at S387 is required for the interaction between Ago and LIM domain-containing protein 1. This protein bridges the Ago-TNRC6 interaction[139]. S387A mutation and the resulting blocking of phosphorylation also minimize trafficking of Ago2-miRNA complexes to multivesicular endosomes and reduce the secretion of exosomes[137]. Taken together, the data indicate that phosphorylation supports miRNA function by stimulating the miRISC assembly[72].

A further well characterized phosphorylation is located at position tyrosine (Y) 393 in the L2 region and neighboring to S387[132–134](Figure 4). Hypoxic stress stimulates the phosphorylation at this residue and is modulated by epidermal growth factor receptor (EGFR)[133]. Another study revealed that overexpressed RAS reversibly blocks protein–tyrosine phosphatase 1B. This inhibition leads to a hyper-phosphorylation of Ago2 at position Y393[134]. Both groups describe a reduced interaction between Ago and Dicer with a phosphorylation at Y393. In addition, phosphorylation at this position prevents miRNA loading of Ago2, impairs the regulation of p21 mRNA and induces senescence[133,134]. In the same line, phosphorylation of Ago2 at Y529 inhibits miRNA loading (Figure 4). This specific residue binds the 5' phosphate and the first nucleotide of guide RNA[71,140,141]. Phosphorylation at Y529 prevents miRNA binding and is known to associate with reduced miRNA binding during macrophage activation[142]. Further phosphorylation sites were detected in the PAZ domain (S253, T303, T307) and in the PIWI domain (S798) but their functions still remain unknown (Figure 4)[132].

1.5.2 The role of Ago2 in cancer and neurological disease

It is known that miRNA regulation is critical in tumorgenesis. As the main interactor of miRNAs, an overexpression of Ago proteins were detected in several carcinomas, like colon cancer[143], head and neck squamous cell cancer[144], and glioma[145]. In these studies, a relation between Ago2 overexpression and tumor growth and survival of cancer patients could be revealed[145,146]. They also discovered that Ago2 was overexpressed in hepatocellular carcinoma tissues and cells and that the overexpression enables oncogenic miRNAs, e.g. miR-21, to repress targets[146,147]. In contrast, the regulatory capacity of tumor suppressive miRNAs, like let-7, was unaffected[146,147]. In addition, a regulatory feedback loop was identified, in which miR-99a can inhibit Ago2 reciprocally. This miRNA was found to be remarkably decreased in hepatocellular carcinoma tissues[146]. Moreover, a decreased expression level of Ago2 protein but not mRNA was found in melanoma[148,149]. Additionally, reduced miRNA and siRNA functionality and phenotypic effects, like higher migration potential of melanoma cells were observed[148]. Interestingly, overexpression of Ago2 protein could block cell and tumor growth[148,149]. Due to different miRNA expression pattern in tissues and association of Ago2 with various processes in cancer, the expression level of Ago2 is variable in different types of cancer[150,151]. According to The Cancer Genome Atlas (TCGA, www.cancergenome.nih.gov), various mutations of Ago2 were identified in cancers, e.g. the mutation S831P was found in melanoma.

Despite cancer, a recent study uncovered an important role of Ago2 in neurological disease[152]. Pircs *et al.*[152] published recently that in Huntington's disease Ago2 accumulates as a result of impaired autophagy in neurons, which express aggregating mutant Huntingtin. The Ago2 accumulation leads to a global alteration of miRNA activity[152]. Taken together, these observations of Ago2 levels and mutations in cancer and neurological disease indicate that the correct Ago2 expression level in different tissues and cells but also intact Ago2 proteins are essential in maintaining appropriate miRNA activity and to ensure health.

1.6 Aims of the thesis

Ago proteins are central components of the small RNA-guided gene silencing pathway. To fulfill their functions, Ago proteins interact with small non coding RNAs, which guide them to specific target RNAs. On the one hand, some Ago proteins are endonucleolytically active and are therefore able to cleave their targets. On the other hand, Ago proteins recruit additional proteins and complexes to mediate translational repression and mRNA decay.

Since Ago proteins play such a pivotal role in gene silencing, it is important to understand the regulation of these proteins by post-translational modifications. It's already known that Ago proteins are targets for post-translational modifications. The best characterized modification on Ago proteins is phosphorylation. However, most phosphorylation sites were measured from overexpressed Ago proteins. The first focus of this thesis is the mass spectrometric identification of endogenous and conserved phosphorylation sites. Additionally, these phosphorylation sites will be characterized regarding their functionality and modifying enzymes will be identified.

Mis-regulation in Ago expression levels or Ago mutations result in diseases, like Huntington's disease or several cancers. A genome screening analysis of various patients showing the same neurological phenotype revealed different, heterozygous point mutations or deletions of Ago2. The second focus of this thesis is the functional characterization of these mutations.

2 Results

2.1 Phosphorylation of endogenous Ago proteins

As a key player of the gene silencing machinery, Ago proteins underlie extensive regulation. Many post-translational modifications of Ago proteins are known (see chapter 1.5), like ubiquitination, hydroxylation and phosphorylation. Here, a systematic and unbiased screen using different purification methods of endogenous Ago proteins are described, followed by the identification of phosphorylation sites using mass spectrometry.

2.1.1 Identification of endogenous phosphorylations in Ago proteins

Since overexpression of tagged proteins can lead to unspecific phosphorylation events, different purification strategies to purify endogenous Ago proteins from human cell lysates were established. On the one hand, a purification with specific monoclonal antibodies against Ago2 or a co-immunoprecipitation (co-IP) with antibodies against TNRC6 proteins was used. On the other hand, a purification strategy, termed Ago-APP (affinity purification by peptide) was chosen to precipitate all Ago proteins[107,154]. Shortly, for the immunoprecipitations, a specific monoclonal antibody against either Ago2 or TNRC6 proteins present in the cell lysate were coupled to protein-G sepharose beads. After washing, lysates, which contain phosphatase inhibitors, were added to the beads, followed by Ago protein elution and analysis using mass spectrometry. The second purification method, the Ago-APP, was performed with a short FLAG-GST-TNRC6B-peptide (T6B_599-683)[107], which was coupled to anti-FLAG M2 affinity agarose gel. The lysates were incubated on the affinity gel, washed, eluted with Lämmli-sample buffer and separated on a SDS-PAGE. Ago bands were excised and the samples were prepared for mass spectrometric analysis. The measurements were performed at least in triplicates. The overlapping potential phosphorylation sites are highlighted in Figure 5 A. The left part of this figure shows a Venn diagram with three biological replicates. The striped area represents the overlap of the phosphorylation sites of Ago in all three replicates. In the right part of this figure, the human Ago proteins are depicted schematically with their domain structure. Within this figure, the green bars represent the phosphorylation sites, which were measured in at least three biological replicates. The orange bars depict the phosphorylation sites measured in two biological replicates. Several phosphorylation sites

are highly conserved between the four human Ago proteins. At the N-terminus, there is one serine (S) as well as one tyrosin (Y), which were phosphorylated on the same peptide. The phosphorylation of a Y, in Ago2 the Y322, which is located in the PAZ domain seems to be phosphorylated in all four human Ago proteins.

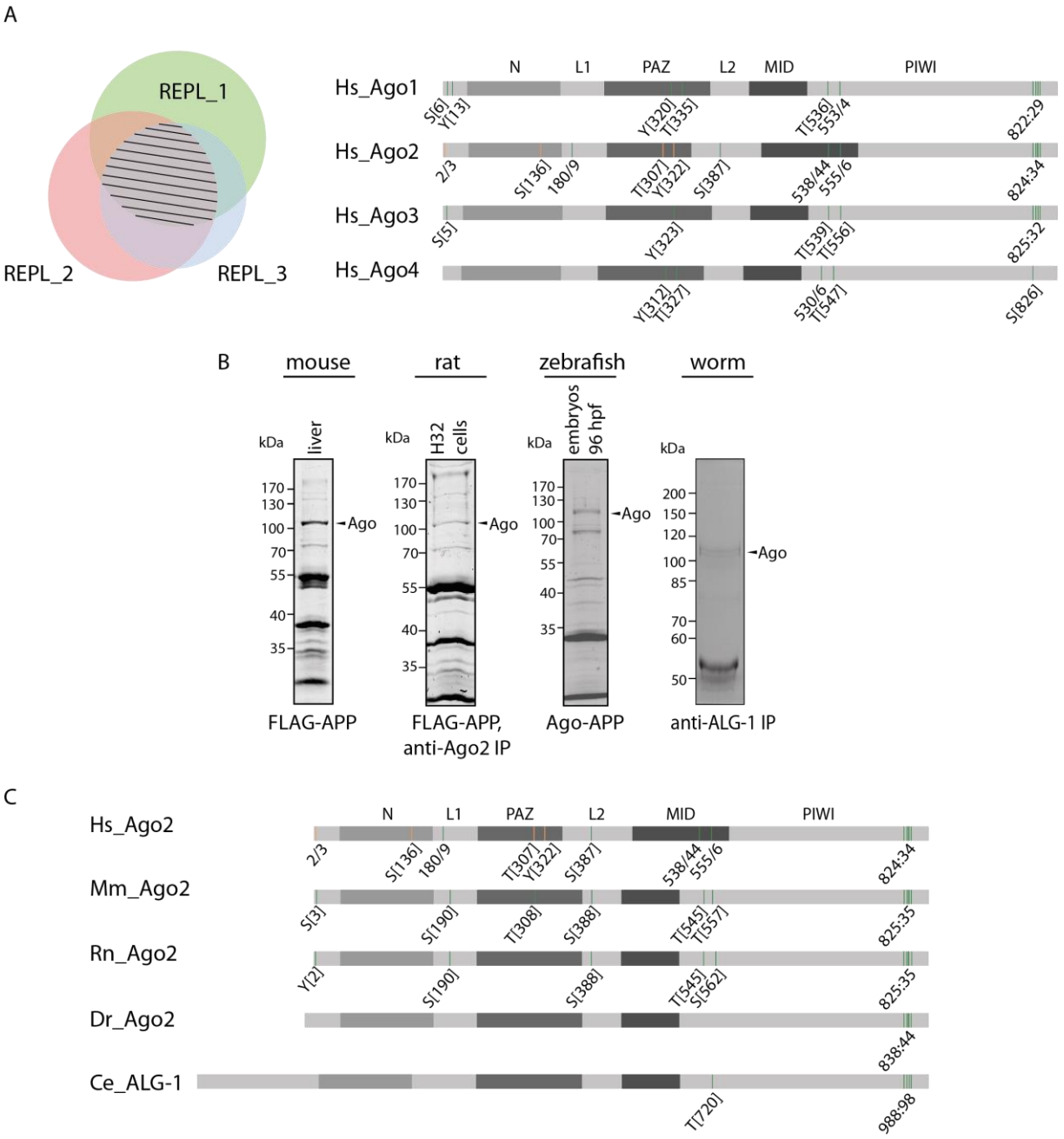

Figure 5 Identification and conservation of potential phosphorylation sites in Ago proteins. (A) Mass spectrometric measurements of human Ago proteins. Left: Venn diagram shows three replicates with an overlapping part, which is marked by stripes. Right: Schematic depiction of all four human Ago proteins and their domains. Green bars represent phosphorylation sites, which were measured at least in three biological replicates. The orange bars represent phosphorylation sites, which were measured in two biological replicates. Those

phosphorylation sites were detected via mass spectrometric analysis after an anti-TNRC6-IP or Ago-APP. (B) Endogenous Ago proteins were purified from human, mouse, rat, zebrafish and *C. elegans* with the indicated method. Here, SDS gels are shown which were stained with Coomassie. (C) Schematic representation of the Ago proteins and their domain structure of various species. The phosphorylation sites are shown as green bars (measured in at least three biological replicates) and orange (measured in two biological replicates). Hs: *Homo sapiens*, Mm: *Mus musculus*, Rn: *Rattus norvegicus*, Dr: *Danio rerio*, Ce: *Ceanorhabditis elegans*. The sample preparation of mouse, zebrafish and *C. elegans* were performed by Dr. Judith Hauptmann.

Prominent phosphorylations, in which single amino acids were detected to be phosphorylated, is found between the residues 530 and 556. Lastly, a cluster phosphorylation at the very C-terminus with five potential residues from 824-834 could be identified up to four times phosphorylated at the same time and within the same peptide. These residues are very well conserved in all four human Ago proteins and appears in a phosphorylation cluster. Only Ago4 showed less phosphorylation sites but this might be due to low abundance of Ago4. The well-characterized phosphorylation site on S387 could only be detected in human Ago2 in our measurements[135,136,139].

To see if those phosphorylation sites are also conserved between different species, material from mouse, rat, zebrafish and *C. elegans* was analyzed as described above (Figure 5 B). All phosphorylation events found on human Ago proteins were also found phosphorylated in these species except for Y322 and S136, which appeared to be human specific (Figure 5 C).

Because of the high conservation, two multiple phosphorylations were analyzed further. First, the peptide around 555-561 (555:61) in human Ago2, which contains four potential residues but was only found to be single phosphorylated in each individual measurement but at different residues. These amino acids are located in the MID domain in close proximity to the binding pocket of the target mRNA that is opposite to the first nucleotide of the miRNA[73,108]. The second phosphorylation cluster was the 824-834 cluster (824:34). This cluster is located on an exposed and flexible loop, which is not resolved in the known human Ago2 crystal structure[71].

2.1.2 Functional analysis of the 555:61 and 824:34 cluster phosphorylation of Ago2

The 555:61 cluster contains four closely located potential phosphorylation sites, but only single phosphorylation events were measured on individual peptides (indicated by the individual boxes, Figure 6 A). In the phosphorylation cluster at residues 824:34, hyper-phosphorylation of single peptides could be detected by mass spectrometry (indicated by one box, Figure 6 A). These phosphorylation events of single or multiple phosphorylated amino acids were readily detected in the spectra of mass spectrometry analysis (Figure 6 B and C). To learn more about those phosphorylated clusters and their potential functions, the phosphorylated residues were mutated into glutamate (E), a phospho-mimicking mutant, and into alanine (A), a non-phosphorylatable mutant, mimicking the unphosphorylated state.

In a first experimental characterization, the constructs were fused to a Lambda N (λN)-peptide and a HA-tag to physically tether them to a luciferase reporter mRNA containing the boxB RNA segment allowing for high affinity binding to λN [155,156] (Figure 6 D). Here, single as well as multiple mutants were analyzed. In this analysis, the single mutants behaved like wild-type (WT) Ago2. Moreover, the cluster mutations which all have potential phosphorylated residues of 824:34 mutated into either E or A, did not show an effect in this tethering assay (Figure 6 D). This approach demonstrates that mutations in the cluster region did not abolish silencing activity and recruitment of downstream factors when artificially tethered to a reporter mRNA target using the λN/boxB system.

Only the phospho-mimicking mutant, in which all residues of the 555:61 cluster were mutated to E, showed a strongly impaired silencing activity (Figure 6 D). This leads to the assumption that downstream factors of the gene silencing machinery cannot be recruited when artificially tethered to a reporter mRNA target using the λN/boxB system.

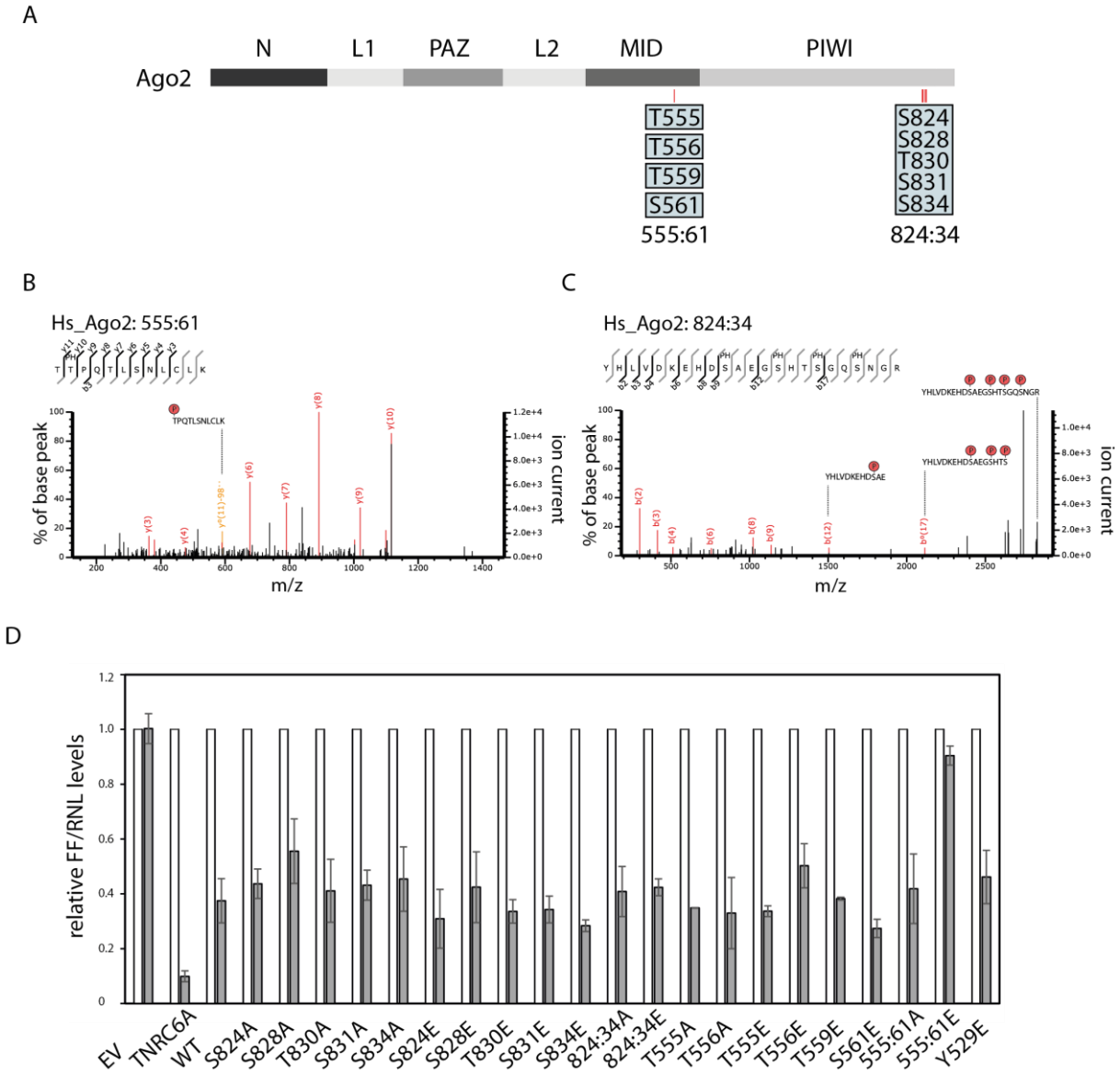

Figure 6 Phosphorylation cluster and their spectra. Schematic representation of human Ago2 and its domain structure. The blue individual boxes represent single phosphorylations on the residues 555-561. One blue box with the residues 824-834 indicates multiple phosphorylations on this peptide. (B) Representative CID fragment spectra of the mono phosphorylated at T556 of human Ago2 peptide (T*p*TPQTLSNLCLK). This spectrum originates from a LC-UHR-QTOF run. Monoisotopic mass: 1397.65 Da, Mascot ion score: 45, expectation value: 3.2e-005, Δ mass: 0.01 Da. (C) Spectra of a four times phosphorylated peptide of human Ago2 (YHLVDKEHD*p*SAEG*p*SHT*p*SGQ*p*SNGR). The phosphorylated sites are S824, S828, S831 and S834 according to Mascot. Monoisotopic mass: 2829.98 Da, Mascot ion score: 31, expectation value: 0.0085, Δ mass: 0.0017 Da. (D) Tethering assay with HA-tagged Ago2 wt and mutants. *Renilla* luciferase (RNL) activity was measured in extracts of HeLa cells. Cells were co-transfected with Ago2 constructs, either with or without λN-peptide, RNL-reporter with 5boxB aptamers, and *Firefly* (FF) luciferase. TNRC6A served as positive control. The expression levels of RNL was normalized to the FF signals (n ≥ 3, SEM).

In a second approach, TNRC6 binding of Ago2 mutants was analyzed. TNRC6 proteins are the main interactors of Ago proteins in context of translational repression and mRNA decay. Therefore, FLAG/HA-tagged constructs immunopurified via anti-FLAG-IP. The beads with the coupled proteins were split for either RNA isolations, followed by Northern Blotting, or eluted

for Western Blot analysis. Co-precipitated TNRC6 proteins were detected by a specific anti-TNRC6 antibody. The TNRC6 binding of the 555:61A mutant is undistinguishable from WT (Figure 7 A, lane 1-2). In contrast, the phospho-mimicking mutant showed an impaired interaction with TNRC6 (Figure 7 A, lane 3). The reduced TNRC6 binding results in impaired silencing activity, as additional factors like deadenylation and decapping complexes will not be recruited. Consistently, the reduced silencing activity could be seen in Figure 6 D.

In a next assay, binding of miRNA was tested. Ago proteins need miRNAs to guide them to specific targets, which are then repressed. After the anti-FLAG-IP, which is mentioned above, Northern Blotting was performed. A probe against the endogenous miR-19b was used to detect the bound miRNA (Figure 7 A). A signal for the bound miR-19b could detected in Ago2 WT and 555:61A mutant (Figure 7 A, lane 1-2), whereas in the 555:61E mutant, only weak signal of the bound miR-19b is visible (Figure 7 A, lane 3). This is consistent with the reduced binding of TNRC6 proteins. With a reduction in miRNA binding, 555:61E mutant could not be guided to the target and TNRC6 proteins could not be recruited. In conclusion, the silencing function of the phosphorylated 555:61 Ago2 protein is inhibited.

To get a complete picture of the silencing activity of the 555:61 phosphorylation mutants, target RNA interaction was tested using qRT-PCR. After an anti-FLAG-IP of the Ago2 proteins, RNA was isolated and cDNA generated. The direct binding of the distinct mRNA of High Mobility group protein HMGI-C (HMGA2), which is a target of let-7, was checked. 555:61A mutant binds this mRNA like Ago2 WT (Figure 7 B). In contrast, 555:61E mutant had a very low affinity to the target, which is correspond with the impaired miRNA binding (Figure 7 B). Y529E mutant, which does not bind miRNAs[132], and GFP served as negative controls and showed no mRNA interaction (Figure 7 B). A decreased miRNA binding of the hyper-phosphorylated 555:61 Ago2 protein results in a low mRNA affinity.

After checking for miRNA binding, these phosphorylation mutants were additionally tested for cleavage activity. After immunoprecipitation of the Ago2 proteins, they were incubated with a radiolabeled substrate RNA. In this *in vitro* cleavage assay, the endogenous miR-19b binds the perfect complementary substrate and cleaves it at a distinct position (indicated by the black bar in Figure 7 C). A signal for the cleavage product was detectable in the lane of 555:61A mutant and is undistinguishable from WT (Figure 7 C, lane 1-2), contrary to 555:61E mutant, which showed only a very weak cleavage product (Figure 7 C, lane 3). The result of impaired cleavage activity of the 555:61E mutant was also shown by Dr. Judith Hauptmann[154]. Consistently with the assays described above, phosphorylation at positions 555:61 results in

an impaired miRNA binding and can therefore interact with mRNA or even cleave perfect complementary targets only in a reduced manner.

Finally, the localization of Ago2 555:61A/E mutants was examined within the cell using immunofluorescence. P-bodies are sites in the cell where RNA metabolism takes place[157] and it is known that Ago proteins localize to p-bodies as well[24,94]. With the anti-HA antibody, Ago2 proteins were detected in green under confocal microscope. An antibody against U6 snRNA-associated Sm-like protein LSm4 (LSm4) detects the endogenous in red (Figure 7 D). LSm4 is a part of the cellular RNA decay machinery and served as a p-body marker. DAPI was used for nuclei staining (blue). While 555:61 un-phosphorylatable mutant showed a co-localization with LSm4 in p-bodies (Figure 7 D, upper panel), 555:61E mutant was not detectable in these structural elements (Figure 7 D, lower panel). In conclusion, the Ago2 555:61 phospho-mimicking mutant is not located in p-bodies, indicating that hyper-phosphorylation at positions 555:61 affect localization within the cell and may also reduce silencing activity. This finding is consistent with the reduced binding of TNRC6 proteins (Figure 7 A), miRNAs (Figure 7 A), mRNAs (Figure 7 B) and the hindered silencing activity (Figure 6 D).

However, in all these approaches the 555:61 non-phosphorylatable mutant behaves like WT (Figure 7). Since only mono-phosphorylated peptides were measured in this peptide and there were no phenotypes with single mutants in the tethering assay (Figure 6 D), this cluster was not characterized further, because effects of multiple phosphorylations could be artificial.

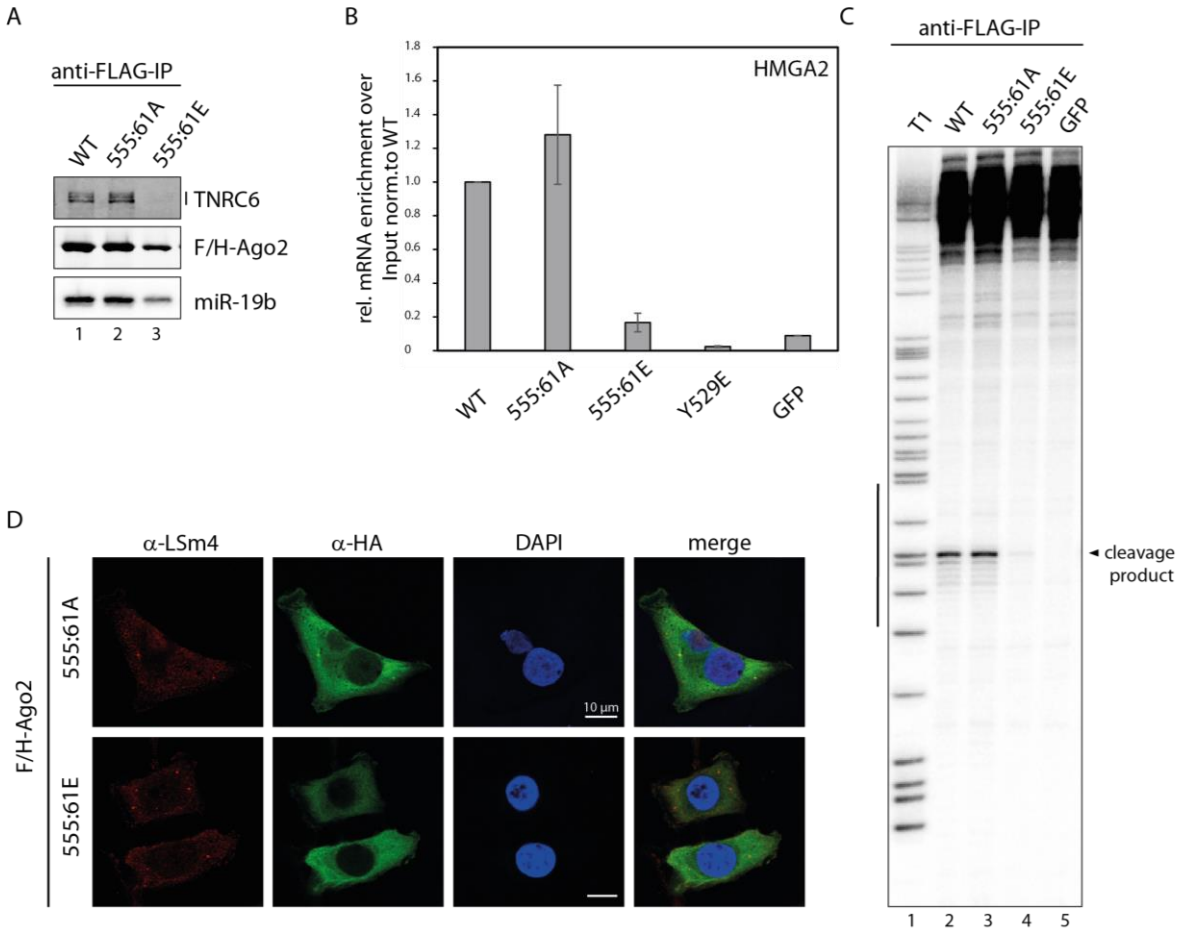

Figure 7 Functional analysis of the 555:61 phosphorylation cluster. (A) Immunofluorescence of HeLa cells transfected with F/H-tagged Ago2 555:61 phosphorylation mutants. Ago2 constructs were detected via anti-HA antibody (green), the endogenous LSm4 is stained in red and serves as p-body marker. The nuclei are stained via DAPI (blue). (B) HEK 293T cells were transfected with F/H-tagged Ago2 constructs, immunopurified with anti-FLAG antibodies, and separated on an SDS-PAGE or urea-gel and analyzed by either Western Blotting or Northern Blotting. Co-precipitated TNRC6 proteins were detected by pan-TNRC6-antnibody, clone 7A9. Ago2 proteins were detected by anti-HA antibody. For detection of the bound miRNAs, radioactively labeled probes against the endogenous miR-19b was used. (C) Cleavage activity of the 555:61 cluster mutants. F/H-Ago2 WT and mutants (GFP as negative control) were transfected in HEK 293T cells, immunopurified via anti-FLAG IP, incubated with a radioactively labeled substrate, which is perfect complementary to the endogenous miR-19b, followed by RNA isolation and separation on an 8 % sequencing gel. The black bar indicates the binding site of miR-19b. RNase T1 digest is labeled with 'T1'. (D) mRNA binding of Ago2 mutants. HeLa cells were transfected with F/H-Ago2 WT or 555:61 A/E mutant. Ago2 Y529E or GFP were transfected as negative controls. After anti-FLAG-IP, RNA isolation and cDNA synthesis, the enrichment of HMGA2 was measured by qRT-PCR over input and normalized to WT.

2.1.3 Hyper-phosphorylation of the 824:34 cluster does not affect miRNA binding and localization

Since there was no effect of the A or E mutant of 824:34 cluster in silencing activity, downstream steps were analyzed next. In a first approach, the miRNA and TNRC6 binding was checked. Therefore, the mutants were overexpressed in HEK 293T cells, immunoprecipitated by anti-FLAG antibodies from lysates, and either RNA isolated for Northern Blot analysis or interacting proteins eluted for Western Blot analysis. Both mutants, the phospho-mimicking and the phospho-lacking mutant, are able to bind TNRC6 proteins like WT suggesting that recruiting of additional factors for translational repression and mRNA degradation are not affected by phosphorylations at these positions (Figure 8 A, lane 2 and 3). These mutants can also interact with miRNAs, like miR-19b, miR-21 and let-7a, as efficient as WT indicating that phosphorylations at 824:34 is not important for small RNA binding and also demonstrate that the mutants are not globally unfolded (Figure 8 A, lane 2 and 3).

Next, the cellular localization of the 824:34A and E mutant was checked. Here, the Ago2 proteins were stained with an antibody against its HA-tag in green, LSm4 functions as p-body marker are shown in red and DAPI was used for nuclei staining in blue. Both mutants co-localize with LSm4 in p-bodies and are indistinguishable from WT (Figure 8 B). This result indicates that hyper-phosphorylation at the 824:34 cluster does not affect localization.

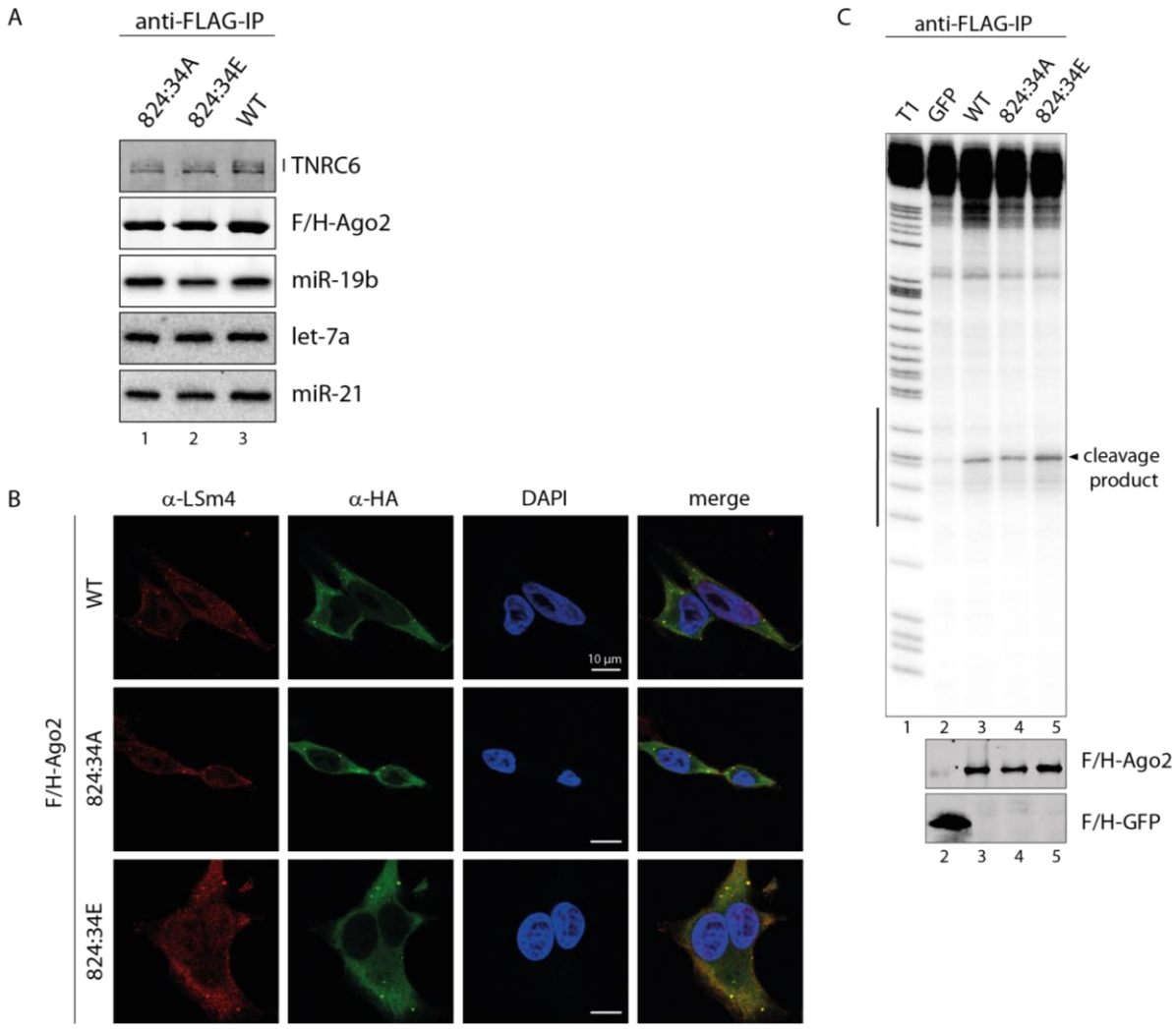

Figure 8 Functional analysis of the 824:34 phosphorylation cluster. (A) Immunofluorescence of HeLa cells transfected with F/H-tagged Ago2 WT and 824:34 phosphorylation mutants as described in Figure 7 A. (B) HEK 293T cells were transfected with F/H-tagged Ago2 constructs, immunopurified with anti-FLAG antibodies, and separated on a SDS-PAGE or urea-gel and analyzed by either Western Blot or Northern Blot. Co-precipitated TNRC6 proteins were detected by pan-TNRC6-antnibody, clone 7A9, and Ago2 proteins were detected by anti-HA antibody. For detection of the bound miRNAs, radioactively labeled probes against the endogenous miR-19b, miR-21 and let-7a were used. (C) Cleavage activity of the 824:34 cluster mutants as described in Figure 7 C. Western Blot was performed for control.

2.1.4 Phosphorylation at the 824:34 cluster is important for mRNA turnover

To examine the endonucleolytic activity of the Ago2 824:34 phosphorylation mutants, *in vitro* cleavage assays were performed. Immunoprecipitated Ago2 proteins were incubated with a radioactively labeled substrate RNA containing a perfect complementary target site for the endogenous miR-19b (Figure 8 C, indicated by a black bar). The cleavage products were analyzed by RNA electrophoresis. Again, the phospho-mimicking mutant as well as the phospho-lacking mutants showed the same activity as WT in this endpoint measurements and are therefore catalytically active indicating that cluster phosphorylation does not generally impair activity (Figure 8 C, lane 4 and 5). GFP served as negative control (Figure 8 C, lane 2).

However, the in vitro cleavage assay might be artificial regarding target RNA binding since the substrate RNA is present in high excess and the products may accumulate over time. A difference in on/off-rates of mRNAs might be detected better at early time points where cleaved substrate is not yet accumulated. After immunoprecipitation, the protein-coupled beads were split into six cups and incubated with radioactively cap-labeled substrate, which is perfect complementary to the endogenous miR-19b. Cleavage activity were tested after different incubation times (1-30 min) with the substrate to elucidate potential differences in cleavage kinetics (Figure 9 A). Western Blot was performed as loading control for the *in vitro* cleavage assays (Figure 9 B). The cleavage assays were repeated in at least triplicates and the cleavage product was quantified to uncleaved target RNA. Indeed, the 824:34 phospho-mimicking mutant showed reduced target cleavage at early timepoints in comparison to WT and the non-phosphorylatable mutant (Figure 9 A). Here, the cleavage kinetic curves of the Ago2 824:34E mutant shows slower target cleavage in comparison to WT or 824:34A mutant suggesting less efficient binding probably by higher off-rates of the hyper-phosphorylated Ago2 protein compared to WT Ago2 (Figure 9 C).

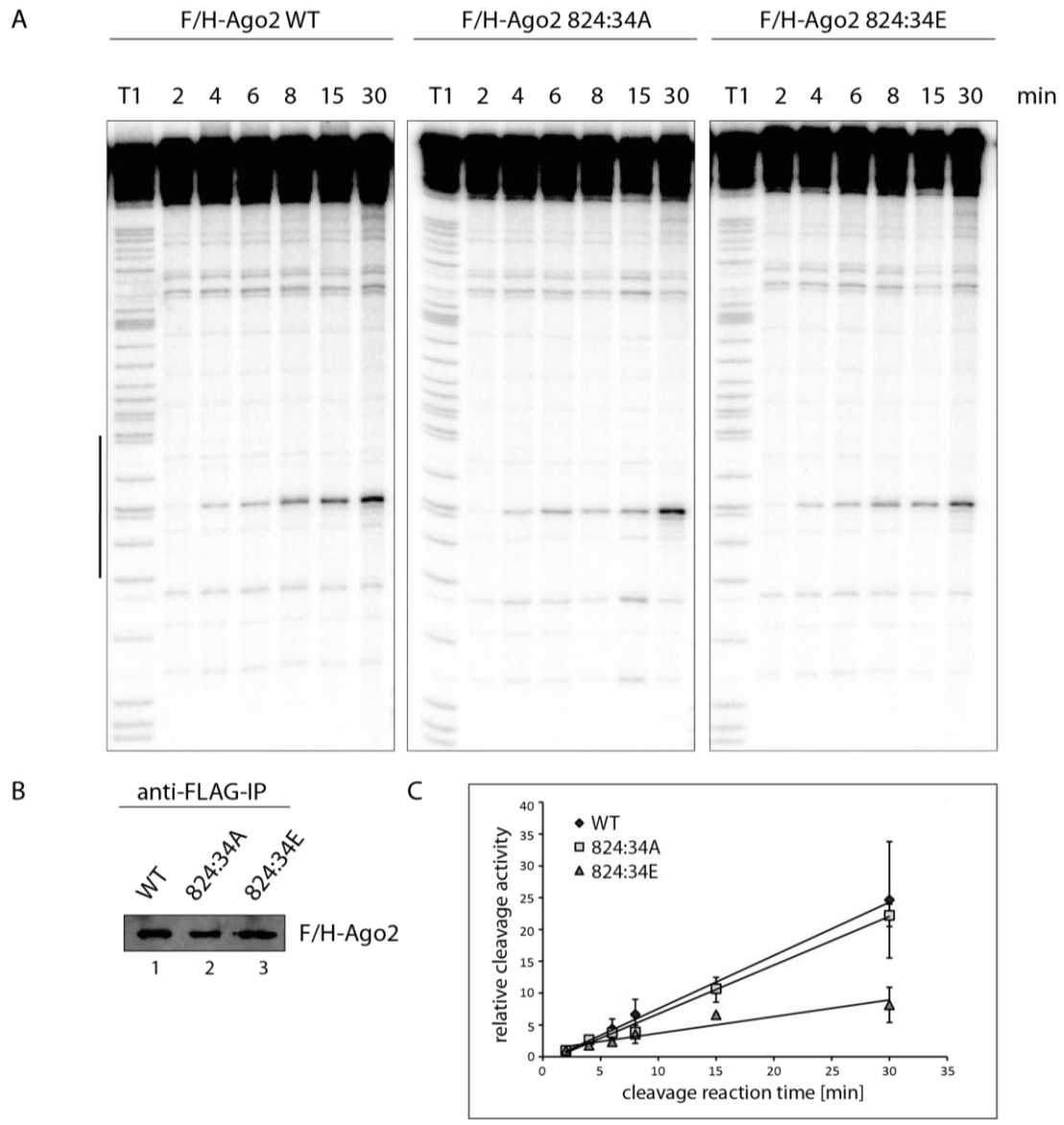

Figure 9 *In-vitro* cleavage kinetics of Ago2 824:34A/E mutants. (A) For cleavage kinetics of Ago2 WT and 824:34 cluster mutants, cleavage assays were performed as described in Figure 7 C but with various reaction times from 1 to 30 min. After anti-FLAG IP, the beads with the bound proteins were split for the cleavage reactions. (B) For loading control, a part of the beads were eluted with Lämmli-sample buffer, loaded on a SDS-gel and analyzed by Western Blot with anti-HA antibody. (C) Quantification of relative cleavage kinetics of Ago2 WT and 824:34A/E mutants, (replicates ≥ 3, SEM).

Lower binding affinity or lower dwelling time on the mRNA substrate could explain the observation of lower cleavage kinetics. Direct endogenous mRNA binding was therefore assessed in the next experiment using RNA-immunoprecipitation (RIP). Ago2 was overexpressed in HEK 293T cells, immunoprecipitated from lysates by their FLAG-tag, followed by RNA isolation. In addition to the IP samples, total RNA from inputs were isolated

to calculate the enrichment over input afterwards. This assay was performed in triplicates with WT, 824:34A and E mutant and as negative control the Ago2 Y529E mutant. This mutant is not able to bind miRNAs and should therefore not bind mRNAs[132]. Co-immunoprecipitated mRNAs were analyzed by microarray (Figure 10 A) and some specific targets were validated by qRT-PCR (Figure 10 B).

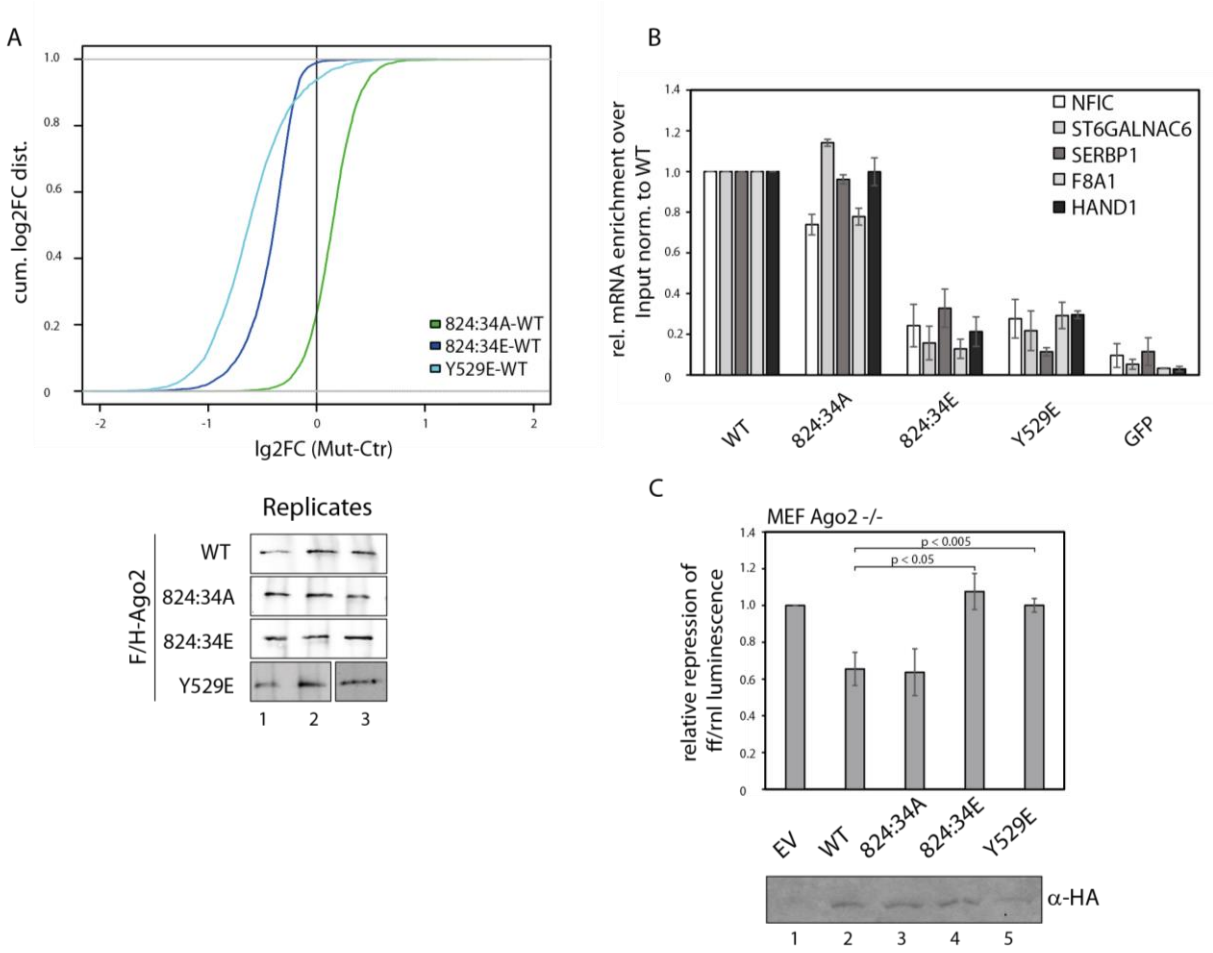

Figure 10 Hyper-phosphorylation of the 824:34 cluster affects mRNA binding. (A) Ago2 WT and phosphorylation mutants (Y529E serves as positive control) were overexpressed in HEK 293T cells, and immunoprecipitated via anti-FLAG-IP. RNA was isolated from three input samples and three biological replicates of each IP sample. The enriched mRNAs were analyzed by microarray, mutant vs. WT. The vertical line at 0 represents the log2FC of zero compared to Ago2 WT. Western Blot was performed for control using anti-HA antibody. (B) For validation of the microarray analysis, RIP experiments were performed as before, cDNA was made and analyzed by qRT-PCR. Different targets (NFIC, ST6GALNAC6, SERBP1, F8A1, HAND1) were analyzed upon binging to Ago2 proteins. GFP and Ago2 Y529E served as negative controls. Relative enrichment over input was normalized to WT Ago2. Analysis was done in biological triplicates and calculated as mean (SEM). (C) Dual luciferase assay was performed on HMGA2-3' UTR to observe the repression by overexpressed Ago2 constructs in MEF Ago2 $^{-/-}$ cells. (Replicates ≥ 3, SEM; p-values were calculated using a two-tailed Student's test) Western Blot was performed as control.

In the microarray analysis depicted in Figure 10 A, the cumulative distribution of the log_2-fold changes (log2FC) of Ago2 mutants in comparison to WT is shown. WT Ago2 associated mRNAs are represented as base line. On the left side of the zero line appeared weaker mRNA binding of the Ago2 mutant versus WT, the right side shows stronger binding. The negative control protein (Ago2 Y529E) bound only weakly to mRNAs, as it was expected since it is deficient of miRNA binding (Figure 10 A, light blue curve). The Ago2 824:34A mutant showed comparably or slightly stronger mRNA binding than the WT protein suggesting that without phosphorylation mRNA have a longer dwell time on Ago2 (Figure 10 A, green curve). Nevertheless, the Ago2 824:34 phospho-mimicking mutant appeared on the left side of the zero line. Hence, a strongly reduced mRNA binding was observed (Figure 10, dark blue curve). These results are consistent with the cleavage results and suggest that the hyper-phosphorylation of the 824:34 cluster interfere with mRNA substrate binding.

For validation of the direct mRNA interaction of Ago2 cluster phosphorylation mutants, the binding of five different targets (NFIC, ST6GALNAC6, SERBP1, F8A1, HAND1), which were identified in the microarray, were analyzed by qRT-PCR. After RIP, the enrichment of these targets was calculated over input and normalized to Ago2 WT. The 824:34 phospho-lacking mutant had a similar binding of mRNAs, while a reduced target binding could be detected with the 824:34E mutant, like the Ago2 Y529E control. Immunoprecipitated GFP served as negative control and did not bind any target above background (Figure 10 B). Consistently, the multiple phosphorylations at positions 824:34 affect mRNA binding in a negative way.

Next, the effect of Ago2 824:34 cluster phosphorylation mutants on small RNA-guided gene silencing was tested in living cells by dual luciferase assay. For this assay, a luciferase reporter under control of the known let-7a target HMGA2-3' UTR was transfected together with WT and mutant Ago2 proteins into Ago2 $^{-/-}$ mouse embryonic fibroblasts (MEFs) to investigate effects of only the transfected Ago2 versions without the endogenous background. Indeed, neither the phospho-mimicking cluster mutant nor the Ago2 Y529E negative control were able to repress the reporter luciferase, whereas the WT and the 824:34A mutant showed mild, but similar inhibition of reporter expression (Figure 10 C). In summary, these observations are pointing to a model, in which the hyper-phosphorylation of the residues 824:34 repels the negative charges of the target from Ago2.

To figure out the step in miRNA-guided gene silencing, where Ago2 is hyper-phosphorylated at the 824:34 cluster, different mutants were used to quantify their phosphorylation level by quantitative mass spectrometry (selected reaction monitoring - SRM). These mutants are trapped in different steps of the gene silencing: The Ago2 Y529E[132] mutant is not able to bind

miRNAs, should therefore not bind mRNA and does not localize in p-bodies. The 555:61A mutant is indistinguishable from WT Ago2 (Figure 7). The 555:61 phospho-mimicking mutant showed reduced miRNA and mRNA binding, no localization in p-bodies, it could not precipitate TNRC6 proteins and was not able to recruit downstream factors of the miRNA-guided gene silencing machinery when tethered to the mRNA (Figure 6 D, Figure 7). And the last mutant, analyzed in this assay was Ago2 620/694W mutant. Here, the binding pockets for the tryptophans (Ws) of TNRC6 proteins were blocked by mutating A620 and leucine (L) at position 694 into Ws in Ago2. This mutant lacked TNRC6 binding and miRNA binding is reduced (Figure 11 A), did not localize in p-bodies (Figure 11 B) but was able to cleave target RNA[158].

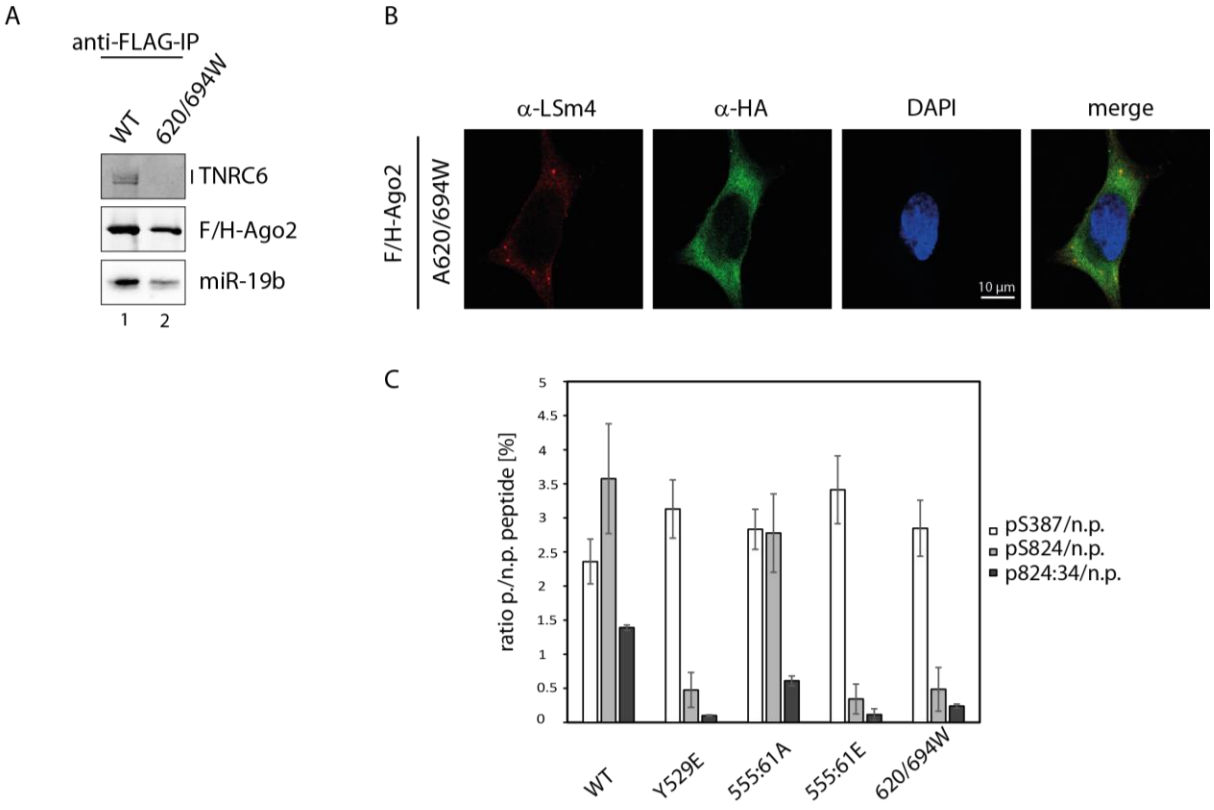

Figure 11 Quantification of phosphorylation levels in various Ago2 mutants. (A) Western Blot Co-IP of FLAG/HA-tagged Ago2 WT and 620/694W mutant described as in Figure 7 B. (B) Localization of Ago2 620/694W. Procedure was the same as in Figure 7 A. (C) The phosphorylation sites S387 and the cluster phosphorylation 824:34 were measured by quantitative mass spectrometry measurements (SRMs). For this, Ago2 mutants were overexpressed in HEK 293T cells, immunopurified by anti-FLAG IP, separated on an SDS-PAGE and stained with Coomassie Blue. The Ago2 bands were excised and prepared for mass spectrometry analysis. Isotope-labeled phosphorylated peptides were spiked into the tryptic in-gel digest. Bars represent the ratio phosphorylated:non-phosphorylated peptide (p./n.p.). Phosphorylation of S387 serves as internal control. Measurements were performed in biological triplicates and calculated as mean (SEM).

To quantify the phosphorylation levels of these proteins, isotope-labeled and phosphorylated peptides were spiked into the sample. First, the Ago2 peptide from amino acid 385 to 395 (SASFNTDPYVR) was spiked in, whereby S387 is phosphorylated or un-phosphorylated. Secondly, the peptide from position 815 to 837 (YHLVDKEHDSAEGSHTSGQSNGR) was used for quantification in an un-phosphorylated form, with a single phosphorylation on S824 and a four times phosphorylated version. For quantification, the ratios were calculated from phosphorylated/un-phosphorylated peptides in percent. Because the phosphorylation at position S387 was unaffected in each Ago2 mutant, this served as an internal control for the measurements (Figure 11 C, white bars). In Ago2 WT, a single phosphorylation level of S824 could be measured at around 3.5 % (Figure 11 C, grey bars) and a multiple phosphorylation level at 1.5 % (Figure 11 C, black bars). Also, the 555:61A mutant showed similar single and quadruple phosphorylation levels. Whereas in the other mutants, which were trapped at various steps of the gene silencing process, a decreasing level of the 824:34 cluster phosphorylation could be detected (Figure 11 C). Altogether, this data suggests a phosphorylation event of Ago 824:34 cluster at a late stage of miRNA-guided gene silencing probably during Ago dissociation from the already silenced mRNA or recycling steps.

2.1.5 Cluster phosphorylation is essential for ALG-1 function *in vivo*

Together with Prof. Dr. Martin Simard (Laval University Cancer Research Centre, Quebec) and his group, we elucidated the function of the Ago2 824:34 cluster phosphorylation *in vivo*. This C-terminal cluster is also very conserved in ALG-1, the Ago2 ortholog in *C. elegans*[159]. The four serines are conserved through all four human Ago proteins and in ALG-1 isoform-a and -b (Figure 12 A). ALG-1 also contains a threonine in this cluster, but at a different position. In collaboration with Dr. Judith Hauptmann (University of Regensburg, Biochemistry I), we investigated phosphorylation of ALG1, using our biochemical strategies. Indeed, multiple phosphorylations were identified in this region from 988 to 998 (Figure 12 B).

Next, Simard's group performed a transgenic rescue assay in an *alg-1* null allele strain *alg-1 (gk214) (alg-1 (0))* and expressed either WT alg-1 gene or mutants. Here, on the one hand single mutations of the position S992 (corresponding to S828 in human Ago2, indicated by a box in Figure 12 A) in phospho-mimicking (E) or phospho-lacking (A) were generated. On the other hand, complete cluster mutations, where the four serines were mutated into A or all potential phosphorylation sites were mutated into E (5A/4E), were used. For this rescue approach, they looked at the alae structure of the worms. Alae is a cuticular structure that

needs a precise developmental program, which is controlled by miRNAs[160]. They observed a strong phenotype in the alae structure of the worms expressing the 5A mutant and also the single S992A mutant (Figure 12 C). These worms showed no rescue of the *alg-1 (0)* resulting gapped alae structures or not even alae formation. However, the AGL-1 WT and the 4E/S992E expressing worms were able to rescue the alae phenotype and had complete alae structures[160] (Figure 12 C).

A

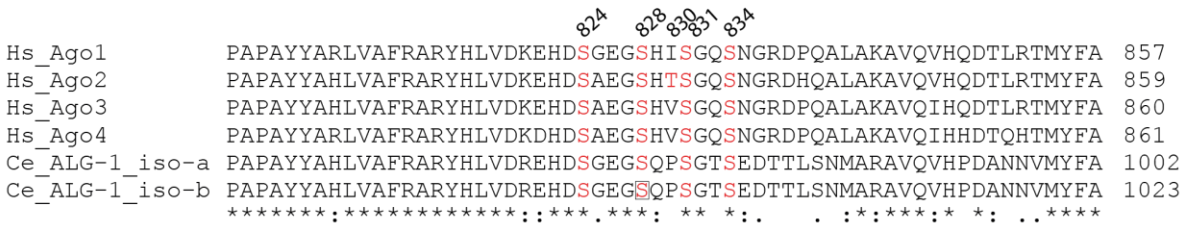

B

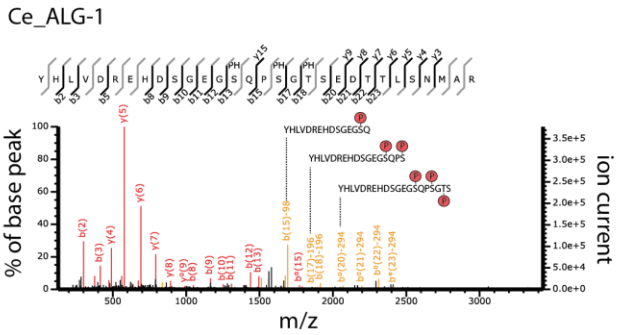

C

Genotype	Array	Complete alae	Gapped alae	No alae	n
wt	Ø	20	0	0	20
alg-1(0)	Ø	17	16	0	33
alg-1(0)	*alg-1(wt)*	23	2	0	25
alg-1(0)	*alg-1(5A)*	5	12	5	22
alg-1(0)	*alg-1(4E)*	34	0	0	34
alg-1(0)	*alg-1(S992A)*	1	16	8	25
alg-1(0)	*alg-1(S992E)*	28	0	0	28

Figure 12 C-terminal phosphorylation cluster is conserved in ALG-1 of *C. elegans*. (A) Alignment of all four human Ago proteins and C. elegans ALG-1 isoform-a and -b using Clustal Omega. (Q9UL18, Q9UKV8, Q9H9G7, Q9HCK5, G5EGR6, G5EES3) (B) Representative CID spectrum of a triple phosphorylated ALG-1 peptide of *C. elegans* (YHLVDREHDSGEGpSQPpSGpTSEDTTLSNMAR). This was generated from a LC-UHR-QTOF analysis. The phosphorylations were detected at position S992, S995 and T997 according to Mascot. Monoisotopic mass: 3,515.34 Da, Mascot ion score: 53, expectation value: 4.8e^{-006}, D mass: 0.01 Da. (C) Overexpressed non-phosphorylatable ALG-1 mutant (988:98A, 5A; S992A) worms were not able to rescue the alae structure in an *alg-1 (0)* background. Phospho-mimicking ALG-1 animals (988:98E, 4E; S992E) rescued the alae formation defects of *alg-1* depleted worms. The number of monitored animals is indicated as 'n'[160].

Furthermore, our collaborators generated phospho-mimicking and non-phosphorylatable ALG-1 S992 mutant worms by CRISPR-based genome editing to avoid artefacts caused by overexpression. With this model system, they could show developmental defects with the

S992A and E mutant but a stronger phenotype with the A mutant. For example, almost all S992A mutant worms died after the transition from larval to adult stage, bursting from the vulva[160]. They also observed an excess number of seam cells of the mutant and *alg-1 (0)* worms in comparison to the 16 seam cells in WT ALG-1 worms[160]. Moreover, the group of Martin Simard monitored a strong de-repression by using transgenic animals expressing a GFP reporter under control of a *lin-41* 3'UTR. This 3'UTR is regulated by *let-7* miRNA in the transition from larval to adult stage and should be repressed in WT worms. But the ALG-1 S992A and E mutant worms were not able to repress the reporter and so a GFP signal was still visible[160]. These assays indicate that the cluster phosphorylation of the 988:98 is essential for ALG-1 function *in vivo*.

2.1.6 Modifying enzymes

In summary, all the results described above point towards an essential role of the Ago 824:34 phosphorylation. It is conceivable that the de-phosphorylation could occur as well, and a phosphorylation-de-phosphorylation cycle might regulate Ago function. Kinases and phosphatases that are involved in phosphorylation and de-phosphorylation of these sites remain unknown. Since a single site mutation (S992) results in a strong phenotype in *C. elegans*, it is unclear if the corresponding site in human Ago2, S828, is more important than the other residues of the 824:34 cluster.

To gain new insights regarding interacting kinases and phosphatases, and thus in the regulation of Ago proteins, mass spectrometry data was analyzed to find interacting partners of Ago proteins. First, published data from Dr. Anne Frohn was scoured to identify relevant kinases and phosphatases[161]. Here, a number of enzymes were found, but the subunits of one phosphatase were exceptional: Protein phosphatase 6 (PP6) and its subunits. This phosphatase is a heterotrimeric complex composed of a catalytic subunit PPP6C, a SAPS domain-containing subunit (PP6R1-3) and an ankyrin repeat-domain containing regulatory subunit (ANKRD28, 44, 52)[162,163]. In the mass spectrometry data of Dr. Anne Frohn SAPS3 or PP6R3, ANKRD28 and PPP6C could be identified as potential interacting partners of Ago2[161].

To test whether these proteins are indeed involved in Ago de-phosphorylation, the single subunits were knocked down via sipools (siTools, Munich). For this experiment, siPools against PPP6C, PP6R1-3 and ANKRD28, 44, 52, and control sipools were transfected into HEK 293T cells and harvested 48 h after knock down. Subsequently, immunoprecipitation of

endogenous Ago2 was performed, followed by a sample preparation for quantitative mass spectrometry with the focus on the phosphorylation cluster 824:34 and the phosphorylation S387 as internal standard for phosphorylation level and comparable amounts of phosphorylated Ago (Figure 13).

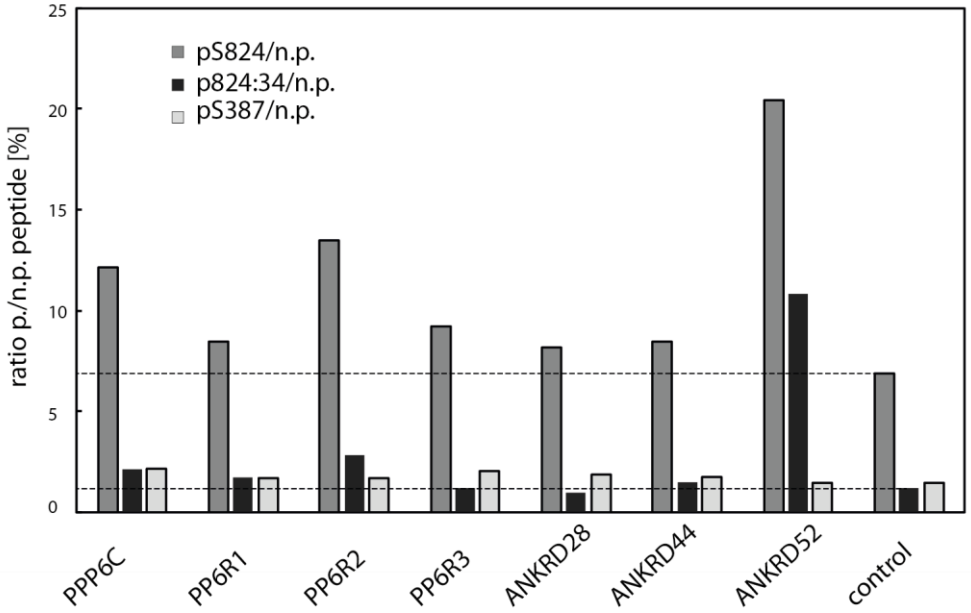

Figure 13 Phosphorylation levels of the 824:34 cluster and S387 in Ago2. The phosphorylation sites S387 and the cluster phosphorylation 824:34 were measured by quantitative mass spectrometry measurements (SRMs). For this, the single subunits of PP6 were knocked down for 48 h in HEK 293T cells, immunopurified by anti-Ago2 IP, separated on a SDS-PAGE and stained with Coomassie Blue. Further procedure was performed as described as in Figure 11. The dashed lines represent the phosphorylation levels of the control knock down.

In the control knock down, a phosphorylation level at approximately 6 % of the total Ago2 protein level was detected when a single S824 phosphorylated peptide was used as reference. About 1 % is phosphorylated at four residues when the four times phosphorylated peptide was spiked in as reference. Upon knocking down the factors of PP6, an increased single phosphorylation level could be measured. Especially upon knock down of ANKRD52, the phosphorylation level of S824 raised to around 20 % (Figure 13). Additionally, an immense increase (around 10 %) of the quadruple phosphorylated 824:34 cluster was observed when ANRKD52 was knocked down (Figure 13). The knock down of PP6R1, PP6R3, ANKRD28 and ANKRD44 showed a slight increased level of the single phosphorylated peptide at position S824 at a level of approximately 0.5-1.5 % (Figure 13). The level of the four times phosphorylated peptides after the knock down of PP6R1, PP6R3, ANKRD28 and AKNRD44 did not change in comparison to the control knock down (Figure 13). Whereas the knock

down of PPP6C results in phosphorylation level of position S824 at approximately 12 % and a multiple phosphorylated peptide 824:34 at around 2 % (Figure 13). Also, an increase in the levels of single phosphorylation (approx. 14 %) and quadruple phosphorylation (approx. 3 %) of the 824:34 peptide was measured in the knock down of PP6R2 (Figure 13). The phosphorylation level of S387 is stable in every sample of this experiment and appears at around 2 % (Figure 13). In conclusion, a phosphatase complex presumably composed of PPP6C-PP6R2-ANKRD52 acts on Ago de-phosphorylation of the 824:34 cluster.

According to this experiment, the most important factor for de-phosphorylation of the 824:34 cluster seems to be ANKRD52 of PP6 holoenzyme. The group of Prof. Dr. Joshua Mendell also confirmed this finding. His group identified PPP6C in combination with ANKRD52 as the phosphatase and casein kinase 1α (CSK1A1/CK1) as responsible kinase for the 824:34 cluster in a genome-wide CRISPR screen[164].

The CSK1A1 as a potential kinase needs an initial phosphorylation to bind and phosphorylate its substrates. The next aim was the identification of the priming site. Therefore, mutants were generated, and their phosphorylation pattern were analyzed. These five mutants have their potential phosphorylation sites mutated to single alanines at position 824, 828, 830, 831, and 834. The single-A mutants were then overexpressed in HEK 293T cells, immunopurified via their FLAG-tag, separated on an SDS-PAGE and prepared for mass spectrometry to assess the phosphorylation pattern of each mutant.

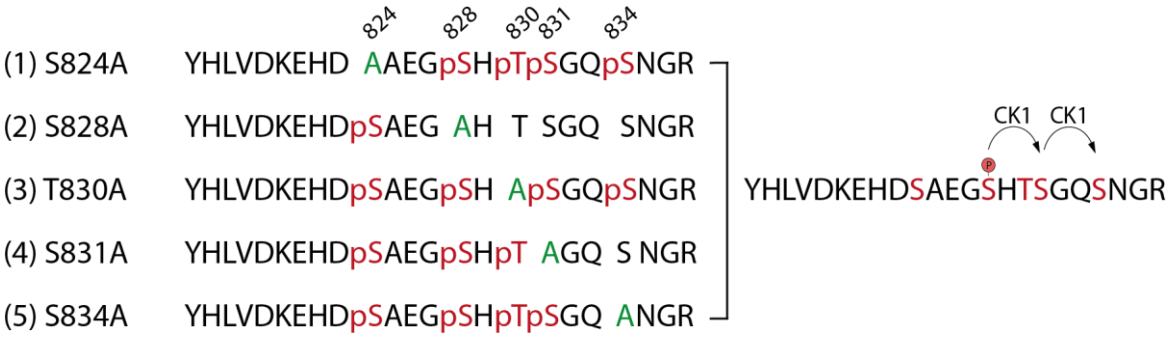

Figure 14 Phosphorylation pattern of different alanine-mutants of the 824:34 cluster. Ago2 824:34 single alanine mutants were generated, overexpressed in HEK 293T cells, immunopurified, separated on an SDS-PAGE and analyzed via mass spectrometry. The phosphorylation pattern of at least three biological replicates of each mutant were measured. Green As mark the mutated serines or threonine. Detected phosphorylated sites are depicted in red with a prefixed 'p'. CK1 is short for CSK1A1. The arrows show phosphorylation events after initial phosphorylation.

Interestingly, the mutation of S824A had no effect on the subsequent phosphorylated sites (Figure 14 (1)). The mutation of the S828A affected the subsequent sites. The residues 830, 831 and 834 showed no phosphorylation, whereas phosphorylation could be detected at S824 (Figure 14 (2)). With the mutation of T830A and S834A, every combination of phosphorylations were measured (Figure 14 (3,5)). In contrast, after mutation of S831A, only the residues before were measured to be phosphorylated, not S834 (Figure 14 (4)). These findings lead to the assumption that S828 is a very important site for the hyper-phosphorylation and could thus be the priming site. After an initial phosphorylation of S828, CSK1A1 phosphorylates the S831, followed by S834 (Figure 14). This is result is consistent with the data obtained in *C. elegans*. When mutating S992 into A, which is corresponding to S828 in human Ago2, the worms showed a strong phenotype (Figure 12 C). This kinase needs an initial phosphorylation and subsequently phosphorylates every third potential residue. Additionally, the group of Prof. Dr. Joshua Mendell performed *in vitro* kinase assays with CSNK1A1[164] and the results correlated with the outcome of the described experiment (Figure 14).

In summary, the protein phosphatase 6, particularly the complex PPP6C-PP6R2-ANKRD52, might be responsible for de-phosphorylation of the 824:34 cluster. The de-phosphorylation may allow Ago to be recycled and go into another round of repression. Furthermore, CSNK1A1 was identified to be involved in phosphorylation of 824:34 cluster, but this kinase needs an initial phosphorylation to be enzymatically active. Here, the phosphorylation of S828 was identified to be very important for hyper-phosphorylation of this cluster and thus may be the priming site for the initial phosphorylation. Other kinases, which are needed i.e. for the priming phosphorylation remain still unknown and will be exciting future research subjects.

2.2 Ago2 mutations result in human neurodevelopmental disorders

In the second part of my thesis, I have biochemically investigated Ago2 mutations found in disease. Ago proteins are known to be key factors in small RNA-guided gene silencing. The group of Prof. Dr. Hans-Jürgen Kreienkamp and Dr. Davor Lessel from the Medical Center Hamburg-Eppendorf discovered Ago2 mutations in human neurodevelopmental disorders. In collaboration, functional effects of these mutations were investigated in biochemical assays.

2.2.1 Ago2 mutations and neurodevelopmental disorders

It is known that mis-regulated Ago expression levels can cause in various diseases, like Huntington's disease[152], or cancer[143,144,146,148,149]. The Kreienkamp/Lessel lab sequenced the genome of different patients. These children showed a similar phenotype: they were mentally retarded and started to talk and walk very late. But it was very interesting that from the exome sequencing results, only heterozygous mutations in Ago2 could be found. They identified eight different point mutations and one deletion of an amino acid: phenylalanine (F)182 deletion (del), leucine (L) 192 into proline (P), glycine (G) at the position 201 mutated into cysteine (C), histidine (H) 203 into glutamine (Q), methionine (M) 364 into T, A367 into P, G733 to arginine (R), and S760 mutated into R (Figure 15 A, red bars). The mutations F182del, L192P, G201C and H203Q are located in the linker 1 (L1) regions, the mutations M364T and A367P are positioned in the linker 2 (L2) region and the mutations G733R and S760R are in the PIWI domain (Figure 15 A). Interestingly, all these mutations independently resulted in a similar phenotype of the children. In addition, the mutation L192P was found in two independent patients, one from the Netherlands and one from Seattle, showing the same phenotype.

In addition, G201 was found once mutated to C and in another patient it was mutated into valine (V). Twins were sequenced with the same phenotype described before with a mutation at C751Y, which is positioned in the PIWI domain (Figure 15 A). The mutation G201V and C751Y were detected at a later stage and could not be included in this work. Altogether, heterozygous mutations in Ago2 appear to result in a neurodevelopmental phenotype in patients, although a second un-mutated copy is present.

2.2.2 Functional analysis of the disease related mutations in Ago2

To analyze effects of these mutations on Ago function, the mutants described above were generated and tested in various assays.

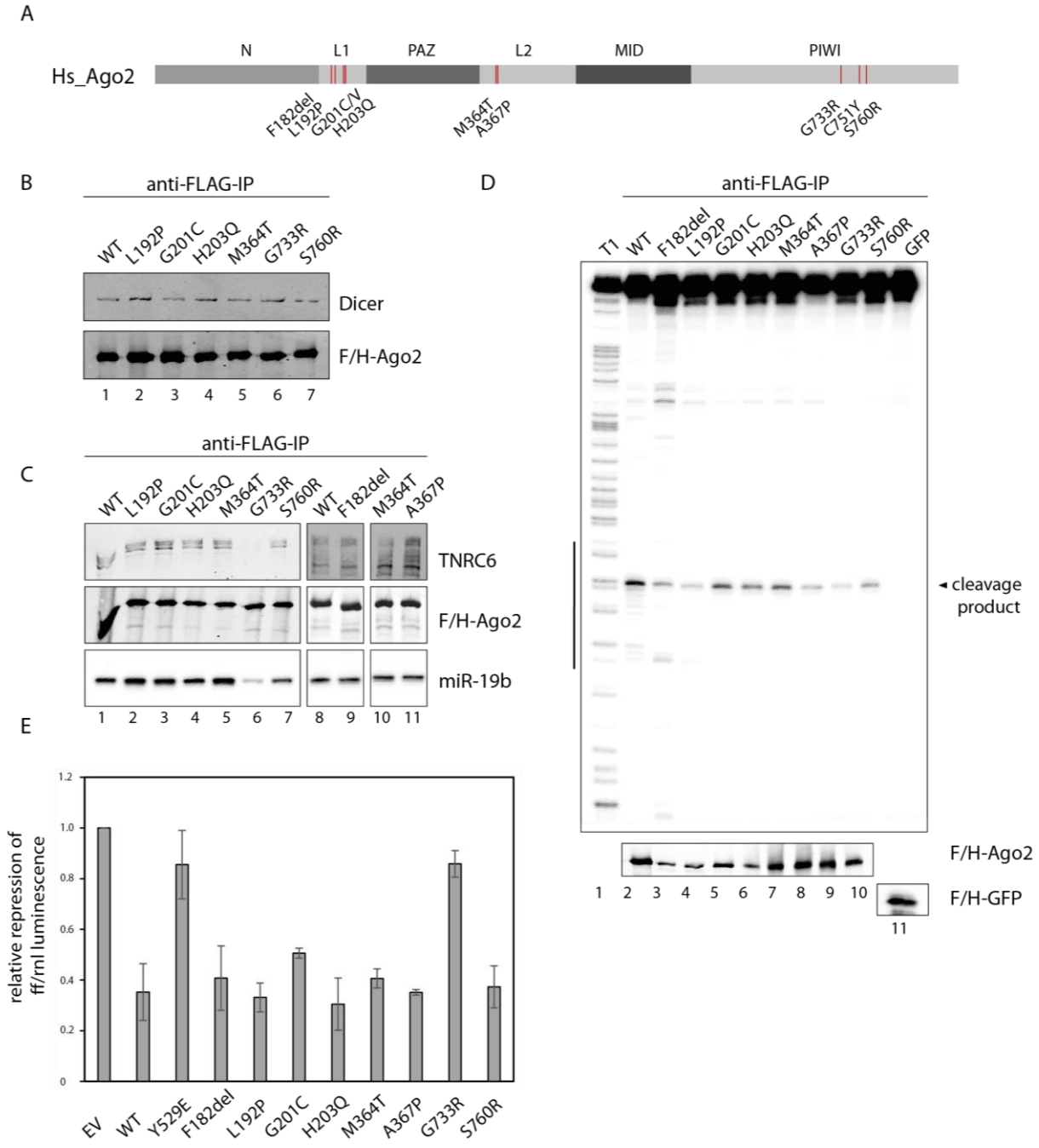

Figure 15 Functional analysis of Ago2 disease related mutants. (A) Schematic depiction of Ago2 and its domain structure. Red bars represent mutations that were found in patients. (B) Co-immunoprecipitation of Dicer. F/H-tagged Ago2 WT and mutants were overexpressed in HEK 293T cells, purified via anti-FLAG antibody, separated on an SDS-PAGE and analyzed via Western Blotting. (C) The procedure was described in (B), but the membrane was incubated with anti-TNRC6 antibody. After the IP, the samples were split on the one hand for Western Blot detection, on the other hand for RNA isolations followed by Northern Blotting. The Northern Blot

was incubated with a radiolabeled probe against endogenous miR-19b. (D) Ago2 cleavage assay. The experiment was performed as described in Figure 7 C. (E) Dual luciferase assay to analyze the silencing ability of Ago2 mutants. Ago2 WT, mutants and empty vector were co-transfected with a plasmid encoding for RNL as control and FF under control of HMGA2-3'UTR in HeLa cells. For calculation, the ratio FF/RNL signals were normalized to empty vector (EV).

First, a co-immunoprecipitation was performed to see the interaction of Ago2 mutants with TNRC6 proteins and/or Dicer. For this, Ago2 WT and mutants were overexpressed in HEK 293T cells, immunopurified via their FLAG-tag, and analyzed by SDS-PAGE. After Western Blotting, the membrane was incubated with anti-HA antibody for Ago2 proteins and either anti-TNRC6 or anti-Dicer antibody. Every tested mutant was able to interact with Dicer (Figure 15 B).

In addition, all Ago2 mutants showed an interaction with TNRC6 proteins (Figure 15 C, lane 1-5 and 7-11), except for mutant G733R. With this mutant, no or reduced signal of TNRC6 proteins could be detected (Figure 15 C, lane 6). In addition to the bound proteins, RNA was isolated after the anti-FLAG IP and the interaction with miR-19b was analyzed. Here, only a weak signal of bound miR-19b could be detected with the mutant G733R (Figure 15 C, lane 6). All the other Ago2 mutants showed a signal for miR-19b comparable to Ago2 WT (Figure 15 C, lane 1-5 and 7-11). These results indicate that Ago2 mutants are loaded with miRNAs correctly by Dicer (Figure 15 B) but the miRNA binding is reduced with mutation G733R (Figure 15 C, lane 3, 8).

After confirming miRNA and TNRC6 binding except for G733R, the next analysis was Ago2 cleavage activity. Therefore, Ago2 WT and mutants were expressed in HEK 293T cells, immunopurified, and incubated with a radioactively labelled target substrate, which is perfect complementary to the endogenous miR-19b. Afterwards, RNA was isolated, and separated on an urea sequencing gel. An Ago2 WT-comparable cleavage activity could be observed for the Ago2 mutants (Figure 15 D, lane 2, 5-8, 10), except for the G733R mutation protein (Figure 15 D, lane 9). Since this mutant showed a reduced miRNA binding, it was not surprising to see a lower cleavage activity. The mutants F182del and L192P showed reduced cleavage products but the in the Western Blot these two proteins appeared to be lower expressed (Figure 15 D, lane 3, 4). That is probably the reason for the decreased cleavage activity. GFP was used as negative control (Figure 15 D, lane 11).

In a next approach, the silencing ability of the mutants was tested using dual luciferase assay. Therefore, Ago2 constructs were expressed in HeLa cells together with a dual luciferase reporter. This reporter expresses Renilla luciferase mRNA for control and Firefly luciferase mRNA under control of HMGA2 3'UTR, which is a known target for let-7. After cell lysis, the

signals were read out by an illuminometer. The relative FF/RNL ratios were calculated and normalized to the empty vector. For negative control, the Ago2 Y529E mutant, which does not bind miRNAs[132], was tested and this mutant showed no repression almost like the empty vector (Figure 15, E). The G733R mutant behaved like the negative control and a strong de-repression could be observed (Figure 15, E). This result is consistent with the reduced miRNA binding and TNRC6 interaction of the G733R mutation. In contrast, all the other mutants showed a repression of the firefly mRNA in the WT range suggesting that these mutations do not affect silencing activity of Ago proteins (Figure 15, E).

For complete functional analysis, the localization of the Ago2 mutants found in patients were examined. For this, Ago2 constructs were overexpressed in HeLa cells, seeded on cover slips, fixed with paraformaldehyde and incubated with anti-LSm4 (red), which served as p-body marker, and anti-HA (green) antibody. The nuclei were stained with DAPI (blue). The localization of the Ago2 mutants gave the same picture as the assays mentioned above: all Ago2 mutants nicely co-localized with the LSm4 in p-bodies, except for the G733R mutant. This one was only found in the cytoplasm but not in dot like structures (Figure 16). Taken together, all tested mutants showed similar behavior to Ago2 WT in the described functional assays, except for the G733R mutant.

Figure 16 Immunofluorescence of Ago2 disease related mutants. Ago2 mutants were overexpressed in HeLa cells, fixed on cover slips and proteins were detected via specific antibodies: anti-HA for Ago2 proteins (green), anti-LSm4 as p-body marker (red) and DAPI for nuclei staining (blue). All mutants were shown separately in immunofluorescence from top to bottom starting with WT.

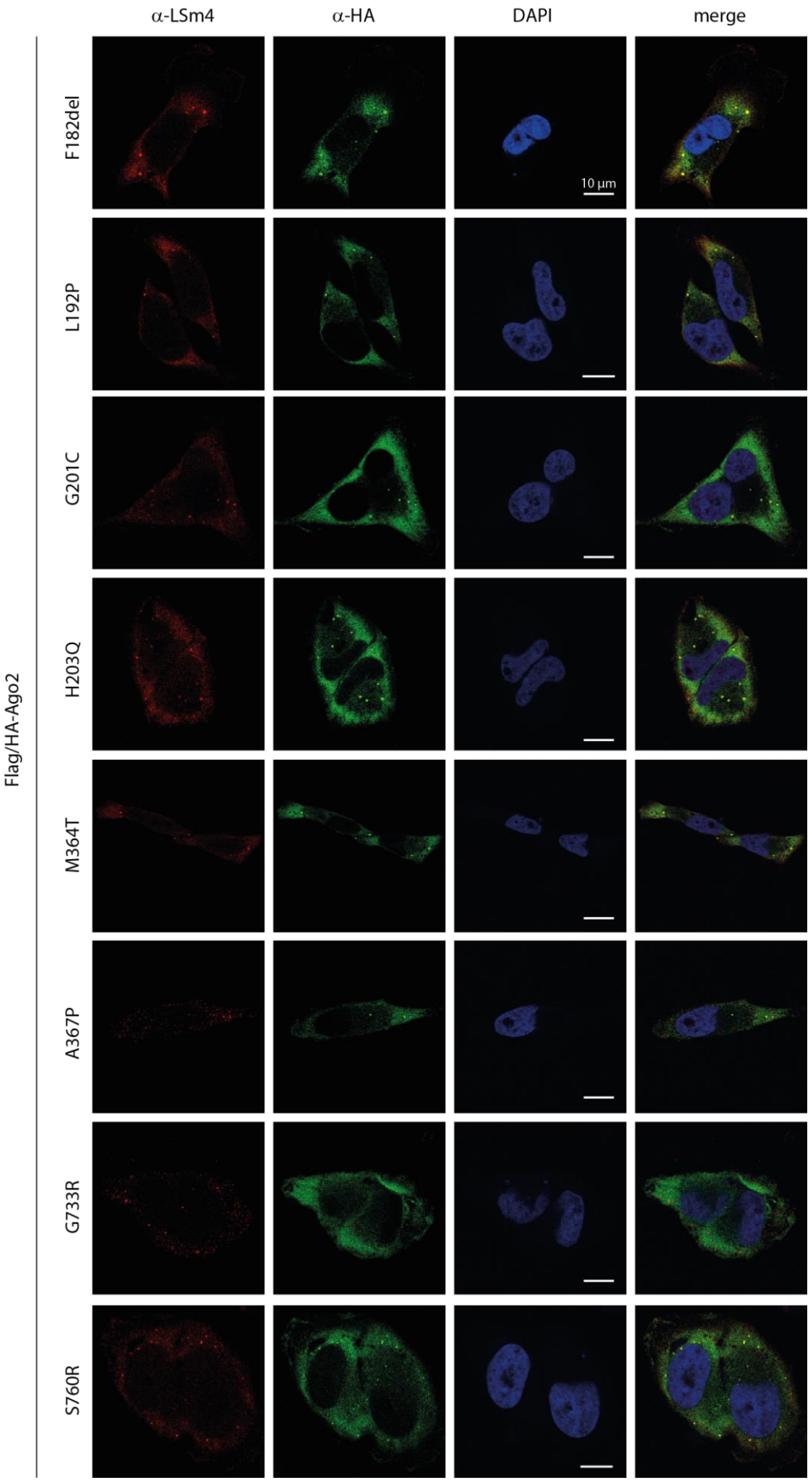
α-LSm4
α-HA
DAPI
merge
Flag/HA-Ago2
F182del
L192P
G201C
H203Q
M364T
A367P
G733R
S760R
10 µm

2.2.3 Mutations affect mRNA binding

With the background of the methods, described in section 2.1.4, the mutants were analyzed concerning their phosphorylation level at the 824:34 cluster, which is near the miRNA-mRNA position. If this is hyper-phosphorylated, the negative charges of the phosphates can lead to the repulsion of bound and negatively charged mRNA. This results in the loss of mRNA (Figure 10, dark blue curve, 824:34E). Without multiple phosphorylations at this peptide, mRNAs can be bound longer or stronger to this Ago protein (shown in Figure 10, green curve, 824:34A). With this knowledge, a link from the phosphorylation level to bound mRNA within a strong phenotype could be established.

To measure the relative phosphorylation levels of the 824:34 cluster, Ago2 mutants, which were found in patients, were overexpressed in HEK 293T cells, immunopurified, analyzed by SDS-PAGE and prepared for mass spectrometry. For relative quantification, unphosphorylated and phosphorylated heavy labelled peptides were spiked into the samples before trypsin digestion (as described in Figure 11). Phosphorylation of S387 served as internal control for the measurements and showed equal levels in each mutant and WT (Figure 17 A, light grey bars). The single phosphorylation S824 was measured in Ago2 WT at levels of approximately 3.5 % of total Ago2, the patient mutants showed single phosphorylation levels from 1-3 % (Figure 17 A, grey bars). Almost no single phosphorylation was measured in the G733R mutant. Looking at the four times phosphorylated version of the 824:34 peptide, a phosphorylation level of around 2 % was measured in the Ago2 WT sample. In all other Ago2 mutants, a heavily reduced level of quadruple phosphorylated peptides could be observed, except for the H203Q mutant. Here, a level up to 3.5 % was measured but with a high error bar. The other mutants showed a decrease of hyper-phosphorylation, which leads to the suggestion that the mRNA might be bound stronger to the Ago proteins because of generally less Ago2 S824:34 cluster phosphorylation (Figure 17 A, black bars).

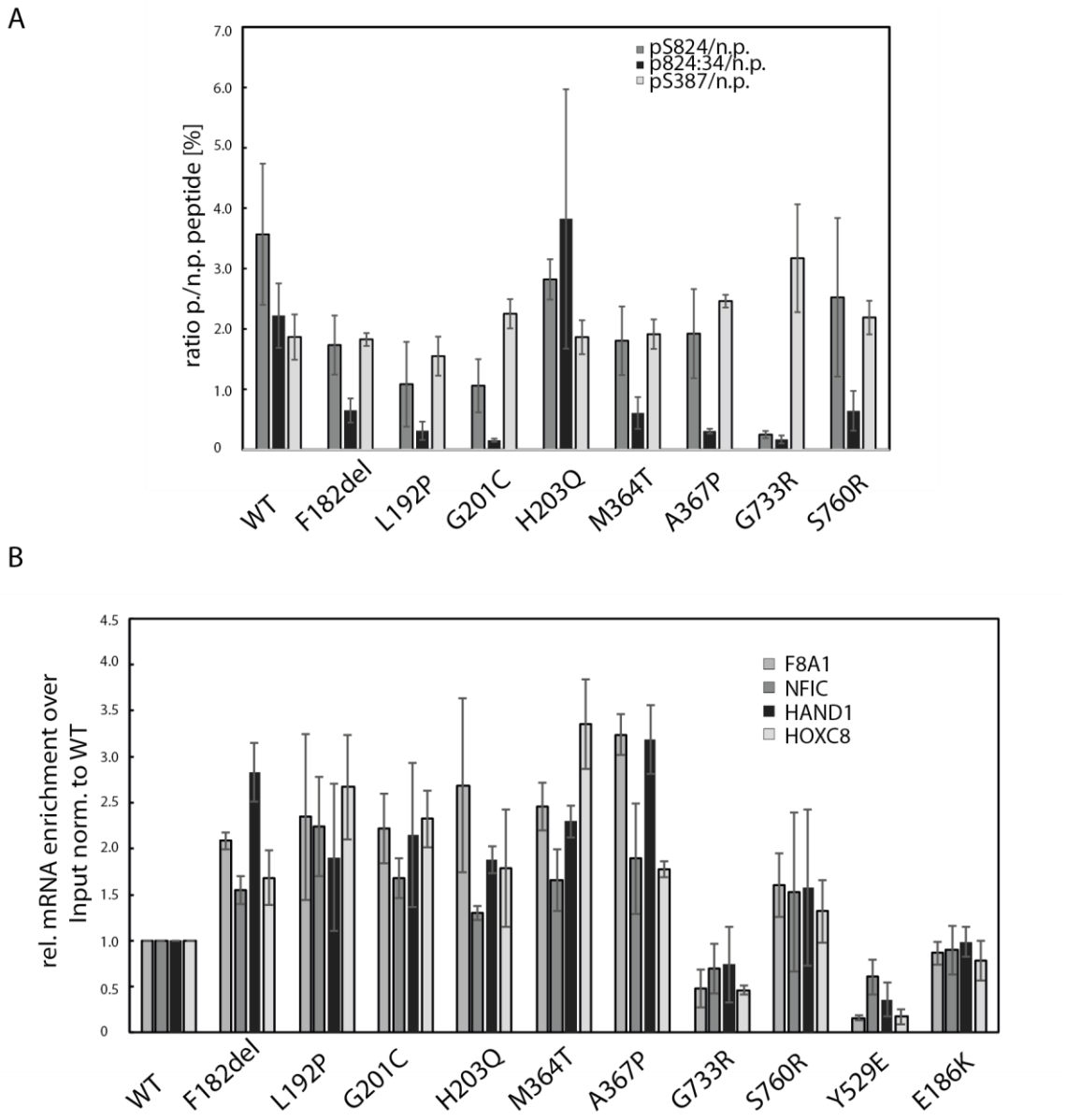

Figure 17 mRNA interaction of Ago2 disease related mutations. (A) Relative quantification of the phosphorylation level. After overexpression of Ago2 mutants in HEK 293T cells, phosphorylation of S387 (light grey bars), S824 (grey bars) and four times phosphorylated 824:34 (black bars) were measured and quantified via SRM. Phosphorylation of S387 serves as internal control. Measurements were performed in biological triplicates and calculated as mean (SEM). (B) RIP experiments were performed as described in Figure 10 A, cDNA was generated and analyzed by qRT-PCR. Different targets (NFIC, ST6GALNAC6, F8A1, HAND1) were analyzed upon binging to Ago2 mutants. GFP and Ago2 Y529E served as negative control. Relative enrichment over input was normalized to WT Ago2. Analysis was done in biological triplicates abs calculated as mean (SEM).

To validate this mRNA binding-hypothesis, RIP experiments were performed and analyzed using qRT-PCR. Therefore, Ago2 WT and mutants were overexpressed in HEK 293T cells, immunopurified with their FLAG-tag, extensively washed, RNA was isolated, and cDNA was generated. Using qRT-PCR, four targets were tested for binding to Ago2 mutants: F8A1, NFIC, HAND1 and HOXC8 (Figure 17 B). For negative control, Ago2 Y529E mutant was used. The enrichment of targets was calculated over input RNA and normalized to Ago2 WT binding. All

mutants showed more target enrichment over input in comparison to WT, except of Ago2 G733R. The enrichment of targets reached from 1.5- up to 3-fold compared to Ago2 WT. As a control, the Ago2 mutant E186K was used. This mutation can be found in normal people without any phenotype. In the qRT-PCR analysis, the Ago2 E186K mutant showed similar mRNA binding to Ago2 WT. Both, the enrichment of targets and hypo-phosphorylation of the 824:34 cluster strengthen the hypothesis that all Ago2 mutants related to the disease show stronger and/or longer interaction with targets, except of Ago2 G733R. This mutant showed weak binding to TNRC6 proteins, miRNA and mRNAs, did not localize in p-bodies. Moreover, it is not phosphorylated on the 824:34 cluster and had less cleavage activity. This mutant seems to be catalytically dead but nevertheless it results in the same neurodevelopmental disease as the other mutations.

3 Discussion

3.1 Endogenous phosphorylation sites of Ago proteins

In this work, a systematic and unbiased mass spectrometry analysis of endogenous Ago phosphorylation sites from different species was performed. Different purification strategies were used to isolate endogenous Ago proteins of human, mouse, rat, zebrafish and *C. elegans*. Subsequently, specific phosphorylation sites were functionally characterized by generating phosphor-lacking and phospho-mimicking mutants, followed by experimental analysis using a large panel of different approaches and assays.

3.1.1 Conservation and positioning of phosphorylation in Ago protein

Many of the measured phosphorylation sites are conserved between the four human Ago proteins. Furthermore, there are also phosphorylation sites, which are conserved in various species. The well-characterized phosphorylation at S387[132,135–137,139] is conserved in mouse and rat. To avoid technical artifacts, measurements were performed in triplicates and only overlapping phosphorylation sites were considered as 'real' phosphorylations (Figure 5 A). Two phosphorylated peptides containing multiple phosphorylatable residues appeared to be very conserved: the first phosphorylations were seen between T555 and S561. This area is located around the binding pocket of the target mRNA that is close to the first miRNA nucleotide (Figure 18 A). This nucleotide is tightly bound to the Ago MID domain and is not involved in the target interactions[73,165]. Here, only single phosphorylations were measured (Figure 6 B). The second phosphorylations, which appear in a cluster, are positioned between S824 to S834. These residues are located on an exposed and most likely flexible loop, which is not resolved in the human Ago2 crystal structure[71,73] (Figure 18 B). The end residues of this loop, which are resolved in the crystal structure, are E821 and G836. Nevertheless, this loop is resolved in the crystal structure of Ago protein QDE-2 protein of *Neurospora crassa*, where it is three residues shorter than in human Ago2[166] (Figure 18 C). However, an alignment with both structures reveals that the loop could potentially reach the bound mRNA:miRNA duplex due to this structural flexibility (Figure 18 C). Therefore, it is likely that the multiple cluster phosphorylations could affect RNA binding caused by repulsion of negative charges on the RNA backbone and the phosphorylated residues found in mass spectrometry. This cluster

contained five phosphorylatable residues and tryptic peptides found in mass spectrometric analysis were up to four times phosphorylated (Figure 6 C). The reason, why phosphorylations could not be measured in our mass spectrometric analysis might be due to technical issues, which are discussed in the following chapter. However, the 824:34 potential phosphorylation sites are conserved in dmAGO1, which is involved in miRNA-guided repression, but not in the dmAGO2, which carries out siRNA-mediated target silencing[164,167,168]. Thus, it is likely that these phosphorylations are only conserved in Ago proteins, which perform miRNA-mediated repression. It is tempting to speculate that cluster phosphorylation could even be a predictor of a miRNA-Ago protein in so far unknown species. All Ago proteins that are involved in miRNA-guided repression that we have examined so far, appear to utilize this mechanism for optimized target release.

3.1.1.1 Technical challenges

In general, phosphorylations are difficult to measure in mass spectrometry[169–171]. First, the ionization efficiency is poor. Second, phosphorylated peptides have a specific fragmentation behavior. This might be due to their negative charges, especially when the peptides are multiply phosphorylated[172]. Moreover, it can be very challenging to assign a phosphorylation to a specific amino acid in case the peptide contains more potentially phosphorylatable residues and the fragment ion spectra do not provide sufficient sequence information[173]. Additionally, redistributions of phosphates to other potentially phosphorylatable residues can happen in the gas phase. These events make the positioning of the phosphates to specific residues very difficult[174]. In many cases less than 5 % of a protein population is phosphorylated. Thus, it is very difficult to get enough endogenous protein material to reliably measure challenging or rare phosphorylation events. In addition, de-phosphorylation can occur during extract preparation. Therefore, it is necessary to include phosphatase-inhibitors while lysate preparation to block phosphatases. Furthermore, tryptic digestions are frequently not complete and this causes missed cleavages[175–177]. In consequence, some peptides are longer than the fully digested ones and can therefore not be included in relative quantification methods like SRM. In this method, heavy labeled peptides with a defined length, with or without phosphorylations, are spiked into the sample and are used for relative quantification[175–179].

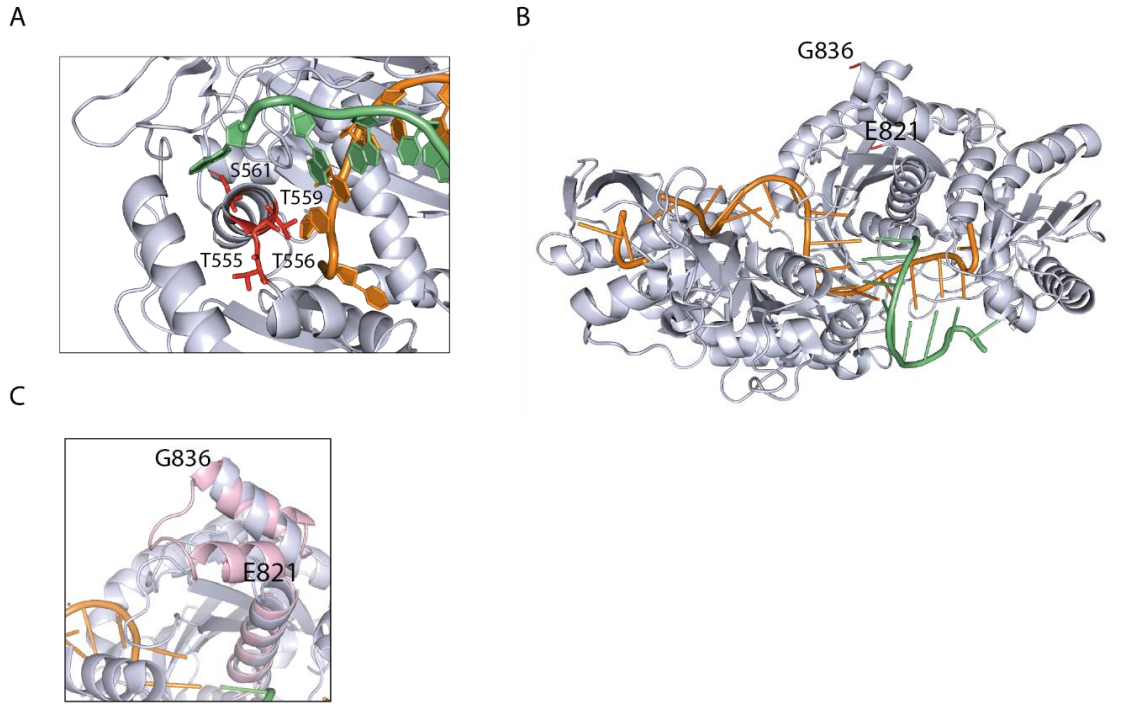

Figure 18 Localization of phosphorylation sites in Ago2. (A) Localization of the phosphorylation sites 555-561. These sites are shown in red, based on the model 4W5O[71]. (B) Position of the unresolved loop starting from E821 to G836. The miRNA is shown in orange, a part of the mRNA is indicated in green[71]. (C) Overlay of similar structures of *Neurospora crassa* Ago protein QDE-2 (pink), based on the model 2YHA[166] and human Ago2 (grey). The corresponding loop of human Ago2 is three residues longer than the loop of QDE-2.

3.1.1.2 Examples for biological functions of cluster phosphorylations

It is known that phosphorylations at serines or threonines tend to appear in clusters in eukaryotes[180]. Various clustered phosphorylations were found with several biological functions[181]. One example are the phosphorylation repeats of the C-terminal domain of RNA polymerase II. The phosphorylations are known to function as specific binding platforms and the pattern changes during transcription allowing for specific binding of different transcription and mRNA processing factors during distinct steps of the transcription cycle[182]. Another example of multiple phosphorylations is found in the Sic1 protein of *Saccharomyces cerevisiae*. This protein is a cyclin-dependent kinase inhibitor and it has been shown that multiple phosphorylation sites contribute to ubiquitination *in vitro* and degradation *in vivo*[183]. Furthermore, for an efficient substrate recognition by Cdc4, a component of the SCF E3 ubiquitin-protein ligase complex, Sic1 requires at least phosphorylations at six out of nine potential phosphorylated residues[184,185]. Cluster or multiple phosphorylations could be more general motifs or mechanisms for protein-protein interactions. Moreover, multiple phosphorylations can disturb membrane association or DNA/RNA binding due to repulsion

of negative charges[160,164,186,187]. Another example for multiple phosphorylated proteins are serine and arginine-rich (SR)-proteins. These proteins are RNA-binding proteins and known as constitutive and alternative splicing regulators. Phosphorylation is necessary for nuclear import of SR-proteins[188] or can allow the recruitment of these proteins from nuclear speckles to RNA during splicing[189]. Phosphorylations are also required for spliceosome assembly and the dynamic switch of the phosphorylation level of SR-proteins modulate splicing[190–193]. Ago proteins may also be regulated by a dynamic switch between hypo- and hyper-phosphorylated state.

3.1.2 Functional analysis of Ago2 cluster phosphorylations

To test the function of the phosphorylation cluster, the phosphorylated serines and threonines were mutated into alanine, a non-phosphorylatable mutant and into glutamate, which served as phospho-mimicking mutant because glutamate contributes a negative charge like those of phosphorylated side chains. Single and cluster mutants were generated and first tested on their function to repress targets when artificially tethered to the mRNA. Since all single, as well as 824:34A/E and 555:61A mutants could repress the target like WT, it is likely that the mutants are folded correctly (Figure 6 D). Additionally, these data also indicate a function of these phosphorylations upstream of deadenylation and translational repression, since downstream silencing is not affected when tethered. On the contrary, the target repression of 555:61E mutant is strongly impaired when tethered (Figure 6 D). Furthermore, this mutant does not localize in p-bodies, shows reduced binding of TNRC6 proteins, mRNA binding is negatively affected and also the cleavage activity is compromised (Figure 7). All this suggests a potentially incorrect folding of the 555:61E mutant. Since only single phosphorylations were measured in mass spectrometry originating from the 555:61 region and the single mutants were indistinguishable from Ago2 WT, we concluded that this region does not contain a simultaneously phosphorylation cluster and discontinued its further examination (Figure 6 B).

Our mass spectrometry data regarding the 824:34 cluster was different. Here, up to quadruple phosphorylations were measured on single peptides from this region (Figure 6 C). The cluster mutants, all five phosphorylatable residues on this peptide mutated into either A or E, were tested in various assays. Both mutants showed WT behavior in subcellular localization, miRNA and TNRC6 binding. In addition, cleavage activity was not affected by phosphorylations after 1.5 h of reaction time (Figure 8). This points towards a generally

functional catalytical activity of both mutants. Since cleavage assays may have reached a plateau after 1.5 h (end-point measurements) with a high excess of substrate, products may accumulate during reaction to similar amounts although mRNA affinities might be different. These difficulties can be overcome by kinetic measurements in a much shorter time window. Indeed, reduced cleavage activity at early time points of the 824:34E mutant were monitored compared to WT and 824:34A mutant (Figure 9). This might be due to lower target RNA affinity or higher off-rate of the phospho-mimicking mutant. To test direct mRNA binding, RNA-immunoprecipitations were performed and analyzed via micro array. The Ago2 Y529E mutant served as a negative control as its miRNA binding is impaired and therefore no mRNAs are bound to it[132]. In fact, a strongly reduced mRNA binding of this mutant was detected in comparison to Ago2 WT. In addition, an impaired mRNA binding could be detected with the 824:34E mutant, which mimics a hyper-phosphorylated state. However, the 824:34A mutant bound mRNAs similar to WT or even stronger (Figure 10 A). Consistently, also in qRT-PCR measurements, the 824:34E mutant demonstrate reduced target RNA binding (Figure 10 B). In living cells, the 824:34 phospho-mimicking mutant was not able to repress the reporter (Figure 10 C). The rather mild effects observed in Figure 10 C might be based on the rather low transfection efficiency.

For elucidation in which step of gene silencing phosphorylation at the loop between the residues E821 and G836 occurs, different mutants were used and analyzed regarding their phosphorylation at the 824:34 cluster. No cluster phosphorylation was detected in Ago2 mutant 620/694W, which is impaired in TNRC6 protein binding due to mutations in of the binding sites. That also indicates that only Ago, which can interact with TNRC6 proteins, is subsequently hyper-phosphorylated. In addition, reduced phosphorylation was measured in the Ago2 Y529E mutant, which cannot bind miRNAs[132], and 555:61E, which showed impaired mRNA binding. In contrast, WT and the 555:61A mutant, which is similar to WT in all utilized assays, contained single and quadruple phosphorylations at the 824:34 cluster (Figure 11 C, grey and black bars). All these quantifications were performed by quantitative mass spectrometry (SRM). Phosphorylation at position S387 served as control and did not differ in any mutants mentioned above, indicating that our results are not due to global phosphorylation artifacts (Figure 11 C, white bars). Notably, all mutants, which are trapped in different stages of gene silencing, showed impaired phosphorylations at the 824:34 cluster. In summary, this suggests that the Ago2 824:34 cluster is hyper-phosphorylated at later stages of small RNA-guided gene silencing. Probably, the phosphorylation event occurs during or for dissociation from silenced mRNPs or recycling steps. This model, however, needs to be validated in more detail.

3.1.3 Cluster phosphorylation is essential for ALG-1 function *in-vivo*

To assess the physiological relevance of the 824:34 cluster phosphorylation, Prof. Dr. Martin Simard (Quebec, Canada) and his group worked with *C. elegans* as model organism. Here, developmental processes and defects can be studied easily. Mutating just one residue, probably the most important residue in this cluster, had strong effects[160]. In summary, the S992 is a very important site in this cluster and its ability to get phosphorylated plays a big role in development.

3.1.4 Modifying enzymes acting on the Ago2 824:34 cluster

Phosphorylations are a general mechanism for regulating Ago protein function[55,132–139]. The key players of this kind of regulation are kinases and phosphatases, which place or remove phosphorylation marks. In the particular case of the Ago2 824:34 cluster phosphorylation, the Protein Phosphatase 6 (PP6) and the Casein Kinase 1 alpha 1 were identified to be involved in the modification of Ago2 824:34 cluster[164]. The relevance of PP6 in this process could also be verified in this work, especially its subunit ANKRD52. This phosphatase is a heterotrimeric complex consisting of a catalytic subunit PPP6C, a SAPS domain-containing subunit (PP6R1-3) and an ankyrin repeat-domain containing regulatory subunit (ANKRD28, 44, 52)[162,163]. In the model of Golden *et al.*[164], the PPP6C-ANKRD52 complex is necessary to dephosphorylate Ago to enable the association with new targets. Of note, PP6R1-3 were not found to be involved in this process although a CRISPR based genome-wide functional screen was performed. However, it is the current view that SAPS proteins serve as scaffolds for PPP6C and ANKRD proteins and are thus required for their function[162,163]. It remains still unknown, how PPP6C can assemble with ANKRD52 without SAPS proteins[194]. In the mass spectrometry analysis of Dr. Anne Frohn, SAPS3 or PP6R3, ANKRD28 and PPP6C could be detected as interacting partners of Ago2[161]. PP6 is ubiquitously expressed in mammalian tissues[195]. Depletion of PPP6C in mouse discovered its essential role in early embryogenesis[196,197]. An upregulated expression of PP6 could be detected in adipose tissues from insulin-resistant mouse models[198], inflammatory bowel disease[199] and various types of cancer[200–202]. In contrast, a downregulated expression of PP6 was observed in other types of cancer[203,204]. It is reported, that levels of PP6 can be controlled by miR-31 and miR-373 and this was linked to some types of cancer[201,204,205]. In human breast cancer, a decreased protein level of PP6, PP6R2 and PP6R3 could be detected. In addition, miR-373 was reported to act

as tumor-promoting miRNA in testicular germ cell tumors[206], esophageal squamous cell carcinoma[207], and hepatocellular carcinoma[204]. PP6 mRNA is a known target of miR-373, thus linking PP6 and hepatocellular carcinoma[204]. It would be very interesting, to measure phosphorylation of Ago in tumors and cancer models containing different levels of these factors. Additionally, the phosphorylation pattern of Ago should be detected after inhibition of miR-373, to see if there is a negative feedback loop between this special miRNA and Ago phosphorylation. Notably, an upregulation of AKNRD52 expression was found in lymphoid neoplasm diffuse large B-cell lymphoma, esophageal carcinoma, cholangio carcinoma, stomach adenocarcinoma and thymoma. A massive decrease in ANKRD52 expression was detected in uterine carcinosarcoma, uterine corpus endometrial carcinoma, thyroid carcinoma, ovarian serous cystadenocarcinoma, cervical squamous cell carcinoma and adrenocortical carcinoma, according to GEPIA database (www.gepia.cancer-pku.cn). In the Human Protein Atlas (www.proteinatlas.org), ANKRD52 was listed to be highly expressed in testis cancer, lung cancer and colorectal cancer. Dr. Hung Ho Xuan (postdoc in the department Biochemistry I, University of Regensburg) generated a mouse model for colorectal cancer in collaboration with Prof. Dr. Christina Hackl (University Hospital Regensburg)[208]. Here, the human colon cancer cell line HT29 was intrasplenically injected into female CB17 mice with an age of 6 weeks[208]. In future experiments, primary tumors and liver metastases will be used for characterization of the link between cancer, ANKRD52 upregulated expression and Ago phosphorylation at Ago2 824:34 cluster.

The kinase CSNK1A1 identified in Golden *et al.*[164] prefers previously phosphorylated substrates and recognizes the consensus sequence (pS/pT/E/D)-X_{1-2}-S/T, which is already mono-phosphorylated[209,210]. Multiple phosphorylations often need a first kinase to set the priming phosphorylation and secondary kinases, which recognize the priming phosphorylation and facilitate subsequent hyper-phosphorylation[211]. Therefore, the question, of the identity of the priming kinase remains unanswered. Our mass spectrometry data suggests that S828 is the most likely priming site. Mutating this site into A, only phosphorylated S824 was found. This indicates that CSNK1A1 most likely only modifies S831 and S834. So, three of five residues are probably phosphorylated by different kinases. Does the S824 also need an initial phosphorylated S828 or is this site phosphorylated separately? This question could be answered in future experiments, with the transfection of Ago2 S828A mutant in a CSNK1A1-deficient background, followed by detection of phosphorylation events. The site T830 is probably not phosphorylated by CSNK1A1, because Golden *et al.*[164] detected no phosphorylation in an *in vitro* kinase assay when mutating all other residues into A. Again, the question rises, which kinase is responsible for phosphorylation at T830?

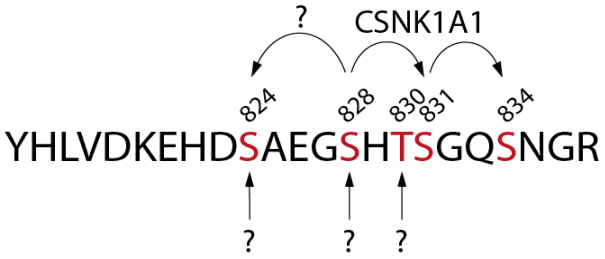

Figure 19 Peptide sequence of 824:34 cluster and summary of kinases. CSNK1A1 recognize previously phosphorylated S828 and phosphorylates S831 and subsequently S834. It is still unclear, which kinase is responsible for the phosphorylation of S824, S828 (priming site) and T830.

Taken together, Ago2 contains a highly flexible loop on the surface of the PIWI domain, which has the potential to reach the target RNA. This exposed loop is easily accessible for kinases and phosphatases and it was indeed found to be hyper-phosphorylated. The loop containing the 824:34 cluster of Ago probably becomes hyper-phosphorylated by CSNK1A1 after repression (Figure 20) but it is also likely that other so far unknown kinases are involved. Negative charges of the phosphates repel the negative charged sugar-phosphate backbone of the mRNA leading to dissociation from the mRNA target. After target release, Ago might be dephosphorylated by the PP6 complex (Figure 20). These findings open many exciting questions: For example, is hyper-phosphorylation of Ago proteins a general mechanism for target release and subsequent target degradation? Do certain RNA binding proteins recruit target-specific kinases or phosphatases upon specific stimuli? Is the Ago2-phosphorylation state of the 824:34 cluster a mechanism to regulate distinct targets that need to be essentially expressed at specific timepoints in development? Will Ago be recycled once it is dephosphorylated and enter another repression round or will it be degraded? Answering these questions will be exciting future research directions in developmental, physiological and pathophysiological contexts.

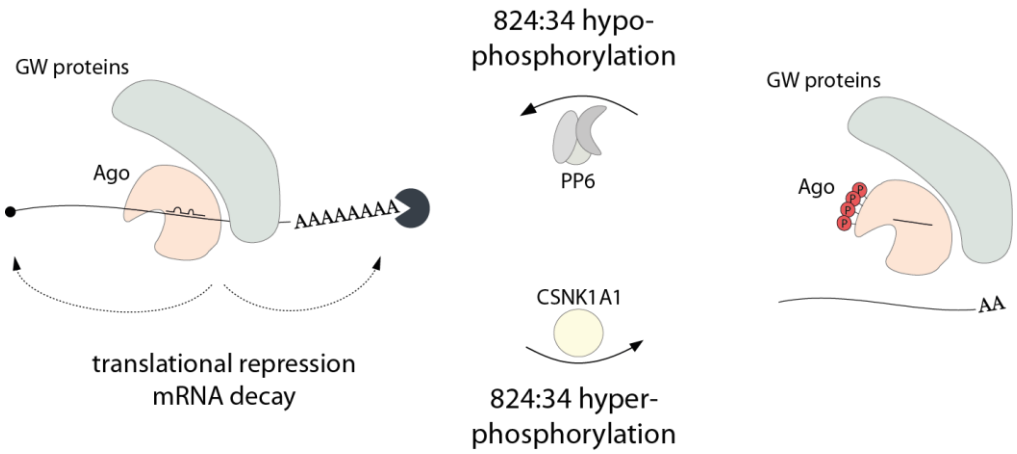

Figure 20 Mechanistic model how Ago phosphorylation might be involved in miRNA-guided gene silencing. Ago is guided by miRNA to target RNA, GW182 proteins are recruited and translational repression and mRNA decay are initiated. After repression, Ago gets hyper-phosphorylated by CSNK1A1 and probably other kinases. Negative charges of the phosphates repel the mRNA and the target is released. After dephosphorylation by PP6, Ago might be recycled and guided to a new mRNA. The other possibility is that Ago is degraded and that phosphorylation functions as a decay signal.

3.1.5 Phosphorylation of Ago proteins – outlook

In this work, several phosphorylation sites on Ago proteins were identified by mass spectrometry. Besides the Ago cluster phosphorylations, it would be very interesting to characterize the remaining phosphorylation sites. This would provide new information about association with binding partners, like Dicer or TNRC6 proteins, cellular localization, binding of RNAs and general stepwise regulation.

To better understand the relevance of Ago-mediated gene silencing, it is necessary to analyze its interaction network. Identifying kinases and phosphatases, which are involved in the de-/phosphorylation events on Ago proteins is challenging, since e.g. kinase motif predictions are often ambiguous. Future approaches for the identification of kinases and phosphatases, which are involved in miRNA-guided gene silencing, could be for example microscope-based screenings. Here, a stable cell line expressing TNRC6A fused to GFP could be used in combination with red-labeled DNA oligonucleotides, which are perfect complementary to abundant mRNAs in the cells. When complexes composed of Ago, miRNA, mRNA and TNRC6 form, combined colors will result in yellow spots. The idea is to use a siRNA library against kinases and phosphatases to knock down specific enzymes and to investigate, if the yellow spots disappear and red and green individual spots are detectable. This hints towards kinases

or phosphatases that are involved in the assembly or dissociation of miRNA-guided gene silencing complexes. These assays are currently established in the lab but are beyond the scope of this PhD thesis.

For the identified phosphorylation sites, not only kinases and phosphatases are mainly unknown but also their impact on cellular signaling pathways remain elusive. It is published that phosphorylation of Ago2 at S387 is induced by cellular stress acting through the p38 MAPK pathway[135]. CSNK1A1 participates in Wnt signaling and functions in a complex with Glycogen synthase kinase-3 (GSK3)[212,213]. The known phosphatase of Ago2 cluster PP6 is also a component of a signaling pathway regulating cell cycle progression in response to IL2 receptor stimulation[214]. Additionally, PP6 downregulates Mitogen-activated protein kinase kinase kinase 7 (MAP3K7/TAK1) activation of the IL1 signaling pathway by de-phosphorylation of TAK1[215]. Identifying and validating one or even more signaling pathways, Ago phosphorylation plays a role in, might be challenging but opens interesting future research directions. Furthermore, disease and cancer relation to Ago phosphorylations will be exciting research topics. For example, Shankar *et al.* published a connection between Ago2 Y393 phosphorylation and EGFR-KRAS signaling in pancreatic cancer development[216].

3.2 Ago2 mutations and the relation to neurodevelopmental disease

Ago proteins are very important actors in the miRNA-guided gene silencing pathway. In difference to other proteins of the AGO family, Ago2 is essential for murine embryonic development. Knocking out Ago2 was lethal in every case[217,218]. Homozygous Ago2 catalytical mutant mice died directly after birth[219]. It is published that mis-regulated Ago expression levels can cause various diseases, like Huntington's disease[152] or cancer[143,144,146,148,149]. These findings emphasize the importance of intact Ago2, especially in embryonic development.

In collaboration with Prof. Dr. Kreienkamp and Dr. Lessel (University Medical Center Hamburg-Eppendorf, Hamburg), genome sequencing of various children was performed. These children suffer from the same neurodevelopmental disorders: they show mental retardation and learn to talk and walk in a late stage. The sequencing resulted in the finding that only unexpected point mutations or deletion at different residues of only Ago2 are present in these children. Even more astonishing, these point mutations/deletion are heterozygous, i.e. an intact WT allele is still present in the genome.

3.2.1 Functional analysis of Ago2 mutants

Interestingly, all individual point/deletion mutants resulted in the same phenotype. Therefore, we asked the question what the mutations have in common to generate the same phenotype.

In vitro analysis revealed that almost all mutants showed WT behavior in protein-protein interactions with Dicer and TNRC6 (Figure 15 B, C). Additionally, miRNA binding (Figure 15 C), repression of a reporter mRNA (Figure 15 E), cleavage activity (Figure 15 D) and cellular localization was indistinguishable from WT Ago2 (Figure 16). However, one mutant, the G733R, failed in every assay and seemed to be catalytically dead. The arginine, which replaced the small glycine, probably disrupts the structure in a way that the protein loses its activity.

Since we found that 824:34 cluster phosphorylation is important for the regulation of target mRNA binding, the phosphorylation of the 824:34 cluster was measured, relatively quantified and compared to WT Ago2 (Figure 17 A). All mutants showed reduced quadruple phosphorylated peptides of the 824:34 cluster. In contrast, the phosphorylation of S387 was at similar levels to WT. This excludes the possibility of poor-quality mass spectrometric measurements and serves as internal standard. According to the hypothesis in chapter 3.1.4,

hyper-phosphorylation of the 824:34 cluster leads to target release because of the repulsion of negative charges. Thus, all mutants might be impaired in dissociation from their mRNA target (Figure 17 A). Only the mutant H203Q gave a higher ratio of quadruple phosphorylated to non-phosphorylated peptide but with a large error bar. This indicates that the measurements differ a lot and the mass spectrometry analysis should be repeated with this mutant to get a reliable result.

For validation of the mRNA binding model, RIP experiments were performed and analyzed via qRT-PCR (Figure 17 B). All mutants showed higher target enrichment in comparison to WT Ago2, except for the G733R mutant, which is the most likely structurally affected as discussed above. For control, the Ago2 mutant E186K was used. This mutation was found in people with no obvious abnormal phenotype. In qRT-PCR experiments, this mutant showed mRNA binding like WT as expected. The higher target RNA enrichment of the other mutants corresponds to the hypo-phosphorylation state of the mutants. Because, if they are not hyper-phosphorylated, the mRNA is bound longer or tighter to the Ago protein. The mRNA release is probably hindered, which would result in a lower off rate or a higher affinity to mRNAs. This "slowdown of the system" may result in impaired development and the observed neurodevelopmental disorders.

3.2.2 Structural localization of phenotypic Ago2 mutations

The first cluster of mutations (F182del, L192P, G201C/V, H203Q) is placed in the linker 1, the next set (M364T, A367P) in linker 2 region and the last set of mutations (G733R, C751Y, S760R) in the PIWI domain (Figure 15 A). Looking into the human Ago2 crystal structure revealed that all mutations cluster around the α-helix-7. Two of the mutated amino acids, the M364 and A367, are directly located on that helix. Additionally, all mutations are close to the bound miRNA:mRNA hybrid (Figure 21).

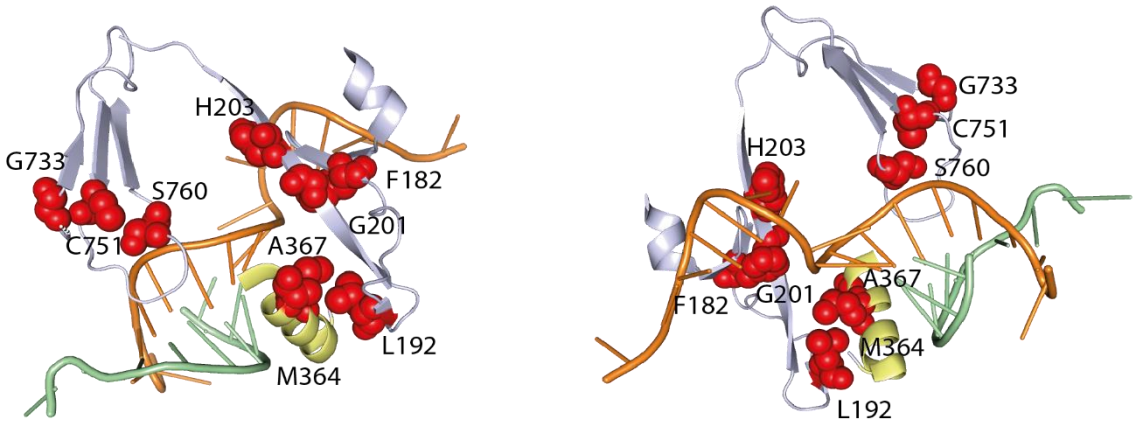

Figure 21 Positioning of patient mutations in the crystal structure of human Ago2 with miRNA/mRNA. Mutations found in patients are shown in red. Parts of Ago2 are indicated in grey and the helix-7 is shown in yellow, based on the model 4W5O[71]. The miRNA is shown in orange, parts of the mRNA are indicated in green.

Klum *et al*. identified Ago2 α-helix-7 as a structural element that is required for speed and fidelity in binding target RNAs[220]. They used biochemical, structural and single-molecule data to show that helix-7 acts as a molecular quality manager or catalyst for seed pairing of miRNA:mRNA. They hypothesize that helix-7 enables target pairing with the positions g6 and g7, which are base numbers of the guide RNA[220]. It is also suggested that the 5' domain (g2-5) of the seed is held by Ago2 in an A-form like conformation[73]. The 3' end of the seed (g6-8) is able to move between different conformations. This movement is controlled by helix-7, which raises the rates of mRNA pairing and un-pairing[220]. Helix-7 stably docks into the minor groove of the miRNA:mRNA duplex and is therefore able to break target binding[220]. When mutating the residues M364 and I365 to A, which are located on helix-7, the affinity of Ago2 to miRNAs was not affected[220]. In contrast, they observed a higher dwell time on off-targets with the mutated helix-7. They conclude that helix-7 also allows Ago2 to efficiently distinguish between targets and off-targets[220]. Interestingly, in this publication, M364 was mutated into A and showed a strong effect in mRNA binding. They also modeled the mutated helix-7 and it shifts backwards, away from the guide RNA[220]. Off-targets and on-targets have a slower off rate and probably block Ago2 for the next round of silencing.

In one patient, a mutation of the same amino acid, M364 to T, was identified and is responsible for the phenotype since helix-7 is not able to function properly. Additionally, the position A367 was mutated into P in another patient. This residue is also located directly on the helix-7. Proline is known to be a helix breaker, which may by the reason why helix-7 cannot be as functional as in a WT Ago2 protein. The mutations F182del, L192P, G201C/V and H203Q are located around helix-7 and close to the miRNA:mRNA duplex. In addition, these mutations

might influence target binding and therefore might be the reason for a changed binding pattern, which may result in a neurodevelopmental disease. Park *et al*. hypothesized that the N-terminal domain is involved in unwinding of the miRNA duplex[221]. When mutating F181 into A, the pre-RISC could be formed successfully but its unwinding activity was much slower than WT Ago2[221]. The deletion of the neighboring phenylalanine F182 in patients might have the same effect. If the unwinding of the miRNA duplex were slower, this mutant would also not be accessible for mRNA at the time of bound miRNA duplex. It also would not be able to form a repressive complex in the period in which unwinding is not completed. The human Ago2 crystal structure displayed that aliphatic segments of the residues R795, I756 and Q757, which are located in the PIWI domain, and the residues I365 and T361 on helix-7 line the minor groove of the guide:target duplex[73]. These sites are making large hydrophobic and van der Waals interactions with the positions 2 to 7 of the miRNA:mRNA duplex[73] (Figure 22). In patients, mutations of the residues G733, C751 and S760 were observed. Replacing these small residues into large amino acids like R or Y might lead to an internal shift of the protein, which might affect the interaction between the residues R795, I756 and Q757 with the minor groove of the RNA duplex and thus the correct target RNA binding.

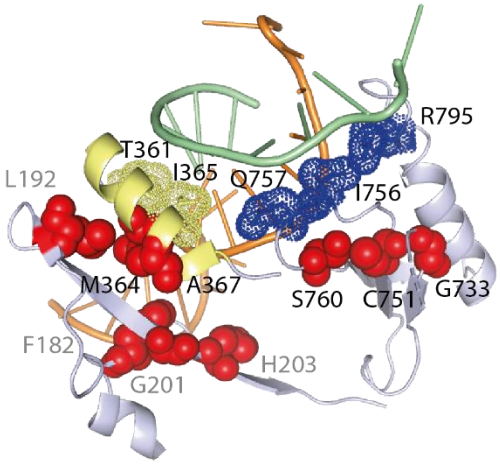

Figure 22 Positioning of patient mutations in relation residues interacting with the minor groove of guide:target duplex. Parts of the crystal structure of Ago2 are shown in grey, based on the model 4W5O[71]. Patient mutations are indicated in red, miRNA in orange and parts of the mRNA in green. The blue dotted residues I756, Q757 and R795 interact with the minor groove of the guide:target duplex. Yellow marks helix-7 and the yellow dotted residues also line the minor groove.

3.2.3 Summary and outlook

In summary, the commonality of all mutations, which were found in patients with the same phenotype, is their localization around the guide:target duplex. These mutants affect the target binding in a way that either off- and on-targets are bound stronger/longer to the miRNA-Ago2 protein complex or the miRNA duplex unwinding is slower during loading of miRNAs into Ago2. Another reason might be that the helix-7 cannot function as a quality manager with the mutations, uncovering off-target mRNAs. In conclusion, all mutants are unable to bind or release the targets or off-targets in a correct way. This would indicate that a part of the real miRNA targets could only be repressed in a reduced fashion, because the defect Ago2 is blocked by off-targets or the prolonged repression of on-targets gives the phenotype. Of note, the Ago2 G733R mutant seems to be catalytically dead but results in the same neurodevelopmental phenotype, whereas all other mutants showed WT behavior in most of the functional analyses. This does not fit completely in the model and the link to the other mutations remains still not fully clear. It should also be checked again, if G733R is the only mutation in this patient.

Of note, two mutations, G201V and C751Y, were identified at a later stage and could not be included in this work. These mutations should be characterized in functional assays, especially on phosphorylation of the 824:34 cluster and mRNA binding. In addition, the F182 deletion mutant should be analyzed upon its ability to unwind the miRNA duplex.

Another important point is the heterozygous occurrence of the mutations. This means that an intact Ago2 is present besides the mutated version. In consequence, two fully functional Ago2 alleles are necessary for a correct neurological development in humans. It would be very interesting to generate mutant mice and look for similar phenotypes. The mouse models might reveal new insights in neurological developmental delay and its relation to Ago2 mutations.

4 Material and Methods

4.1 Consumables and chemicals

All used chemicals were obtained from Sigma-Aldrich (St. Louis, USA), Merck (Whitehouse Station, USA), Roth (Karlsruhe, Germany), AppliChem GmbH (Darmstadt, Germany) and Thermo Fisher Scientific (Waltham, USA). They were ordered at the highest degree of purity.

Radiochemicals were purchased from Hartmann Analytic GmbH (Braunschweig, Germany). Oligonucleotides were synthesized by Metabion GmbH (Planegg, Germany) and cell culture reagents were obtained from Sigma-Aldrich (St. Louis, USA). Frequently used enzymes, nucleotides, and molecular weight markers were purchased from Thermo Fisher Scientific (Waltham, USA).

4.2 Buffers and solutions

name	**contents**
2 ×HEPES-buffered saline	274 mM NaCl, 1.5 mM Na_2HPO_4, 54.6 mM HEPES (pH 7.1)
NET buffer	50 mM Tris/HCl pH 7.5, 150 mM NaCl, 5 mM EDTA, 0.5 % NP-40,
	10 % Glycerol, 1 mM NaF, 0.5 mM DTT, 1 mM AEBSF
NET washing buffer	NET buffer with 300 mM NaCl
RIPA buffer	50 mM Tris/HCl, pH 7.5, 150 mM NaCl, 0.1 % SDS, 1 % sodium deoxycholate,1 % NP-40, 1 mM NaF, 0.5 mM DTT, 1 mM AEBSF
5 × SDS sample buffer (Lämmli)	300 mMTris/HCl pH 6.8, 10 % SDS, 62.5 % glycerol, 0.05 % bromophenol blue,
	10 % β-mercaptoethanol
SDS-Running buffer	25 mM Tris, 192 mM glycine, 1 % SDS
Towbin Blotting Buffer	25 mM Tris, 192 mM glycine, 20 % methanol (pH 8.6)
TBS-T	10 mM Tris, 150 mM NaCl, 0.1 % Tween (pH 8)
2 × RNA sample buffer	bromophenol blue and xylene cyanol in formamide

10 × TBE	890 mM Tris, 890 mM boric acid, 20 mM EDTA
20 × SSC	3 M NaCl, 0.3M trisodium citrate (pH 7)
50 × Denhardt's solution	1 % Bovine serum albumin fraction V, 1 % Polyvinylpyrrolidon K30, 1 % Ficoll 400
Hybridization solution	1 × SSC, 20 mM Na_2HPO_4 pH 7.2, 7 % SDS, 1 × Denhardt's solution
Wash buffer I	5 × SSC, 1 % SDS
Wash buffer II	1 × SSC, 1 % SDS
10 × GT buffer	400 mM Tris pH 8, 60 mM MgCl2, 150 mM DTT, 20 mM spermidine
carrier RNA solution	25 µM sodium citrate pH 5.0, 7.5 M urea, 1 mM EDTA, 0.1 µg/µl yeast tRNA (Ambion), 0.05 % bromophenol blue, 0.05 % xylene cyanol
RNase T1 dilution	25 µM sodium citrate pH 5.0, 7.5 M urea, 1 mM EDTA, 5 U/µl RNase T1 (Fermentas),0.05 % bromophenol blue, 0.05 % xylene cyanol
Renilla Luciferase buffer pH 5.0	2.2 mM Na_2EDTA, 0.22 M K_xPO_4 pH 5.1, 0.44 mg/ml BSA, 1.1 M NaCl, 1.3 mM NaN_3
Firefly Luciferase buffer	470 µM D-luciferine, 530 µM ATP, 270 µM coenzyme A, 20 mM tricine, 5.34 mM magnesium sulfate heptahydrate, 0.1 mM EDTA
3 × Translation Mix	200 mM KCl, 20 mM $MgCl_2$, 25 mM DTT, 5 mM ATP, 1 mM GTP, 0.5 U/µl RiboLock RNase Inhibitor
Coomassie Staining	10 % acetic acid, 30 % ethanol, 0.25 % Coomassie R250
Coomassie Destaining	10 % acetic acid, 20 % ethanol

Table 1 Buffers and solutions

4.3 Bacterial strain and cell lines

The bacterial strain XL1-blue was used in this work. (Genotype: *F- recA1 enA1 gyrA96 thi-1 hsdR17 supE44 relA1 lac F'[proAB lacI^{q}ZΔM15 Tn10 (Tet^R)]*)

The cell lines are listed in Table 2.

cell line	specification
HEK 293T	human embryonic kidney cells
HeLa	human cervical cancer cells
H32	rat hypothalamic cells
MEF Ago2$^{-/-}$	mouse embryonic fibroblast cells, Ago2 knock out (k.o.)

Table 2 cell lines

4.4 Vectors, constructs and oligonucleotides

4.4.1 Vectors

Used vectors are listed in Table 3.

vector name	resistance	tag	applications
VP5	Amp	N-terminal HA- and FLAG-tag	eukaryotic expression vector
pCIneo NHA	Amp	λ-phage N-peptide followed by HA-tag	mammalian expression vector tethering assays
pCIneo HA		HA-tag	mammalian expression vector tethering assays

Table 3 Vectors

4.4.2 Constructs

FLAG/HA-tagged GFP and human Ago2 were described before[77]. Ago2 824:34A/E and 555:61A/E mutants were generated by 3-way blunt end ligation (Dr. Judith Hauptmann, University of Regensburg)[154]. To obtain the Ago2 mutants, 'Quik-Change' PCR strategy (site-directed mutagenesis) was used. For tethering assays, the constructs were cloned into the mammalian expression vector pCIneo via *Not*I/*Eco*RI.

4.4.3 Oligonucleotides

All used oligonucleotides were diluted in water to a concentration of 10 µM (primers) or 20 µM (probes) and stored at -20°C. The oligonucleotides used for cloning are listed inTable 4, others are listed in Table 5.

construct name	orientation	primer sequence (5'→3')
Ago2 F182del_2	fwd	GCCGCTCCTTCACCGCGTCCGAAGGCTGCTCTAA
Ago2 F182del_2	rev	TTAGAGCAGCCTTCGGACGCGGTGAAGGAGCGGC
Ago2 E186K	fwd	CTTCACCGCGTCCAAAGGCTGCTCTAAC
Ago2 E186K	rev	GTTAGAGCAGCCTTTGGACGCGGTGAAG
Ago2 L192P	fwd	GAAGGCTGCTCTAACCCTCCTGGCGGGGGCCGAGAAGTG
Ago2 L192P	rev	CACTTCTCGGCCCCCGCCAGGAGGGTTAGAGCAGCCTTC
Ago2 G201C	fwd	CGAGAAGTGTGGTTTTGCTTCCATCAGTCCG
Ago2 G201C	rev	CGGACTGATGGAAGCAAAACCACACTTCTCG
Ago2 H203Q	fwd	GGTTTGGCTTCCAGCAGTCCGTCCGGC
Ago2 H203Q	rev	GCCGGACGGACTGCTGGAAGCCAAACC
Ago2 M364T	fwd	CAGACCTCAACCACGATCAGAGCGACTG
Ago2 M364T	rev	CAGTCGCTCTGATCGTGGTTGAGGTCTG
Ago2 A367P	fwd	CAACCATGATCAGACCGACTGCTAGGTCG
Ago2 A367P	rev	CGACCTAGCAGTCGGTCTGATCATGGTTG
Ago2 A620W	fwd	GCAGCATGGACTGGCACCCCAATCGCTACT
Ago2 A620W	rev	AGTAGCGATTGGGGTGCCAGTCCATGCTGC
Ago2 L694W	fwd	GCCTGTATCAAGTGGGAAAAAGACTAC
Ago2 L694W	rev	GTAGTCTTTTTCCCACTTGATACAGGC
Ago2 G733R	fwd	GAAACATTCCAGCACGCACGACTGTGGAC
Ago2 G733R	rev	GTCCACAGTCGTGCGTGCTGGAATGTTTC
Ago2 S760R	fwd	CATCCAGGGGACACGCAGGCCTTCGC
Ago2 S760R	rev	GCGAAGGCCTGCGTGTCCCCTGGATG

Table 4 Oligonucleotides for cloning

oligonucleotide	orientation	sequence (5'→3')
Probes for Northern Blotting		
miR-19b	fwd	TCAGTTTTGCATGGATTTGCACA
miR-21	fwd	TCAACATCAGTCTGATAAGCTA
let-7a	fwd	AACTATACAACCTACTACCTCA
Sequencing primers		
T7	fwd	TAATACGACTCACTATAGGG
M13	fwd	TGTAAAACGACGGCCAGT
M13	rev	CAGGAAACAGCTATGACCATG
pCIneo Seq	rev	TGCATTCTAGTTGTGGTTTG
pCIneo fwd	fwd	GCGTTTCTGATAGGCACCTATTG
Ago2 seq1	fwd	GGCACAGCCAGTAATCGAGT
Ago2 seq2	fwd	CGGAAGTCCATCTGAAGTCCT

Table 5 Oligonucleotides for Northern Blotting and sequencing

4.5 Antibodies

antibody	origin	application	dilution	supplier
antibodies against endogenous proteins				
α-Ago2, clone 11A9	rat	WB, IP	1:5	Dr. E. Kremmer/Dr. Regina Feederle, Helmholtz Zentrum München
α-TNRC6A-C, clone 7A9	rat	WB, IP	1:5	
antibody against tags				
α-HA, clone 16B12	mouse	WB	1:1000	Covance Research Products
secondary antibody				
α rat IRDye® 800CW	goat	WB	1:10000	LI-COR Bioscience
α mouse IRDye® 800CW	goat	WB	1:15000	LI-COR Bioscience
Alexa Fluor 488	mouse	IF	1:400	Thermo Fisher Scientific
Alexa Fluor 555	chicken	IF	1:400	Thermo Fisher Scientific

Table 6 primary and secondary antibodies. WB: Western Blot, IP: immunoprecipitation, IF: immunofluorescence

4.6 Technical Equipment

For imaging of Western Blots Odyssey Infrared Imaging System (LI-COR Biosciences, Lincoln, USA) was used. The supplier of Personal Molecular Imager™ (Phosphorimager) is Bio-Rad Laboratories (Hercules, USA).

4.7 Producing DNA constructs

4.7.1 Polymerase chain reaction (PCR)

All mutants in this thesis were generated by site-directed mutagenesis ('Quik Change'). This PCR method uses mutagenic primers to change or delete single/several amino acids. After amplification, the template DNA was removed by *Dpn*I digestion. The components and conditions of the PCR reaction are listed below.

PCR Mix 50 µl		**Cycling Conditions**		
50 ng	template DNA	Initial denaturation	98°C	30 s
1×	HF buffer	Denaturation	98°C	10 s
0.2 mM	dNTPs	Annealing	55°C	30 s
0.2 µM	reverse primers	Elongation	72°C	1 min/kb
0.2 µM	forward primers	Terminal elongation	72°C	10 min
1 U	Phusion DNA Polymerase			
				18 cycles

After the PCR reaction and *Dpn*I digestion, the products were purified by NucleoSpin® Gel and PCR Clean-up kit (MACHEREY-NAGEL GmbH). For preparative digestion, FastDigest restriction enzymes (Thermo Fisher Scientific) were added to the whole PCR reaction and incubated at 37°C for 3-6 h. Afterwards, the DNA was separated on a 1 % agarose gel and purified by the kit named above.

Ligation were performed with 50 ng of the cut vector and 4× molar excess of the restricted insert, 0.1 U/µl T4 Ligase (Thermo Fisher Scientific), appropriate buffers and PEG 4000. The reaction was incubated for 1 h at 23°C, followed by transformation.

4.7.2 Transformation of *Escherichia coli* (*E. coli*) with plasmids

After defrosting chemically competent *E. coli* cells (*XL1-Blue*), approximately 0.5 µg plasmid DNA was added and were incubated for 20 min on ice. Afterwards, the cells were incubated at 42°C for 1 min, followed by a cooling step on ice. An additional incubation step in antibiotic-free LB-medium at 37°C is not necessary, because Ampicillin, as a beta-lactam antibiotic, inhibits the cell-wall synthesis of bacteria. At the end, they were plated on LB-Amp plates and incubated over night at 37°C. For retransformations, 30 µl were plated containing LB medium and Ampicillin.

4.7.3 Preparation of plasmid DNA from *E. coli*

A 5 ml overnight culture was centrifuged at 15,000 g and the DNA was purified with the NucleoSpin® Plasmid Kit of MACHEREY-NAGEL GmbH according to the manufacturer's protocol. Plasmid DNA was eluted with 50 µl dH_2O. For fast DNA extraction, 2 ml of the overnight culture were pelleted and resuspended in 40 µl EasyPrep Buffer. The samples were incubated at 99°C for 1 min, followed by a 15 min centrifugation at 15,000 g. For restriction analysis, 5 µl of the supernatant were digested with 0.1 µl FastDigest enzyme(s) (Thermo Fisher Scientific) in a total volume of 10 µl.

The plasmid DNA was sequenced by Macrogen (Amsterdam, The Netherlands) with the sequencing primers listed in Table 5.

4.8 Protein-based methods

4.8.1 Cell culture

Human cells (HEK 293T, HeLa) were cultivated under standard conditions (37°C, 5 % CO_2) using Dulbecco's modified Eagle's medium (DMEM, Sigma-Aldrich) including 10 % FBS (Sigma-Aldrich) and 1 % Penicillin/Streptomycin (Sigma-Aldrich).

4.8.1.1 Transfection by calcium phosphate

HEK 293T cells were transfected using calcium phosphate. 5-10 µg DNA and 123 µl 2 M $CaCl_2$ were filled up to 1 ml with water in one reaction tube. This mixture was added to a second tube containing 1 ml 2 × HEPES buffered saline while shaking. After 10 min incubation, the whole 2 ml solution was added to the cells with about 30 % confluency on a 15 cm plate. The cells were harvested after 48 h.

4.8.1.2 Transfection by Lipofectamin 2000

HeLa or MEF Ago2 $^{-/-}$ cells were transfected with Lipofectamin 2000 (Thermo Fisher Scientific) and Optimem according to the manufacturer's protocol. Here, a reverse transfection was used. For tethering assay, 300 ng λ-NHA/HA-constructs, 120 ng Renilla-5BoxB luciferase and 80 ng Firefly luciferase were filled up to 25 µl with Optimem per well of an 48 well-plate. In a second reaction, 1 µl Lipofectamin 2000 was mixed with 24 µl Optimem. After adding the DNA solution to the Lipofectamin 2000 solution, it was incubated for 10 min and applied to the medium. The cells were then split on the 48 well-plate onto medium supplemented with the Lipofectamin-DNA mix. For luciferase reporter assays, 400 ng of VP5-Ago2 constructs and 125 ng of the plasmid encoding for Firefly luciferase mRNA under control of HMGA2 3' UTR and the mRNA of a Renilla luciferase as transfection control were cotransfected. For Immunofluorescence (IF), cells were transfected with 300 ng VP5-Ago2 constructs.

4.8.1.3 Transfection by Lipofectamin RNAiMAX

For knockdown experiments with a subsequent mass spectrometry analysis, Lipofectamin RNAiMAX (Thermo Fisher Scientific) was mixed with 16 µl of 10 µM siPool (siTools, Munich) in Optimem, according to the manufacturer's protocol. The mixture was supplemented to the cell culture media and HEK 293T cells were seeded on 10 cm plates to a confluency of about 60-80 %. After 24 h, cells were transferred to 15 cm plates, followed by splitting on three 15 cm plates 48 h after transfection. Finally, the cells were harvested 72 h after transfection.

4.8.2 Lysate preparation from harvested cells

For harvesting cells, the medium was completely removed and the cells were washed with cold PBS once. To scrape the cells off the plate, a rubber policeman was used and the cell suspension was transferred into a 1.5 ml reaction tube. After 10 min centrifugation at 200 g, the supernatant was removed and the cells were lysed in 1 ml NET lysis buffer, respectively. Generally, an incubation time of 20 min on ice and a centrifugation step for 20 min at 15,000 g were applied.

4.8.3 Immunoprecipitation (IP)

For immunoprecipitation of endogenous proteins, monoclonal antibodies were coupled to Protein G Sepharose (GE Healthcare). Therefore, 30-100 µl beads were washed with cold PBS twice and incubated with 1-5 ml hybridoma supernatant overnight. The beads were washed with cold PBS twice to remove unbound antibody. Thereafter, the lysate was added to the beads and incubated for 2 h at 4°C. For an IP of TNRC6, an only 1.5 h rotation step is necessary. For immunoprecipitation of overexpressed FLAG/HA-tagged proteins, anti-FLAG M2 affinity agarose gel (Sigma-Aldrich) was used and washed twice with cold PBS before incubation with lysate. After incubation, the beads with bound proteins were centrifuged for 1 min at 1000 g and the supernatant was removed. The affinity matrix was washed with lysis buffer three times, followed by washing with PBS once. In the last washing step, a new reaction tube was used to minimize the contamination by protein bound to the reaction tube surface. Finally the beads were eluted by addition of an appropriated amount of 2.5 × Laemmli sample buffer.

4.8.4 SDS-PAGE, Western Blot and Coomassie staining

After elution, half of the volume was loaded on 10 % SDS polyacrylamide gels. The gels were run at 180 V.

Stacking gel	125 mM Tris/HCl pH 6.8, 0.1 % SDS, 0.15 % TEMED, 5 % Acrylamide/Bis solution (37.5:1), 0.05 % APS
Resolving gel	380 mM Tris/HCl PH 8.8, 0.1 % SDS, 0.1 % TEMED, 6–10 % Acrylamide/Bis solution (37.5:1), 0.05 % APS

For Western Blot analysis, a stack of three Whatman papers and a Hybond ECL membrane (GE Healthcare), matching the size of the gel, were soaked with 1 ×Towbin Blotting Buffer and placed on the positive electrode. The SDS gel was put above, followed by three soaked Whatman papers. The semi dry Western Blot was run at 10 V for 1.5 h. For bigger proteins, wet blot was used and run for 16 h at 30 V and 4°C. After blotting, the membrane was blocked in 5 % milk in 1x TBS-T for 1 h. The primary antibody was incubated also for at least 1 h at room temperature (RT), if possible overnight at 4°C in blocking solution. To remove unbound antibody, the membrane was washed with TBS-T three times. Thereafter, the secondary antibody was incubated for 1 h in blocking solution, the blot was washed three times and scanned with the Odyssey Infrared Imaging System (BioRad).

For Coomassie staining, the SDS PAGE is incubated right after running in Coomassie solution for about 1 h. After staining, the gel gets destained in destaining solution and changed several times until the protein bands can be distinguished from the rest of the gel.

4.8.5 Mass Spectrometry

<u>Phosphorylation site identification</u>

Distinct bands of an SDS-gel after affinity-purification were excised and washed with 50 mM NH_4HCO_3, 50 mM NH_4HCO_3/acetonitrile (3:1), 50 mM NH_4HCO_3/acetonitrile (1:1) and acetonitrile. After washing, the samples were lyophilized for 1 h. For reduction and alkylation of cysteines, the gel pieces were incubated with DTT and Iodoacetamide, followed by the

washing steps and the lyophilization mentioned above. After *in gel* tryptic digest overnight at 37 °C with approximately 2 µg trypsin per 100 µl gel volume (Trypsin Gold, mass spectrometry grade, Promega), Peptides were first extracted with 100 mM NH_4HCO_3, followed by 50 mM NH_4HCO_3 in 50 % acetonitrile. The eluates were combined, lyophilized and reconstituted in 20 µl 1 % TFA prior LC-MS/MS. The peptides were separated by reversed-phase chromatography on an UltiMate 3000 RSLCnano System (Thermo Fisher Scientific, Dreieich) which was equipped with C18 Acclaim Pepmap100 preconcentration column (100 µm i.D.x20 mm, Thermo Fisher Scientific). For the separation of the peptides, a linear gradient of 4 % to 40 % acetonitrile in 0.1 % formic acid over 90 min at a flow rate of 300 nl/min. Via a CaptiveSpray nanoflow electrospray source, the LC was coupled to a maXis plus UHR-QTOF System (Bruker Daltonics, Bremen). Data-dependent acquisition of MS/MS spectra by CID fragmentation was done at a resolution of minimum 60000 for MS and MS/MS scans. The MS spectra rate of the precursor scan was 2 Hz processing a mass range between m/z 175 and m/z 2000. Via the Compass 1.7 acquisition and processing software (Bruker Daltonics) a dynamic method with a fixed cycle time of 3 s and an m/z dependent collision energy adjustment between 34 and 55 eV was used. Via Data Analysis 4.2 (Bruker Daltonics), raw data were processed. For database search, Protein Scape 3.1.3 (Burker Daltonics) in connection with Mascot 2.5.1 (Matrix Science) was applied. The following search parameters were used: enzyme specificity trypsin with two missed cleavages allowed, precursor tolerance 10 ppm, MS/MS tolerance 0.04 Da, variable modifications: propionamide modification and carbamidomethylation of cysteine, oxidation of methionine, deamidation of asparagine and glutamine, phosphorylation of serine, threonine and tyrosine. With a Mascot peptide ion-score cut-off of 15, phosphopeptide fragment sprectra were evaluated using Biotools 3.2 (Bruker Daltonics)[160].

SRM-quantification of phosphopeptides

For phosphorylation stoichiometry determination of selected phosphopeptides, stable isotope-labeled peptides in phosphorylated and unphosphorylated state were used as internal standards. Heavy labeled peptides were synthesized as quantified SpikeTides-TQL (JPT Innovative Peptide solutions) with a $^{13}C^{15}N$-labeled C-terminal lysine or arginine:

SASFNTDPYVR	SA***pS***FNTDPYVR
YHLVDKEHDSAEGSHTSGQSNGR	YHLVDKEHD***pS***AEGSHTSGQSNGR, YHLVDKEHD***pS***AEG***pS***HT***pS***GQ***pS***NGR

100 fmol of each labeled peptide were spiked into the samples before the overnight *in-gel* tryptic digests. The samples were then processed as described above. To generate a SRM (Selected Reaction Monitoring) method, the software Skyline (MacCoss Lab Software, Seattle, USA) was used. The first step is to build a spectral library from several LC-MS/MS discovery runs (DDA, data dependent analysis) on the hybrid triple quadrupole/linear ion trap instrument QTRAP4500 (SCIEX). According to their occurrence in the DDA runs, precursor charge states +2, +3, +4 with either 3 or 4 transitions were included in the targeted method and the resulting transition list was imported into the instrument software (Analyst 1.6.1). Additionally, the parameters were set for the SRM method: Q1 and Q3 set to unit resolution (0.7 m/z half-maximum peak width), dwell time 20 ms, cycle time < 3 s. Next, a scheduled SRM method was generated in Skyline by annotating peptide retention times from the initial SRM run and setting the parameters with a cycle time of 2 s and a retention time window of 5 min. The LC-MS/MS system consisted of an UltiMate 3000 RSLCnano System (Thermo Fisher Scientific, Dreieich) coupled via NanoSprayII source (SCIEX) to a QTRAP4500. Peptide separation was conducted on an Acclaim Pepmap100 C18 preconcentration column (100 µm i.D.x20 mm, Thermo Fisher) in front. The run was performed at a flow rate of 300 nl/min on a 60 min linear gradient of 4 % to 40 % acetonitrile in 0.1 % formic acid. After importing the .wiff files of the SRM measurements into Skyline, the quantification of phosphorylated or non-phosphorylated peptides was conducted by calculating the heavy-to-light ratios of the peak areas of the respective transitions. With the whole amount of detected peptides were set to 100 %, the phosphorylated peptides could be relatively quantified[160].

4.9 RNA-based methods

4.9.1 RNA isolation

For cleavage assays and Northern Blotting, RNA was isolated with 1 ml TRIzol (Thermo Fisher Scientific) and 200 µl cloroform. The samples were shaken vigorously for 15 sec and centrifuged at 15,000 g for 10 min. For RNA precipitation, the aqueous phase were transferred into 2.5 volumes of ethanol and 1 µl Glycogen RNA grade (Thermo Fisher Scientific) and incubated overnight at -20°C. Subsequently, RNA was pelleted by centrifugation at 15,000 g for 30 min. After a washing step with 70 % ethanol, the RNA pellet was resuspended in water or 2 × RNA sample buffer.

4.9.2 RNA separation by Urea polyacrylamide gels and Northern Blotting

For RNA separation, 8–12 % Urea polyacrylamide gels (Rotiphorese, Roth) were used. After a pre-run at 400 V in 1x TBE, the wells were washed and the RNA samples were loaded to the bottom of each well. 8 % urea gels were run at 400 V for 1 h, 12 % gels run 1.5 h.

The Northern Blot was performed with three Whatman papers soaked with bidest. water and an Amersham Hybond-N membrane (GE Healthcare), which were placed on the positive electrode. The gel was washed with water, and put on the stack, followed by three bidest. water soaked Whatman papers. Northern Blotting was performed at 20V for 30 min. Thereafter, the RNA 5' ends were crosslinked to the membrane via EDC crosslinking solution. EDC supports the phosphoramidate bond between 5'-phosphate of RNA and amine of the membrane. A Whatman paper was soaked with this solution, the membrane was placed on this paper with the RNA side facing up, wrapped in cling film and incubated at 50°C for 1 h. Probes, listed in Table 5, were labeled with ^{32}P-γ-ATP on the 5' end by T4 Polynucleotide Kinase (Thermo Fisher Scientific) at 37°C for 30 min. The reaction was stopped by adding 30 µl 30 mM EDTA and purified by Sephadex G25 columns (GE Healthcare) to purify labeled probes from free ^{32}P-γ-ATP.

After crosslinking, the membrane was washed with water and dried. The radioactively labeled probe was incubated with the membrane in hybridization solution at 50°C overnight. After washing steps with wash-buffer I twice and with wash-buffer II once ten minutes each,

the blot was wrapped in cling film, exposed to a screen and scanned with phospho-imaging system (BioRad).

4.9.2.1 Quantitative real-time PCR (qRT-PCR)

The RNA of Input and IP samples were isolated using TRIzol (Thermo Fisher Scientific) and a second step with chloroform. For cDNA synthesis, 1 µg of the Input and complete RNA yield of the IP samples were first digested with DNaseI (Thermo Fisher Scientific). After the digest, cDNA was synthesized using First Strand cDNA synthesis kit (Thermo Fisher Scientific) with random hexamers, following the manufacturer's protocol. qRT-PCR was performed with Sso Fast Eva Green Mix (Bio-Rad). The primer which were used in this thesis are: ST6GALNAC6, fwd 5'-CATTCGTGGTTGAGCACAGG, rev 5'-CCGCTGGCTGCAGTAGTT; NFIC, fwd 5'-GACCTGTACCTGGCCTACTTTG, rev 5'-CACACCTGACGTGACAAAGCTC; SERBP1, fwd 5'-ACATCCATAATCAGCCACCA, rev 5'-AAGCTGTCTGCTGCCCAAAT[222]; HMGA2, fwd 5'-CTGCTATACACAAGCAATGCAAG, rev 5'-GTAAGGAGATTGCTTCTTTAACTG[222], F8A1, fwd 5'-GTTTGCGTCTGGGGAGGAAT, rev 5'-TGGTAACGTTCAGCCAACGA; HAND1, fwd 5'-GGAGTCCGCAGAAGGGTTAAA, rev 5'-CGGGCAAGGCTGAAAATGAG; HOXC8, fwd 5'-CGGAGACGCCTCCAAATTCT, rev 5'-GCCTTGTCCTTCGCTACTGT. qRT-PCRs were run on a CFX96 cycler (Bio-Rad) and data was analyzed using ΔΔCt method.[160]

4.9.3 RISC cleavage assay

4.9.3.1 *In vitro* transcription

The composition of an *in vitro* transcription reaction is listed below.

***In vitro* transcription, 200 µl**	
NTPs	20 mM
DTT	10 mM
Triton X-100	1 %
Spermidin	2 mM
$MgCl_2$	25 mM
Tris/HCl pH 8	30 mM
template (here 86.1)	10 µg
pyrophosphatase	0.2 µl
T7 RNA polymerase	20 µg

Table 7 Components of *in vitro* transcription reaction

A T7 RNA Polymerase (purified by Dres. Nora Treiber and Thomas Treiber, Biochemistry I, University of Regensburg) was used for *in vitro* transcriptions. The reaction was incubated at 37°C for 3-4 h. After incubation, 40 U DNase I (Thermo Fisher Scientific) were added and incubated for 15 min at 37°C to remove template DNA.

For *in vitro* transcription, 400 ng of the DNA template were used. The *in vitro* transcribed RNA was separated on an 8 % urea gel. The transcription product was visualized by UV shadowing and excised. After elution from gel by RNA Elution Buffer at 65°C for 1 h while shaking, the liquid was transferred in a new reaction tube. The RNA was precipitated with 2.5 volumes of ethanol and resuspended in bidest. water.

4.9.3.2 Cap-labeling of the target RNA

For cap-labeling, the *in vitro* transcribed RNA was incubated in a cap labelling reaction for 4 h at 37°C. The cap-labeled RNA was separated on an 8 % urea polyacrylamide gel, visualised by UV shadowing, excised, and eluted from gel incubating in RNA Elution Buffer at 10°C over night while shaking. Thereafter, the RNA was precipitated in 2.5 volumes ethanol and pelleted by centrifugation for 30 min at 15,000 g. The supernatant was removed and the RNA pellet was resuspended in 15 µl bidest. water.

cap labeling reaction, 20 µl	
GT buffer	1 ×
S-Adenosyl methionine	25 µM
RiboLock RNase Inhibitor	0.5 U/µl
Guanylyltransferase	10 %
^{32}P-α-GTP	1 µCi/µl

Table 8 Composition of a cap-labeling reaction

4.9.3.3 RISC cleavage assay

The cleavage reaction was performed directly after anti-FLAG immunoprecipitation. The beads were washed as described before. 25 % of the total immunoprecipitate was separated for subsequent analysis by Western Blotting. Thereafter, translation mix was added to a final concentration of 1 × translation mix and the reaction was started by addition of 1-2 Bq/cm^2 cap-labeled target RNA per sample. The reaction was incubated for 0-1.5 h at 37°C and stopped by addition of TRizol (Thermo Fisher Scientific) and Cloroform, shaking and centrifuging, followed by precipitation overnight at -20°C in ethanol with 20 µg glycogen RNA grade (Thermo Fisher Scientific). After pelleting, the RNA was resuspended in 10 µl RNA sample buffer.

The radiolabeled target RNA was also partially digested by RNase T1 and was used as ladder in for cleavage assays. For this reaction, 83.6 µl of carrier RNA solution and 4 µl of RNase T1 were mixed and added to 1-2 Bq/cm^2 radiolabeled target RNA. The mixture was incubated at

50°C for 10 min. Thereafter, the reaction was immediately transferred to -20°C. 2 µl of this ladder were loaded on the sequencing gel[77,154,223].

4.9.4 Autoradiographic sequencing gels

Samples of RISC cleavage assays were loaded onto 8 % urea sequencing gels (Rotiphorese, Roth). The sequencing gel was poured and run in a SequiGen Sequencing Cell (21x40 cm, 0.4 mm spacers, 16-well plastic comb, supplied by BioRad-Laboratories). The glass plate connected to the buffer tank was treated with Sigmacote® (Sigma-Aldrich) to facilitate gel pouring and disassembly, the other one was treated with 1 M NaOH, to increase roughness. Each well was washed before loading the samples. For loading MiniFlex Flat tips (Sorenson BioScience) were used. The gel was run at 50 W for about 1.5 h. After running, the gel was transferred onto Whatman paper, wrapped with cling film and vacuum-dried at 80°C for 1 h. Then, the gel was exposed to a screen and scanned at a phospho-imaging system (BioRad).

4.10 Tethering Assays

HeLa cells were transfected in triplicates as described above (4.8.1.2). After 48 h, the medium was completely removed and the cells were lysed by addition of 100 µl 1x Passive Lysis buffer (Promega, Madison, USA). The cells were shaken at 600 rpm for 15 min at RT. Thereafter, 20 µl of each sample were transferred into 96-wells and used for measurements. For measurements, the Luciferase-Reader (Berthold) was used in combination with Renilla- and Firefly-buffers. Shortly before use, 10 µl of the Renilla substrate coelenterazine (1.43 mM) were added to 10 ml Renilla buffer, and 333 µl DTT (1 M) were added to 10 ml Firefly buffer. For control, blanks and cells transfected with empty vectors (pCI neo) were measured. The ratio of Firefly:Renilla-reads was used for evaluation and the reads of the NHA-tagged plasmid samples were normalized with the appropriate HA samples.

4.11 Dual Luciferase Assay

For the dual luciferase assay, HeLa cells were cotransfected with 125 ng pMIR-HMGA2 reporter[107] and 400 ng VP5-Ago2 constructs[154,160] in 48-well format using Lipofectamin 2000 (4.8.1.2). The empty vector VP5 served as a control. 48 h after transfection, cells were lysed with Passive Lysis Buffer (Promega) while shaking. Luciferase substrates were purchased from PJK Cryosystems and the luciferase activity was measured on the Mithras LB940 luminometer (Berthold Technologies). The Firefly/Renilla luminescence ratios were calculated for each sample and normalized to the ratio in the empty vector control sample.

4.12 Immunofluorescence

The immunofluorescence (IF) were conducted as described previously[224]. Briefly, 24 h after transfection with 300 ng of the plasmids, cells were seeded on microscopy slides in 24-well plates to about a confluency of 50 %. Again, after 24 h, cells were first washed twice with warm PBS, incubated for 10 min with 3.7 % PFA in PBS at 37°C, stopped with 100 mM glycine in PBS for 5 min at 37°C and washed twice with PBS. The cells were then permeabilized with 0.2 % TX-100 in PBS for 15 min at RT and washed trice with PBS + 0.05 % TX-100 + 1 % BSA. Cells were blocked in this solution for 1 h. The cells were incubated in PBS + 0.05 % TX-100 + 1 % BSA supplemente4d with the first antibody for 1 h. After four washing steps with the blocking solution, cells were again incubated for 1 h with the second antibody, followed by four washings. At the end, the slides were mounted with Prolong Gold containing DAPI (Thermo Fisher Scientific – Life Technologies). Confocal microscopy was performed on a TCSSP8 (Leica Microsystems) equipped with acousto-optical beam splitter, 405 nm laser (DAPI), argon laser (488 nm for Alexa 488), and DPSS laser 561 nm (for Alexa 555).

4.13 GeneChip microarray assay

Preparation of the samples for microarray hybridization was performed as described in the Affymatrix GeneChip WT PLUS Reagent Kit User Manual (Affimetrix, Inc., Santa Clara, CA, USA). Shortly, to generate double-stranded cDNA, 4-100 ng of the IP-RNA were used. ERCC spike-in (Thermo Fisher Scientific) were added (1 µl ERCC 1:50,000 per ng input RNA; 1 µl

ERCC 1:250,000 per ng precipitated RNA). Of subsequently synthesized cRNA 15 µg were purified and reversely transcribed into sense-strand cDNA, where unnatural dUTP residues were incorporated. For fragmentation of the sense-stranded cDNA, a combination of uracil DNA glycosylase (UDG) and apurinic/apyrimidinic endonuclease 1 (APE 1) followed by a terminal labeling with biotin. 3.8 µg of the fragmented and labeled sense-stranded cDNA were hybridized to Affymetrix Human Gene 2.1 ST Array Plates. The Affymetrix GeneTitan system was used for hybridization, washing, staining and scanning, under control of the Affymetrix GeneChip Command Console software v4.2. Processing of the samples was carried out at an Affymetrix Service Provider and Core Facility, "KFB – Center of Excellence for Fluorescent Bioanalytics" (Regensburg, Germany)[160].

4.14 Bioinformatic analysis

4.14.1 Microarray

The RNA-IP (RIP) microarray data were processed in R version 3.3.0 [R core Team2016] with the oligo package (oligo_1.36.0)[225] using the built-in Affymetrix annotation (pd.hugene.2.1.st_3.14.1). For calibration of samples with different precipitated Ago quantities and their associated mRNAs to a fixed mRNA amount, ERCC RNA Spike-In Mix (Thermo Fisher Scientific) was added in proportion to the precipitated mRNA amount (4.13). Subsequently, the spike-in amounts were used for normalization in bioinformatics analysis. Following data quality control, ERCC spike-in intensities were used for vsn normalization of the different Affymetrix single color microarrays. Limma was used for analysis of differential precipitation in RIP assays. First, data were filtered to contain only transcripts enriched over input (log2FC Ago2 WT IP vs input >0), with the result of 4,200 transcripts. With these transcripts, cumulative distributions of the log2FC of mutant IP versus WT IP were drawn to globally analyze mRNA binding. A further reduction of the transcripts to the ones with a false discovery rate of the moderated t-test within limma below 0.3 for all three mutants versus WT comparisons helped to focus on the significant changes in mRNA binding. This resulted in 103 transcripts. In the GEO database www.ncbi.nlm.nih.gov/geo/ the microarray data is deposited and assigned the identifier GSE92698[160].

4.14.2 Sequence alignments

Protein sequences were retrieved from www.uniprot.org and the alignments were performed by Clustal Omega (www.ebi.ac.uk/Tools/msa/clustalo/).

Homo sapiens: Ago1 Q9UL18, Ago2 Q9UKV8, Ago3 Q9H9G7, Ago4 Q9HCK5

Caenorhabditis elegans: ALG1 G5EES3

Appendix

Mass spectrometry data – phosphorylation sites

Table 9 Potential phosphorylation sites in human Ago2

Peptide	Residue [phospho-site]	score REPL_1	score REPL_2	score REPL_3
MYSGAGPALAPPAPPPPIQGYAFKPPPRPDFGTSGR	Y[2]/S[3]	25.0		25.0
WVSCVSLQALHDALSGR	S[136]	34.1		30.0
SFFTASEGCSNPLGGGR	S[180]/S[189]	92.5	47.8	23.9
RPASHQTFPLQQESGQTVECTVAQYFK	S[307]	43.3		23.8
YPHLPCLQVGQEQK	Y[322]	27.2	38.0	
SASFNTDPYVR	S[387]	45.7	42.7	61.3
VGDTVLGMATQCVQMK	T[538]/T[544]	26.1	44.9	30.4
TTPQTLSNLCLK	T[555]/T[556]	57.2	45.5	44.9
YHLVDKEHDSAEGSHTSGQSNGR/DPQALAK	S[824]	93.6	113.0	102.2
YHLVDKEHDSAEGSHTSGQSNGR/DPQALAK	S[828]	78.2	126.0	19.6
YHLVDKEHDSAEGSHTSGQSNGR/DPQALAK	T[830]	66.4		17.6
YHLVDKEHDSAEGSHTSGQSNGR/DPQALAK	S[834]	26.5		
YHLVDKEHDSAEGSHTSGQSNGR/DPQALAK	S[824]/S[828]	28.4		22.5
YHLVDKEHDSAEGSHTSGQSNGR/DPQALAK	S[824]/S[834]	22.0	16.9	
YHLVDKEHDSAEGSHTSGQSNGR/DPQALAK	S[828]/T[830]	17.9	49.8	18.1
YHLVDKEHDSAEGSHTSGQSNGR/DPQALAK	S[828]/S[831]		24.3	
YHLVDKEHDSAEGSHTSGQSNGR/DPQALAK	T[830]/S[831]	43.5	43.9	
YHLVDKEHDSAEGSHTSGQSNGR/DPQALAK	S[831]/S[834]		24.0	
YHLVDKEHDSAEGSHTSGQSNGR/DPQALAK	S[828]/T[830]/S[831]	16.0		
YHLVDKEHDSAEGSHTSGQSNGR/DPQALAK	S[824]/S[828]/T[830]	22.7	31.3	18.8
YHLVDKEHDSAEGSHTSGQSNGR/DPQALAK	S[828]/T[830]/S[831]/S[834]	26.5		22.1
YHLVDKEHDSAEGSHTSGQSNGR/DPQALAK	S[824]/S[828]/T[830]/S[834]		27.0	

Table 10 Potential phosphorylation sites in human Ago1

Peptide	Residue [phospho-site]	score REPL_1	score REPL_2	score REPL_3
MEAGPSGAAAGAYLPPLQQVFQAPR	S[6]	63.7	59.2	59.7
MEAGPSGAAAGAYLPPLQQVFQAPR	Y[13]	45.8		33.2
YPHLPCLQVGQEQK	Y[320]		27.2	39.1
HTYLPLEVCNIVAGQR	T[335]			52.3
RVGDTLLGMATQCVQV	T[536]		32	38.5
TSPQTLSNLCLK	T[553]/S[554]		45	41.7
YHLVDKEHDSGEGSHISGQSNGR/DPQALAK	S[822]	27.2	82.8	24
YHLVDKEHDSGEGSHISGQSNGR/DPQALAK	S[826]	35.3	19.7	31.1
YHLVDKEHDSGEGSHISGQSNGR/DPQALAK	S[829]	26.1		
YHLVDKEHDSGEGSHISGQSNGR/DPQALAK	S[832]	18.4	23.5	
YHLVDKEHDSGEGSHISGQSNGR/DPQALAK	S[822]/S[826]			29.1
YHLVDKEHDSGEGSHISGQSNGR/DPQALAK	S[822]/S[829]		42.6	17.2
YHLVDKEHDSGEGSHISGQSNGR/DPQALAK	S[822]/S[832]		18	
YHLVDKEHDSGEGSHISGQSNGR/DPQALAK	S[829]/S[832]	16.5		
YHLVDKEHDSGEGSHISGQSNGR/DPQALAK	S[826]/S[829]	37.6	47.7	
YHLVDKEHDSGEGSHISGQSNGR/DPQALAK	S[826]/S[829]/S[832]	20.3	23.6	
YHLVDKEHDSGEGSHISGQSNGR/DPQALAK	S[822]/S[826]/S[829]	49.4		20.9

Table 11 Potential phosphorylation sites in human Ago3

Peptide	Residue [phospho-site]	score REPL_1	score REPL_2	score REPL_3
MEIGSAGPAGAQPLLMVPR	S[5]	66.7	36.9	31.4
YPHLPCLQVGQEQK	Y[323]		27.2	39.1
RVGDTLLGMATQCVQVK	T[539]	42.4	32	38.5
TSPQTLSNLCLK	T[556]		45	41.7
YHLVDKEHDSAEGSHVSGQSNGR/DPQALAK	S[825]	48.2	16	25.7
YHLVDKEHDSAEGSHVSGQSNGR/DPQALAK	S[829]	31.9	39.2	39.6
YHLVDKEHDSAEGSHVSGQSNGR/DPQALAK	S[832]	28.8	23.5	19.4
YHLVDKEHDSAEGSHVSGQSNGR/DPQALAK	S[835]	22.3		16.7
YHLVDKEHDSAEGSHVSGQSNGR/DPQALAK	S[825]/S[829]			21.1
YHLVDKEHDSAEGSHVSGQSNGR/DPQALAK	S[832]/S[835]	16.5		
YHLVDKEHDSAEGSHVSGQSNGR/DPQALAK	S[829]/S[832]	32.9		18.8
YHLVDKEHDSAEGSHVSGQSNGR/DPQALAK	S[829]/S[835]	24.4		
YHLVDKEHDSAEGSHVSGQSNGR/DPQALAK	S[825]/S[829]/S[832]	22.3		
YHLVDKEHDSAEGSHVSGQSNGR/DPQALAK	S[825]/S[832]/S[835]	21.9	23.6	
YHLVDKEHDSAEGSHVSGQSNGR/DPQALAK	S[825]/S[829]/S[832]/S[835]	15.6		

Table 12 Potential phosphorylation sites in human Ago4

Peptide	Residue [phospho-site]	score REPL_1	score REPL_2	score REPL_3
YPHLPCLQVGQEQK	Y[312]	41.9	27.2	39.1
HTYLPLEVCNIVAGQR	T[327]	49.1		52.3
RVGDTLLGMATQCVQVK	T[530]/T[536]	26	32	38.5
TSPQTLSNLCLK	T[547]	75.6	45	41.7
YHLVDKDHDSAEGSHVSGQSNGR/DPQALAK	S[826]	18.1	25.4	19

Table 13 Potential phosphorylation sites in mouse Ago2

Peptide	Residue [phospho-site]	score REPL_1	score REPL_2	score REPL_3
MYSGAGPVLASPAPTTSPIPGYAFKPPPRPDFGTTGR	S[3]			28,11
SFFTASEGCSNPLGGGR	S[190]			17,16
RPASHQTFPLQQESGQTVECTVAQYFK	T[308]			24,42
SASFNTDPYVR	S[388]		49.5	54,29
VGDTVLGMATQCVQMK	T[545]		20	
TTPQTLSNLCLK	T[557]			
YHLVDKEHDSAEGSHTSGQSNGR/DPQALAK	S[825]	75.5	66.2	104,43
YHLVDKEHDSAEGSHTSGQSNGR/DPQALAK	S[829]	67.3	85.8	38,68
YHLVDKEHDSAEGSHTSGQSNGR/DPQALAK	T[831]		18.7	
YHLVDKEHDSAEGSHTSGQSNGR/DPQALAK	S[832]	48.2	35.1	
YHLVDKEHDSAEGSHTSGQSNGR/DPQALAK	S[835]	33.7	17.7	
YHLVDKEHDSAEGSHTSGQSNGR/DPQALAK	S[829]/S[832]			22,82
YHLVDKEHDSAEGSHTSGQSNGR/DPQALAK	S[829]/T[831]			
YHLVDKEHDSAEGSHTSGQSNGR/DPQALAK	S[825]/S[829]	19.8	37.7	
YHLVDKEHDSAEGSHTSGQSNGR/DPQALAK	T[831]/S[832]	37.1		
YHLVDKEHDSAEGSHTSGQSNGR/DPQALAK	S[825]/S[829]/T[831]	26	46.7	18,43
YHLVDKEHDSAEGSHTSGQSNGR/DPQALAK	S[829]/T[831]/S[832]	38.4		15,32
YHLVDKEHDSAEGSHTSGQSNGR/DPQALAK	S[829]/T[831]/S[832]/S[835]		17.9	16,28
YHLVDKEHDSAEGSHTSGQSNGR/DPQALAK	S[825]/T[831]/S[832]/S[835]			22,46

Peptide	Residue [phospho-site]	score REPL_4	score REPL_5	score REPL_6
MYSGAGPVLASPAPTTSPIPGYAFKPPPRPDFGTTGR	S[3]	20,23	23,85	29,86
SFFTASEGCSNPLGGGR	S[190]		23,17	
RPASHQTFPLQQESGQTVECTVAQYFK	T[308]			19,78
SASFNTDPYVR	S[388]	55,8	31,45	66,81
VGDTVLGMATQCVQMK	T[545]	16,55		
TTPQTLSNLCLK	T[557]			15,52
YHLVDKEHDSAEGSHTSGQSNGR/DPQALAK	S[825]	84,43	70,89	26,76
YHLVDKEHDSAEGSHTSGQSNGR/DPQALAK	S[829]	37,96	34,14	74,8
YHLVDKEHDSAEGSHTSGQSNGR/DPQALAK	T[831]	36,21		
YHLVDKEHDSAEGSHTSGQSNGR/DPQALAK	S[832]	14,07	19,14	27,25
YHLVDKEHDSAEGSHTSGQSNGR/DPQALAK	S[829]/T[831]	46,03	30,88	
YHLVDKEHDSAEGSHTSGQSNGR/DPQALAK	S[825]/S[829]	23,64	43,79	
YHLVDKEHDSAEGSHTSGQSNGR/DPQALAK	T[831]/S[832]	27,55		
YHLVDKEHDSAEGSHTSGQSNGR/DPQALAK	S[825]/S[829]/T[831]	29,15	29,52	22,78
YHLVDKEHDSAEGSHTSGQSNGR/DPQALAK	S[829]/T[831]/S[832]			18,18
YHLVDKEHDSAEGSHTSGQSNGR/DPQALAK	S[829]/T[831]/S[832]/S[835]	24,67		

Peptide	Residue [phospho-site]	score REPL_7	score REPL_8
MYSGAGPVLASPAPTTSPIPGYAFKPPPRPDFGTTGR	S[3]		21,47
SFFTASEGCSNPLGGGR	S[190]		32,07
RPASHQTFPLQQESGQTVECTVAQYFK	T[308]	34,4	
SASFNTDPYVR	S[388]	45,06	49,21
VGDTVLGMATQCVQMK	T[545]	20,1	39,21
TTPQTLSNLCLK	T[557]		
YHLVDKEHDSAEGSHTSGQSNGR/DPQALAK	S[825]	66,99	96,35
YHLVDKEHDSAEGSHTSGQSNGR/DPQALAK	S[829]	85,73	53,59
YHLVDKEHDSAEGSHTSGQSNGR/DPQALAK	T[831]		17,53
YHLVDKEHDSAEGSHTSGQSNGR/DPQALAK	S[832]	14,5	32,34
YHLVDKEHDSAEGSHTSGQSNGR/DPQALAK	S[829]/S[832]		14,08
YHLVDKEHDSAEGSHTSGQSNGR/DPQALAK	T[831]/S[832]		40,3
YHLVDKEHDSAEGSHTSGQSNGR/DPQALAK	S[825]/S[829]/T[831]	19	27,62
YHLVDKEHDSAEGSHTSGQSNGR/DPQALAK	S[829]/T[831]/S[832]		16,4
YHLVDKEHDSAEGSHTSGQSNGR/DPQALAK	S[829]/T[831]/S[832]/S[835]	27,97	32,2
YHLVDKEHDSAEGSHTSGQSNGR/DPQALAK	S[825]/T[831]/S[832]/S[835]		24,94

Table 14 Potential phosphorylation sites in rat Ago2

Peptide	Residue [phospho-site]	score REPL_1	score REPL_2	score REPL_3
MYSGAGPVLASPAPTTSPIPGY	Y[2]	24,85	13,65	
SFFTASEGCSNPLGGGRE	S[190]	30,73		
SASFNTDPYVR	S[388]	62,28	44,04	42.1
VGDTVLGMATQCVQMK	T[545]	20,3	17,35	20.5
TLSNLCLKINVK	S[562]	20,99		
YHLVDKEHDSAEGSHTSGQSNGR	S[825]	91,74	95,58	75.5
YHLVDKEHDSAEGSHTSGQSNGR	S[829]	67.9	47,61	58.4
YHLVDKEHDSAEGSHTSGQSNGR	S[835]			27.6
YHLVDKEHDSAEGSHTSGQSNGR	S[829]/S[832]		23,83	
YHLVDKEHDSAEGSHTSGQSNGR	S[829]/T[831]	30		
YHLVDKEHDSAEGSHTSGQSNGR	S[825]/S[829]	61		
YHLVDKEHDSAEGSHTSGQSNGR	T[831]/S[832]	29,96	21,14	
YHLVDKEHDSAEGSHTSGQSNGR	S[832]/S[835]	21,57		
YHLVDKEHDSAEGSHTSGQSNGR	S[825]/S[829]/T[831]	28,63		
YHLVDKEHDSAEGSHTSGQSNGR	S[825]/S[829]/S[835]	26,33		

Table 15 Potential phosphorylation sites in zebrafish Ago2

Peptide	Residue [phospho-site]	score REPL_1	score REPL_2	score REPL_3
YHLVDKEHDSAEGSHTSGQSNGR	S[838]	40.6	48.1	33,83
YHLVDKEHDSAEGSHTSGQSNGR	S[842]	29.5	20	41,14
YHLVDKEHDSAEGSHTSGQSNGR	T[844]			14,02

Table 16 Potential phosphorylation sites in *C. elegans* ALG-1

Peptide	Residue [phospho-site]	score REPL_1	score REPL_2	score REPL_3
TTPQTLSNLCLK	T[720]		38,73	30,13
YHLVDR/EHDSGEGSQPSGTSEDTTLSNMAR	S[988]	85.2		96,3
YHLVDR/EHDSGEGSQPSGTSEDTTLSNMAR	S[992]	114	111,55	123,47
YHLVDR/EHDSGEGSQPSGTSEDTTLSNMAR	S[995]	35		28,2
YHLVDR/EHDSGEGSQPSGTSEDTTLSNMAR	T[997]	20.4	26,96	27,47
YHLVDR/EHDSGEGSQPSGTSEDTTLSNMAR	S[988]/S[992]		52,76	
YHLVDR/EHDSGEGSQPSGTSEDTTLSNMAR	S[992]/S[995]	67.4	60,28	56,15
YHLVDR/EHDSGEGSQPSGTSEDTTLSNMAR	S[995]/T[997]	41.2		44,62
YHLVDR/EHDSGEGSQPSGTSEDTTLSNMAR	T[997]/S[998]		35,14	38,43
YHLVDR/EHDSGEGSQPSGTSEDTTLSNMAR	S[992]/S[995]/T[997]	39.1	58,87	56,68
YHLVDR/EHDSGEGSQPSGTSEDTTLSNMAR	S[995]/T[997]/S[998]	21	42,8	38,64
YHLVDR/EHDSGEGSQPSGTSEDTTLSNMAR	S[988]/S[992]/S[995]		27,49	17,25

List of Abbreviations

Units were abbreviated according to the International System of Units. Chemical names not indicated below were abbreviated according to the International Union of Pure and Applied Chemistry (IUPAC) recommendations.

A / Ala	Alanine
aa	amino acid
AEBSF	4-(2-aminoethyl) benzenesulfonyl .uoride hydrochloride
Ago	Argonaute
Ago-APP	Ago affnity purification by peptides
Amp	ampicillin
ANKRD28, 44, 52	Serine/threonine-protein phosphatase 6 regulatory ankyrin repeat subunit A-B// Ankyrin repeat domain-containing protein 28, 44, 52
APS	ammonium persulphate
ATP	adenosine triphosphate
bp	base pair(s)
BSA	bovine serum albumin
C / Cys	Cysteine
C. elegans	Caenorhabditis elegans
cDNA	complementary DNA
CDS	coding sequence
CoIP	co-immunoprecipitation
CSNK1A1	Casein kinase I isoform alpha
CTD	C-terminal domain
D. melanogaster	Drosophila melanogaster
Da	Dalton
Del	deletion
DMEM	Dulbecco's Modified Eagle's Medium
DNA	deoxyribonucleic acid
dNTP	deoxynucleoside triphosphate
ds	double-stranded
dsRBD	double-stranded RNA binding domain

dT	desoxythymidine
DTT	dithiothreitol
E / Glu	Glutamate
EDC	1-ethyl-3-(3-dimethyl-aminopropyl)-carbodiimid
EDTA	ethylenediaminetetraacetic acid
EGFR	epithelial growth factor receptor
eIF	eukaryotic initiation factor
ERK	extracellular signal–regulated protein kinases
EtBr	ethidium bromide
Exp	Exportin
F / Phe	Phenylalanine
FBS	fetal bovie serum
G / Gly	Glycine
g	gram
GAPDH	glyceraldehyde 3-phosphate dehydrogenase
GDP	guanosine diphosphate
GFP	green .uorescent protein
GSH	glutathione
GSK3	glycogen synthase kinase 3_
GST	glutahione-S-transferase
GTP	guanosine triphosphate
H / His	Histidine
h	hour
H. sapiens	Homo sapiens
HA	hemagglutinin
HEK 293T	human embryonic kidney 293T
HEPES	4-(2-hydroxyethyl)-1-piperazineethanesulfonic acid
HMGA2	high mobility group AT hook 2
HSP90	heat shock protein 90
Imp	Importin
IP	immunoprecipitation

IPTG	isopropyl _-D-1-thiogalactopyranoside
K / Lys	Lysine
k	kilo
kb	kilobase
L / Leu	Leucine
l	liter
LB	lysogeny broth
M / Met	Methionine
M	molar
MAPK	MAP (mitogen-activated protein) kinase
MAP3K7 / TAK1	Mitogen-activated protein kinase kinase kinase 7
MAPKAPK2	MAP-activated protein kinase 2
MCS	multiple cloning site
min	minute
miRISC	miRNA induced silencing complex
miRNA	microRNA
miRNP	micro-ribonucleoprotein
MKK	MAPK kinase
mRNA	messenger RNA
MS	mass spectrometry, mass spectrometric
Neo	neomycine
NES	nuclear localization signal
NMR	nuclear magnetic resonance
nt	nucleotides(s)
o/n	over night
OD	optical density
ORF	open reading frame
P / Pro	Proline
PABP	poly(A)-binding protein
PACT	protein activator of the interferon-induced protein kinase
PAGE	polyacrylamide gel electrophoresis

PAM2	PABP interacting motif 2
PAN2/3	PAB-dependent poly(A)-specific ribonuclease subunit 2/3
PAR-CLIP	Photoactivatable-Ribonucleoside-Enhanced Crosslinking and IP
PAZ	PIWI-Argonaute-Zwille
P-bodies	processing bodies
PBS	Phosphate buffered saline
PBS(-T)	phosphate-buffered saline (containing Tween 20)
PCR	polymerase chain reaction
piRNA	Piwi-interacting RNA
piRNA	PIWI-interacting RNA
PIWI	P-element-induced wimpy testes
PNK	polynucleotide kinase
PPP6C	Serine/threonine-protein phosphatase 6 catalytic subunit
PP6R1-3	Serine/threonine-protein phosphatase 6 regulatory subunit 1-3
pre-miRNA	precursor miRNA
pri-miRNA	primary miRNA
PTGS	post-transcriptional gene silencing
PTM	post-translational modification
PTP1B	protein tyrosine phosphatase 1B
Q / Gln	Glutamine
qRT-PCR	quantitative real-time polymerase chain reaction
R / Arg	Arginine
RAS	rat sarcoma
RIPA	radioimmunoprecipitation assay
RISC	RNA-induced silencing complex
RNA	ribonucleic acid
RNAi	RNA interference
RNP	ribonucleoprotein
rpm	revolutions per minute
RRM	RNA recognition motif
RT	room temperature

S / Ser	Serine
S. pombe	Schizosaccaromyces pombe
S. cerevisiae	Saccharomyces cerevisiae
SDS	sodium dodecyl sulfate
sec	second
shRNA	short hairpin RNA
siRNA	small interfering RNA
snoRNA	small nucleolar RNA
SRM	selected reaction monitoring
ss	single-stranded
SSC	saline-sodium citrate buffer
T / Thr	Threonine
TBE	Tris/Borate/EDTA buffer
TBS	Tris buffered saline
TBS(-T)	Tris-buffered saline (containing Tween 20)
TEMED	tetramethylethylenediamine
TRBP	transactivating response RNA binding protein
TRIM71	tripartite motif-containing protein 71
tRNA	transfer RNA
UBA	ubiquitin-associated
UTP	uridine triphosphate
UTR	untranslated region
V / Val	Valine
W / Trp	Tryptophan
w/v	weight per volume
wt / WT	wild type
Y / Tyr	Tyrosine

List of Figures

List of Tables

Bibliography

1. Fire, A. *et al.* Potent and specific genetic interference by double-stranded RNA in Caenorhabditis elegans.pdf. *Nature* **391**, 806–11 (1998).

2. Ender, C. & Meister, G. Argonaute proteins at a glance. *J. Cell Sci.* **123**, 1819–23 (2010).

3. Rana, T. M. Illuminating the silence: understanding the structure and function of small RNAs. *Nat. Rev. Mol. Cell Biol.* **8**, 23–36 (2007).

4. Kim, V. N., Han, J. & Siomi, M. C. Biogenesis of small RNAs in animals. *Nat. Rev. Mol. Cell Biol.* **10**, 126–39 (2009).

5. Cai, X., Hagedorn, C. H. & Cullen, B. R. Human microRNAs are processed from capped, polyadenylated transcripts that can also function as mRNAs. *RNA* **10**, 1957–66 (2004).

6. Lee, Y. *et al.* MicroRNA genes are transcribed by RNA polymerase II. *EMBO J.* **23**, 4051–60 (2004).

7. Raver-Shapira, N. & Oren, M. Tiny Actors, Great Roles: microRNAs in p53's Service. *Cell Cycle* **6**, 2656–2661 (2007).

8. Denli, A. M., Tops, B. B. J., Plasterk, R. H. a, Ketting, R. F. & Hannon, G. J. Processing of primary microRNAs by the Microprocessor complex. *Nature* **432**, 231–5 (2004).

9. Gregory, R. I. *et al.* The Microprocessor complex mediates the genesis of microRNAs. *Nature* **432**, 235–40 (2004).

10. Landthaler, M., Yalcin, A. & Tuschl, T. The Human DiGeorge Syndrome Critical Region Gene 8 and Its D. melanogaster Homolog Are Required for miRNA Biogenesis. *Curr. Biol.* **14**, 2162–2167 (2004).

11. Han, J. *et al.* The Drosha-DGCR8 complex in primary microRNA processing. *Genes Dev.* **18**, 3016–27 (2004).

12. Kwon, S. C. *et al.* Structure of Human DROSHA. *Cell* **164**, 81–90 (2016).

13. Quick-Cleveland, J. *et al.* The DGCR8 RNA-Binding Heme Domain Recognizes Primary MicroRNAs by Clamping the Hairpin. *Cell Rep.* **7**, 1994–2005 (2014).

14. Weitz, S. H., Gong, M., Barr, I., Weiss, S. & Guo, F. Processing of microRNA primary transcripts requires heme in mammalian cells. *Proc. Natl. Acad. Sci.* **111**, 1861–1866 (2014).

15. Nguyen, T. A. *et al.* Functional Anatomy of the Human Microprocessor. *Cell* **161**, 1374–1387 (2015).

16. Herbert, K. M. *et al.* A heterotrimer model of the complete Microprocessor complex revealed by single-molecule subunit counting. *RNA* **22**, 175–183 (2016).

17. Bohnsack, M. T. Exportin 5 is a RanGTP-dependent dsRNA-binding protein that mediates nuclear export of pre-miRNAs. *RNA* **10**, 185–191 (2004).

18. Kim, Y.-K., Kim, B. & Kim, V. N. Re-evaluation of the roles of *DROSHA* , *Exportin 5* , and *DICER* in microRNA biogenesis. *Proc. Natl. Acad. Sci.* **113**, E1881–E1889 (2016).

19. Yi, R. Exportin-5 mediates the nuclear export of pre-microRNAs and short hairpin RNAs. *Genes Dev.* **17**, 3011–3016 (2003).

20. Lund, E. & Dahlberg, J. E. Substrate Selectivity of Exportin 5 and Dicer in the Biogenesis of MicroRNAs. *Cold Spring Harb. Symp. Quant. Biol.* **71**, 59–66 (2006).

21. Gregory, R. I., Chendrimada, T. P., Cooch, N. & Shiekhattar, R. Human RISC Couples MicroRNA Biogenesis and Posttranscriptional Gene Silencing. *Cell* **123**, 631–640 (2005).

22. Taylor, D. W. *et al.* Substrate-specific structural rearrangements of human Dicer. *Nat. Struct. Mol. Biol.* **20**, 662–670 (2013).

23. Wang, H.-W. *et al.* Structural insights into RNA processing by the human RISC-loading complex. *Nat. Struct. Mol. Biol.* **16**, 1148–1153 (2009).

24. Meister, G. *et al.* Identification of novel argonaute-associated proteins. *Curr. Biol.* **15**, 2149–55 (2005).

25. MacRae, I. J., Ma, E., Zhou, M., Robinson, C. V. & Doudna, J. A. In vitro reconstitution of the human RISC-loading complex. *Proc. Natl. Acad. Sci.* **105**, 512–517 (2008).

26. Zhang, H., Kolb, F. A., Jaskiewicz, L., Westhof, E. & Filipowicz, W. Single Processing Center Models for Human Dicer and Bacterial RNase III. *Cell* **118**, 57–68 (2004).

27. MacRae, I. J. Structural Basis for Double-Stranded RNA Processing by Dicer. *Science* **311**, 195–198 (2006).

28. Lau, P.-W., Potter, C. S., Carragher, B. & MacRae, I. J. Structure of the Human Dicer-TRBP Complex by Electron Microscopy. *Structure* **17**, 1326–1332 (2009).

29. Redfern, A. D. *et al.* RNA-induced silencing complex (RISC) Proteins PACT, TRBP, and Dicer are SRA binding nuclear receptor coregulators. *Proc. Natl. Acad. Sci.* **110**, 6536–6541 (2013).

30. Lee, H. Y., Zhou, K., Smith, A. M., Noland, C. L. & Doudna, J. A. Differential roles of human Dicer-binding proteins TRBP and PACT in small RNA processing. *Nucleic Acids Res.* **41**, 6568–6576 (2013).

31. Heyam, A., Lagos, D. & Plevin, M. Dissecting the roles of TRBP and PACT in double-stranded RNA recognition and processing of noncoding RNAs: Roles of TRBP and PACT in double-stranded RNA recognition. *Wiley Interdiscip. Rev. RNA* **6**, 271–289 (2015).

32. Kok, K. H., Ng, M.-H. J., Ching, Y.-P. & Jin, D.-Y. Human TRBP and PACT Directly Interact with Each Other and Associate with Dicer to Facilitate the Production of Small Interfering RNA. *J. Biol. Chem.* **282**, 17649–17657 (2007).

33. Kim, Y. *et al.* Deletion of Human tarbp2 Reveals Cellular MicroRNA Targets and Cell-Cycle Function of TRBP. *Cell Rep.* **9**, 1061–1074 (2014).

34. Chendrimada, T. P. *et al.* TRBP recruits the Dicer complex to Ago2 for microRNA processing and gene silencing. *Nature* **436**, 740–4 (2005).

35. Lee, H. Y. & Doudna, J. A. TRBP alters human precursor microRNA processing in vitro. *RNA* **18**, 2012–2019 (2012).

36. Wilson, R. C. *et al.* Dicer-TRBP Complex Formation Ensures Accurate Mammalian MicroRNA Biogenesis. *Mol. Cell* **57**, 397–407 (2015).

37. Fareh, M. *et al.* TRBP ensures efficient Dicer processing of precursor microRNA in RNA-crowded environments. *Nat. Commun.* **7**, 13694 (2016).

38. Song, M.-S. & Rossi, J. J. Molecular mechanisms of Dicer: endonuclease and enzymatic activity. *Biochem. J.* **474**, 1603–1618 (2017).

39. Dueck, A., Ziegler, C., Eichner, A., Berezikov, E. & Meister, G. microRNAs associated with the different human Argonaute proteins. *Nucleic Acids Res.* **40**, 9850–62 (2012).

40. Miyoshi, K., Okada, T. N., Siomi, H. & Siomi, M. C. Characterization of the miRNA-RISC loading complex and miRNA-RISC formed in the Drosophila miRNA pathway. *RNA N. Y. N* **15**, 1282–91 (2009).

41. Nakanishi, K. Anatomy of RISC: how do small RNAs and chaperones activate Argonaute proteins?: Anatomy of RISC. *Wiley Interdiscip. Rev. RNA* **7**, 637–660 (2016).

42. Kawamata, T. & Tomari, Y. Making RISC. *Trends Biochem. Sci.* **35**, 368–376 (2010).

43. Czech, B. *et al.* An endogenous small interfering RNA pathway in Drosophila. *Nature* **453**, 798–802 (2008).

44. Ghildiyal, M. *et al.* Endogenous siRNAs derived from transposons and mRNAs in Drosophila somatic cells. *Science* **320**, 1077–81 (2008).

45. Kawamura, Y. *et al.* Drosophila endogenous small RNAs bind to Argonaute 2 in somatic cells. *Nature* **453**, 793–797 (2008).

46. Okamura, K. *et al.* The Drosophila hairpin RNA pathway generates endogenous short interfering RNAs. *Nature* **453**, 803–6 (2008).

47. Siomi, M. C., Sato, K., Pezic, D. & Aravin, A. A. PIWI-interacting small RNAs: the vanguard of genome defence. *Nat. Rev. Mol. Cell Biol.* **12**, 246–258 (2011).

48. Weick, E.-M. & Miska, E. A. piRNAs: from biogenesis to function. *Development* **141**, 3458–3471 (2014).

49. Czech, B. & Hannon, G. J. One Loop to Rule Them All: The Ping-Pong Cycle and piRNA-Guided Silencing. *Trends Biochem. Sci.* **41**, 324–337 (2016).

50. Pfaff, J. *et al.* Structural features of Argonaute-GW182 protein interactions. *PNAS* **110**, E3770–9 (2013).

51. Matranga, C., Tomari, Y., Shin, C., Bartel, D. P. & Zamore, P. D. Passenger-strand cleavage facilitates assembly of siRNA into Ago2-containing RNAi enzyme complexes. *Cell* **123**, 607–20 (2005).

52. Rand, T. a, Petersen, S., Du, F. & Wang, X. Argonaute2 cleaves the anti-guide strand of siRNA during RISC activation. *Cell* **123**, 621–9 (2005).

53. Bohmert, K. *et al.* AGO1 defines a novel locus of Arabidopsis controlling leaf development. *EMBO J.* **17**, 170–80 (1998).

54. Yigit, E. *et al.* Analysis of the C. elegans Argonaute family reveals that distinct Argonautes act sequentially during RNAi. *Cell* **127**, 747–57 (2006).

55. Meister, G. Argonaute proteins: functional insights and emerging roles. *Nat. Rev. Genet.* **14**, 447–459 (2013).

56. Tolia, N. H. & Joshua-Tor, L. Slicer and the Argonautes. *Nat. Chem. Biol.* **3**, 36–43 (2007).

57. Aravin, A. a, Sachidanandam, R., Girard, A., Fejes-Toth, K. & Hannon, G. J. Developmentally regulated piRNA clusters implicate MILI in transposon control. *Science* **316**, 744–7 (2007).

58. Kuramochi-Miyagawa, S. *et al.* Mili, a mammalian member of piwi family gene, is essential for spermatogenesis. *Development* **131**, 839–49 (2004).

59. Hutvagner, G. & Simard, M. J. Argonaute proteins: key players in RNA silencing. *Nat. Rev. Mol. Cell Biol.* **9**, 22–32 (2008).

60. Fabian, M. R. & Sonenberg, N. The mechanics of miRNA-mediated gene silencing: a look under the hood of miRISC. *Nat. Struct. Mol. Biol.* **19**, 586–593 (2012).

61. Zander, A. *et al.* Guide-independent DNA cleavage by archaeal Argonaute from Methanocaldococcus jannaschii. *Nat. Microbiol.* **2**, 17034 (2017).

62. Willkomm, S., Zander, A., Gust, A. & Grohmann, D. A Prokaryotic Twist on Argonaute Function. *Life* **5**, 538–553 (2015).

63. Willkomm, S., Makarova, K. S. & Grohmann, D. DNA silencing by prokaryotic Argonaute proteins adds a new layer of defense against invading nucleic acids. *FEMS Microbiol. Rev.* **42**, 376–387 (2018).

64. Willkomm, S. *et al.* Structural and mechanistic insights into an archaeal DNA-guided Argonaute protein. *Nat. Microbiol.* **2**, 17035 (2017).

65. Song, J.-J. Crystal Structure of Argonaute and Its Implications for RISC Slicer Activity. *Science* **305**, 1434–1437 (2004).

66. Yuan, Y.-R. *et al.* Crystal structure of A. aeolicus argonaute, a site-specific DNA-guided endoribonuclease, provides insights into RISC-mediated mRNA cleavage. *Mol. Cell* **19**, 405–19 (2005).

67. Swarts, D. C. *et al.* DNA-guided DNA interference by a prokaryotic Argonaute. *Nature* **507**, 258–261 (2014).

68. Wang, Y. *et al.* Structure of an argonaute silencing complex with a seed-containing guide DNA and target RNA duplex. *Nature* **456**, 921–6 (2008).

69. Olovnikov, I., Chan, K., Sachidanandam, R., Newman, D. K. & Aravin, A. a. Bacterial argonaute samples the transcriptome to identify foreign DNA. *Mol. Cell* **51**, 594–605 (2013).

70. Nakanishi, K., Weinberg, D. E., Bartel, D. P. & Patel, D. J. Structure of yeast Argonaute with guide RNA. *Nature* 1–9 (2012). doi:10.1038/nature11211

71. Schirle, N. T. & MacRae, I. J. The Crystal Structure of Human Argonaute2. *Science* (2012). doi:10.1126/science.1221551

72. Gebert, L. F. R. & MacRae, I. J. Regulation of microRNA function in animals. *Nat. Rev. Mol. Cell Biol.* (2018). doi:10.1038/s41580-018-0045-7

73. Schirle, N. T., Sheu-Gruttadauria, J. & MacRae, I. J. Structural basis for microRNA targeting. *Science* **346**, 608–613 (2014).

74. Kwak, P. B. & Tomari, Y. The N domain of Argonaute drives duplex unwinding during RISC assembly. *Nat. Struct. Mol. Biol.* **19**, 145–151 (2012).

75. Schwarz, D. S. *et al.* Asymmetry in the assembly of the RNAi enzyme complex. *Cell* **115**, 199–208 (2003).

76. Khvorova, A., Reynolds, A. & Jayasena, S. D. Functional siRNAs and miRNAs Exhibit Strand Bias. 8

77. Meister, G. *et al.* Human Argonaute2 mediates RNA cleavage targeted by miRNAs and siRNAs. *Mol. Cell* **15**, 185–197 (2004).

78. Liu, J. *et al.* Argonaute2 is the catalytic engine of mammalian RNAi. *Science* **305**, 1437–41 (2004).

79. Wang, Y. *et al.* Nucleation, propagation and cleavage of target RNAs in Ago silencing complexes. *Nature* **461**, 754–61 (2009).

80. Betel, D., Koppal, A., Agius, P., Sander, C. & Leslie, C. Comprehensive modeling of microRNA targets predicts functional non-conserved and non-canonical sites. *Genome Biol.* **11**, R90 (2010).

81. Agarwal, V., Bell, G. W., Nam, J.-W. & Bartel, D. P. Predicting effective microRNA target sites in mammalian mRNAs. *eLife* **4**, (2015).

82. Wong, N. & Wang, X. miRDB: an online resource for microRNA target prediction and functional annotations. *Nucleic Acids Res.* **43**, D146–D152 (2015).

83. Bartel, D. P. MicroRNAs: target recognition and regulatory functions. *Cell* **136**, 215–33 (2009).

84. Schirle, N. T., Sheu-Gruttadauria, J., Chandradoss, S. D., Joo, C. & MacRae, I. J. Water-mediated recognition of t1-adenosine anchors Argonaute2 to microRNA targets. *eLife* **4**, (2015).

85. Chandradoss, S. D., Schirle, N. T., Szczepaniak, M., MacRae, I. J. & Joo, C. A Dynamic Search Process Underlies MicroRNA Targeting. *Cell* **162**, 96–107 (2015).

86. Moore, M. J. *et al.* miRNA–target chimeras reveal miRNA 3′-end pairing as a major determinant of Argonaute target specificity. *Nat. Commun.* **6**, (2015).

87. Grosswendt, S. *et al.* Unambiguous Identification of miRNA:Target Site Interactions by Different Types of Ligation Reactions. *Mol. Cell* **54**, 1042–1054 (2014).

88. Kim, D. *et al.* General rules for functional microRNA targeting. *Nat. Genet.* **48**, 1517–1526 (2016).

89. Helwak, A., Kudla, G., Dudnakova, T. & Tollervey, D. Mapping the Human miRNA Interactome by CLASH Reveals Frequent Noncanonical Binding. *Cell* **153**, 654–665 (2013).

90. Grimson, A. *et al.* MicroRNA Targeting Specificity in Mammals: Determinants beyond Seed Pairing. *Mol. Cell* **27**, 91–105 (2007).

91. Broughton, J. P., Lovci, M. T., Huang, J. L., Yeo, G. W. & Pasquinelli, A. E. Pairing beyond the Seed Supports MicroRNA Targeting Specificity. *Mol. Cell* **64**, 320–333 (2016).

92. Jonas, S. & Izaurralde, E. Towards a molecular understanding of microRNA-mediated gene silencing. *Nat. Rev. Genet.* **16**, 421–433 (2015).

93. Guo, H., Ingolia, N. T., Weissman, J. S. & Bartel, D. P. Mammalian microRNAs predominantly act to decrease target mRNA levels. *Nature* **466**, 835–840 (2010).

94. Liu, J. *et al.* A role for the P-body component GW182 in microRNA function. *Nat. Cell Biol.* **7**, 1261–6 (2005).

95. Ding, L., Spencer, A., Morita, K. & Han, M. The developmental timing regulator AIN-1 interacts with miRISCs and may target the argonaute protein ALG-1 to cytoplasmic P bodies in C. elegans. *Mol. Cell* **19**, 437–47 (2005).

96. Rehwinkel, J. A crucial role for GW182 and the DCP1:DCP2 decapping complex in miRNA-mediated gene silencing. *RNA* **11**, 1640–1647 (2005).

97. Baillat, D. & Shiekhattar, R. Functional dissection of the human TNRC6 (GW182-related) family of proteins. *Mol. Cell. Biol.* **29**, 4144–55 (2009).

98. Behm-Ansmant, I. *et al.* mRNA degradation by miRNAs and GW182 requires both CCR4:NOT deadenylase and DCP1:DCP2 decapping complexes. *Genes Dev.* **20**, 1885–98 (2006).

99. Patel, P. H., Barbee, S. A. & Blankenship, J. T. GW-Bodies and P-Bodies Constitute Two Separate Pools of Sequestered Non-Translating RNAs. *PLOS ONE* **11**, e0150291 (2016).

100. Kamenska, A. *et al.* The DDX6–4E-T interaction mediates translational repression and P-body assembly. *Nucleic Acids Res.* **44**, 6318–6334 (2016).

101. Zipprich, J. T., Bhattacharyya, S., Mathys, H. & Filipowicz, W. Importance of the C-terminal domain of the human GW182 protein TNRC6C for translational repression. *RNA* **15**, 781–793 (2009).

102. Braun, J. E., Huntzinger, E., Fauser, M. & Izaurralde, E. GW182 proteins directly recruit cytoplasmic deadenylase complexes to miRNA targets. *Mol. Cell* **44**, 120–33 (2011).

103. Chekulaeva, M. *et al.* miRNA repression involves GW182-mediated recruitment of CCR4–NOT through conserved W-containing motifs. *Nat. Struct. Mol. Biol.* **18**, 1218–1226 (2011).

104. Fabian, M. R. *et al.* miRNA-mediated deadenylation is orchestrated by GW182 through two conserved motifs that interact with CCR4-NOT. *Nat. Struct. Mol. Biol.* **18**, 1211–7 (2011).

105. Huntzinger, E. & Izaurralde, E. Gene silencing by microRNAs: contributions of translational repression and mRNA decay. *Nat. Rev. Genet.* **12**, 99–110 (2011).

106. Christie, M., Boland, A., Huntzinger, E., Weichenrieder, O. & Izaurralde, E. Structure of the PAN3 Pseudokinase Reveals the Basis for Interactions with the PAN2 Deadenylase and the GW182 Proteins. *Mol. Cell* **51**, 360–373 (2013).

107. Hauptmann, J. *et al.* Biochemical isolation of Argonaute protein complexes by Ago-APP. *Proc. Natl. Acad. Sci.* **112**, 11841–11845 (2015).

108. Elkayam, E. *et al.* Multivalent Recruitment of Human Argonaute by GW182. *Mol. Cell* **67**, 646-658.e3 (2017).

109. Lazzaretti, D., Tournier, I. & Izaurralde, E. The C-terminal domains of human TNRC6A, TNRC6B, and TNRC6C silence bound transcripts independently of Argonaute proteins. *RNA* **15**, 1059–66 (2009).

110. Takimoto, K., Wakiyama, M. & Yokoyama, S. Mammalian GW182 contains multiple Argonaute-binding sites and functions in microRNA-mediated translational repression. *RNA* **15**, 1078–89 (2009).

111. Till, S. *et al.* A conserved motif in Argonaute-interacting proteins mediates functional interactions through the Argonaute PIWI domain. *Nat. Struct. Mol. Biol.* **14**, 897–903 (2007).

112. Lian, S. L. *et al.* The C-terminal half of human Ago2 binds to multiple GW-rich regions of GW182 and requires GW182 to mediate silencing. *RNA* **15**, 804–813 (2009).

113. Chen, C.-Y. a, Zheng, D., Xia, Z. & Shyu, A.-B. Ago-TNRC6 triggers microRNA-mediated decay by promoting two deadenylation steps. *Nat. Struct. Mol. Biol.* **16**, 1160–6 (2009).

114. Braun, J. E. *et al.* A direct interaction between DCP1 and XRN1 couples mRNA decapping to 5' exonucleolytic degradation. *Nat. Struct. Mol. Biol.* **19**, 1324–1331 (2012).

115. Mathys, H. *et al.* Structural and Biochemical Insights to the Role of the CCR4-NOT Complex and DDX6 ATPase in MicroRNA Repression. *Mol. Cell* **54**, 751–765 (2014).

116. Jackson, R. J., Hellen, C. U. T. & Pestova, T. V. The mechanism of eukaryotic translation initiation and principles of its regulation. *Nat. Rev. Mol. Cell Biol.* **11**, 113–127 (2010).

117. Hinnebusch, A. G. Molecular Mechanism of Scanning and Start Codon Selection in Eukaryotes. *Microbiol. Mol. Biol. Rev.* **75**, 434–467 (2011).

118. Fukaya, T., Iwakawa, H. & Tomari, Y. MicroRNAs Block Assembly of eIF4F Translation Initiation Complex in Drosophila. *Mol. Cell* **56**, 67–78 (2014).

119. Meijer, H. A. *et al.* Translational Repression and eIF4A2 Activity Are Critical for MicroRNA-Mediated Gene Regulation. *Science* **340**, 82–85 (2013).

120. Fukao, A. *et al.* MicroRNAs Trigger Dissociation of eIF4AI and eIF4AII from Target mRNAs in Humans. *Mol. Cell* **56**, 79–89 (2014).

121. Kobayashi, H., Shoji, K., Kiyokawa, K., Negishi, L. & Tomari, Y. Iruka Eliminates Dysfunctional Argonaute by Selective Ubiquitination of Its Empty State. *Mol. Cell* (2018). doi:10.1016/j.molcel.2018.10.033

122. Rybak, A. *et al.* The let-7 target gene mouse lin-41 is a stem cell specific E3 ubiquitin ligase for the miRNA pathway protein Ago2. *Nat. Cell Biol.* **11**, 1411–20 (2009).

123. Smibert, P., Yang, J.-S., Azzam, G., Liu, J.-L. & Lai, E. C. Homeostatic control of Argonaute stability by microRNA availability. *Nat. Struct. Mol. Biol.* **20**, 789–95 (2013).

124. Bronevetsky, Y. *et al.* T cell activation induces proteasomal degradation of Argonaute and rapid remodeling of the microRNA repertoire. *J. Exp. Med.* **210**, 417–32 (2013).

125. Wilkinson, K. A. & Henley, J. M. Mechanisms, regulation and consequences of protein SUMOylation. *Biochem. J.* **428**, 133–145 (2010).

126. Sahin, U., Lapaquette, P., Andrieux, A., Faure, G. & Dejean, A. Sumoylation of Human Argonaute 2 at Lysine-402 Regulates Its Stability. *PLoS ONE* **9**, e102957 (2014).

127. Josa-Prado, F., Henley, J. M. & Wilkinson, K. A. SUMOylation of Argonaute-2 regulates RNA interference activity. *Biochem. Biophys. Res. Commun.* **464**, 1066–1071 (2015).

128. Qi, H. H. *et al.* Prolyl 4-hydroxylation regulates Argonaute 2 stability. *Nature* **455**, 421–4 (2008).

129. Leung, A. K. L. *et al.* Poly(ADP-ribose) regulates stress responses and microRNA activity in the cytoplasm. *Mol. Cell* **42**, 489–99 (2011).

130. Leung, A. K. L., Todorova, T., Ando, Y. & Chang, P. Poly(ADP-ribose) regulates post-transcriptional gene regulation in the cytoplasm. *RNA Biol.* **9**, 542–548 (2012).

131. Seo, G. J. *et al.* Reciprocal Inhibition between Intracellular Antiviral Signaling and the RNAi Machinery in Mammalian Cells. *Cell Host Microbe* **14**, 435–445 (2013).

132. Ruedel, S. *et al.* Phosphorylation of human Argonaute proteins affects small RNA binding. *Nucleic Acids Res.* **39**, 2330–2343 (2011).

133. Shen, J. *et al.* EGFR modulates microRNA maturation in response to hypoxia through phosphorylation of AGO2. *Nature* 1–5 (2013). doi:10.1038/nature12080

134. Yang, M. *et al.* Dephosphorylation of Tyrosine 393 in Argonaute 2 by Protein Tyrosine Phosphatase 1B Regulates Gene Silencing in Oncogenic RAS-Induced Senescence. *Mol. Cell* 782–790 (2014). doi:10.1016/j.molcel.2014.07.018

135. Zeng, Y., Sankala, H., Zhang, X. & Graves, P. R. Phosphorylation of Argonaute 2 at serine-387 facilitates its localization to processing bodies. *Biochem. J.* **413**, 429–436 (2008).

136. Horman, S. R. *et al.* Akt-Mediated Phosphorylation of Argonaute 2 Downregulates Cleavage and Upregulates Translational Repression of MicroRNA Targets. *Mol. Cell* 1–12 (2013). doi:10.1016/j.molcel.2013.03.015

137. McKenzie, A. J. *et al.* KRAS-MEK Signaling Controls Ago2 Sorting into Exosomes. *Cell Rep.* **15**, 978–987 (2016).

138. Lopez-Orozco, J. *et al.* Functional analyses of phosphorylation events in human Argonaute 2. *RNA* **21**, 2030–2038 (2015).

139. Bridge, K. S. *et al.* Argonaute Utilization for miRNA Silencing Is Determined by Phosphorylation-Dependent Recruitment of LIM-Domain-Containing Proteins. *Cell Rep.* **20**, 173–187 (2017).

140. Ma, J.-B. *et al.* Structural basis for 5'-end-specific recognition of guide RNA by the A. fulgidus Piwi protein. *Nature* **434**, 666–70 (2005).

141. Parker, J. S., Roe, S. M. & Barford, D. Structural insights into mRNA recognition from a PIWI domain–siRNA guide complex. *Nature* **434**, 663–666 (2005).

142. Mazumder, A., Bose, M., Chakraborty, A., Chakrabarti, S. & Bhattacharyya, S. N. A transient reversal of miRNA-mediated repression controls macrophage activation. *EMBO Rep.* **14**, 1008–16 (2013).

143. Li, L., Yu, C., Gao, H. & Li, Y. Argonaute proteins: potential biomarkers for human colon cancer. *BMC Cancer* **10**, (2010).

144. Chang, S. S., Smith, I., Glazer, C., Hennessey, P. & Califano, J. A. EIF2C Is Overexpressed and Amplified in Head and Neck Squamous Cell Carcinoma. *ORL* **72**, 337–343 (2010).

145. Feng, B., Hu, P., Lu, S.-J., Chen, J.-B. & Ge, R.-L. Increased Argonaute 2 Expression in Gliomas and its Association with Tumor Progression and Poor Prognosis. *Asian Pac. J. Cancer Prev.* **15**, 4079–4083 (2014).

146. Zhang, J. *et al.* MiRNA-99a directly regulates AGO2 through translational repression in hepatocellular carcinoma. *Oncogenesis* **3**, e97–e97 (2014).

147. Cheng, N., Li, Y. & Han, Z.-G. Argonaute2 promotes tumor metastasis by way of up-regulating focal adhesion kinase expression in hepatocellular carcinoma. *Hepatology* **57**, 1906–1918 (2013).

148. Völler, D., Reinders, J., Meister, G. & Bosserhoff, A.-K. Strong reduction of AGO2 expression in melanoma and cellular consequences. *Br. J. Cancer* **109**, 3116–3124 (2013).

149. Tattikota, S. G. *et al.* Argonaute2 Mediates Compensatory Expansion of the Pancreatic β Cell. *Cell Metab.* **19**, 122–134 (2014).

150. Hayes, J., Peruzzi, P. P. & Lawler, S. MicroRNAs in cancer: biomarkers, functions and therapy. *Trends Mol. Med.* **20**, 460–469 (2014).

151. Ye, Z., Jin, H. & Qian, Q. Argonaute 2: A Novel Rising Star in Cancer Research. *J. Cancer* **6**, 877–882 (2015).

152. Pircs, K. *et al.* Huntingtin Aggregation Impairs Autophagy, Leading to Argonaute-2 Accumulation and Global MicroRNA Dysregulation. *Cell Rep.* **24**, 1397–1406 (2018).

153. Maciotta, S., Meregalli, M. & Torrente, Y. The involvement of microRNAs in neurodegenerative diseases. *Front. Cell. Neurosci.* **7**, (2013).

154. Hauptmann, J. Human Argonaute proteins: Analysis of endonucleolytic activity and endogenous phosphorylation sites. (University of Regensburg, 2014).

155. Gehring, N. H., Hentze, M. W. & Kulozik, A. E. Chapter 23 Tethering Assays to Investigate Nonsense-Mediated mRNA Decay Activating Proteins. in *Methods in Enzymology* **448**, 467–482 (Academic Press, 2008).

156. Pillai, R. S. Tethering of human Ago proteins to mRNA mimics the miRNA-mediated repression of protein synthesis. *RNA* **10**, 1518–1525 (2004).

157. Eulalio, A., Behm-Ansmant, I. & Izaurralde, E. P bodies: at the crossroads of post-transcriptional pathways. *Nat. Rev. Mol. Cell Biol.* **8**, 9–22 (2007).

158. Graus, V. Charakterisierung von Argonaut-TNRC6-Bindungsmutanten und regulatorische Zusammenhänge der Dicer-abhängigen miRNA Prozessierung. (2016).

159. Vasquez-Rifo, A. *et al.* Developmental Characterization of the MicroRNA-Specific C. elegans Argonautes alg-1 and alg-2. *PLoS ONE* **7**, e33750 (2012).

160. Huberdeau, M. Q. *et al.* Phosphorylation of Argonaute proteins affects mRNA binding and is essential for microRNA-guided gene silencing in vivo. *EMBO J.* **36**, 2088–2106 (2017).

161. Frohn, A. *et al.* Dicer-dependent and -independent Argonaute2 protein interaction networks in mammalian cells. *Mol. Cell. Proteomics* **11**, 1442–56 (2012).

162. Stefansson, B., Ohama, T., Daugherty, A. E. & Brautigan, D. L. Protein Phosphatase 6 Regulatory Subunits Composed of Ankyrin Repeat Domains †. *Biochemistry* **47**, 1442–1451 (2008).

163. Stefansson, B. & Brautigan, D. L. Protein Phosphatase 6 Subunit with Conserved Sit4-associated Protein Domain Targets IκBε. *J. Biol. Chem.* **281**, 22624–22634 (2006).

164. Golden, R. J. *et al.* An Argonaute phosphorylation cycle promotes microRNA-mediated silencing. *Nature* **542**, 197–202 (2017).

165. Elkayam, E. *et al.* The Structure of Human Argonaute-2 in Complex with miR-20a. *Cell* **150**, 100–110 (2012).

166. Boland, A., Tritschler, F., Heimstädt, S., Izaurralde, E. & Weichenrieder, O. Crystal structure and ligand binding of the MID domain of a eukaryotic Argonaute protein. *EMBO Rep.* **11**, 522–7 (2010).

167. Iwasaki, S., Kawamata, T. & Tomari, Y. Drosophila Argonaute1 and Argonaute2 Employ Distinct Mechanisms for Translational Repression. *Mol. Cell* **34**, 58–67 (2009).

168. Miyoshi, K. Slicer function of Drosophila Argonautes and its involvement in RISC formation. *Genes Dev.* **19**, 2837–2848 (2005).

169. Blackburn, K. & Goshe, M. B. Challenges and strategies for targeted phosphorylation site identification and quantification using mass spectrometry analysis. *Brief. Funct. Genomic. Proteomic.* **8**, 90–103 (2009).

170. Dephoure, N., Gould, K. L., Gygi, S. P. & Kellogg, D. R. Mapping and analysis of phosphorylation sites: a quick guide for cell biologists. *Mol. Biol. Cell* **24**, 535–542 (2013).

171. Gafken, P. R. & Lampe, P. D. Methodologies for Characterizing Phosphoproteins by Mass Spectrometry. *Cell Commun. Adhes.* **13**, 249–262 (2006).

172. Steen, H., Jebanathirajah, J. A., Rush, J., Morrice, N. & Kirschner, M. W. Phosphorylation Analysis by Mass Spectrometry: Myths, Facts, and the Consequences for Qualitative and Quantitative Measurements. *Mol. Cell. Proteomics* **5**, 172–181 (2006).

173. Boersema, P. J., Mohammed, S. & Heck, A. J. R. Phosphopeptide fragmentation and analysis by mass spectrometry. *J. Mass Spectrom.* **44**, 861–878 (2009).

174. Palumbo, A. M. & Reid, G. E. Evaluation of Gas-Phase Rearrangement and Competing Fragmentation Reactions on Protein Phosphorylation Site Assignment Using Collision Induced Dissociation-MS/MS and MS ^{3}. *Anal. Chem.* **80**, 9735–9747 (2008).

175. Lawless, C. & Hubbard, S. J. Prediction of Missed Proteolytic Cleavages for the Selection of Surrogate Peptides for Quantitative Proteomics. *OMICS J. Integr. Biol.* **16**, 449–456 (2012).

176. Picotti, P. *et al.* A database of mass spectrometric assays for the yeast proteome. *Nat. Methods* **5**, 913–914 (2008).

177. Lange, V., Picotti, P., Domon, B. & Aebersold, R. Selected reaction monitoring for quantitative proteomics: a tutorial. *Mol. Syst. Biol.* **4**, (2008).

178. MacLean, B. *et al.* Effect of Collision Energy Optimization on the Measurement of Peptides by Selected Reaction Monitoring (SRM) Mass Spectrometry. *Anal. Chem.* **82**, 10116–10124 (2010).

179. Shi, T. *et al.* Advancing the sensitivity of selected reaction monitoring-based targeted quantitative proteomics. *PROTEOMICS* **12**, 1074–1092 (2012).

180. Schweiger, R. & Linial, M. Cooperativity within proximal phosphorylation sites is revealed from large-scale proteomics data. *Biol. Direct* **5**, 6 (2010).

181. Serber, Z. & Ferrell, J. E. Tuning Bulk Electrostatics to Regulate Protein Function. *Cell* **128**, 441–444 (2007).

182. Phatnani, H. P. & Greenleaf, A. L. Phosphorylation and functions of the RNA polymerase II CTD. *Genes Dev.* **20**, 2922–36 (2006).

183. Verma, R. Phosphorylation of Sic1p by G1 Cdk Required for Its Degradation and Entry into S Phase. *Science* **278**, 455–460 (1997).

184. Nash, P. *et al.* Multisite phosphorylation of a CDK inhibitor sets a threshold for the onset of DNA replication. *Nature* **414**, 514–21 (2001).

185. Deshaies, R. J. & Ferrell, J. E. Multisite phosphorylation and the countdown to S phase. *Cell* **107**, 819–22 (2001).

186. Pufall, M. a *et al.* Variable control of Ets-1 DNA binding by multiple phosphates in an unstructured region. *Science* **309**, 142–5 (2005).

187. Strickfaden, S. C. *et al.* A Mechanism for Cell-Cycle Regulation of MAP Kinase Signaling in a Yeast Differentiation Pathway. *Cell* **128**, 519–531 (2007).

188. Lai, M.-C., Lin, R.-I. & Tarn, W.-Y. Transportin-SR2 mediates nuclear import of phosphorylated SR proteins. *Proc. Natl. Acad. Sci.* **98**, 10154–10159 (2001).

189. Ngo, J. C. K. *et al.* Interplay between SRPK and Clk/Sty Kinases in Phosphorylation of the Splicing Factor ASF/SF2 Is Regulated by a Docking Motif in ASF/SF2. *Mol. Cell* **20**, 77–89 (2005).

190. Prasad, J., Colwill, K., Pawson, T. & Manley, J. L. The Protein Kinase Clk/Sty Directly Modulates SR Protein Activity: Both Hyper- and Hypophosphorylation Inhibit Splicing. *Mol. Cell. Biol.* **19**, 6991–7000 (1999).

191. Cao, W., Jamison, S. F. & Garcia-Blanco, M. A. Both phosphorylation and dephosphorylation of ASF/SF2 are required for pre-mRNA splicing in vitro. *RNA J.* 1456–1467 (1997).

192. Zhou, Z. & Fu, X.-D. Regulation of splicing by SR proteins and SR protein-specific kinases. *Chromosoma* **122**, 191–207 (2013).

193. Jakubauskiene, E., Vilys, L., Makino, Y., Poellinger, L. & Kanopka, A. Increased Serine-Arginine (SR) Protein Phosphorylation Changes Pre-mRNA Splicing in Hypoxia. *J. Biol. Chem.* **290**, 18079–18089 (2015).

194. Ohama, T. The multiple functions of protein phosphatase 6. *Biochim. Biophys. Acta BBA - Mol. Cell Res.* **1866**, 74–82 (2019).

195. Nagaraj, N. *et al.* Deep proteome and transcriptome mapping of a human cancer cell line. *Mol. Syst. Biol.* **7**, 548–548 (2014).

196. Ogoh, H. *et al.* The protein phosphatase 6 catalytic subunit (Ppp6c) is indispensable for proper post-implantation embryogenesis. *Mech. Dev.* **139**, 1–9 (2016).

197. Ye, J. *et al. PP6* Controls T Cell Development and Homeostasis by Negatively Regulating Distal TCR Signaling. *J. Immunol.* **194**, 1654–1664 (2015).

198. Flowers, J. B. *et al.* Abdominal obesity in BTBR male mice is associated with peripheral but not hepatic insulin resistance. *Am. J. Physiol.-Endocrinol. Metab.* **292**, E936–E945 (2007).

199. Hagiwara, K. *et al.* Identification of Genes Upregulated in the Inflamed Colonic Lesions of Crohn's Disease. *Biochem. Biophys. Res. Commun.* **283**, 130–135 (2001).

200. Shen, Y. *et al.* Serine/threonine protein phosphatase 6 modulates the radiation sensitivity of glioblastoma. *Cell Death Dis.* **2**, e241–e241 (2011).

201. Ivanov, S. V. *et al.* Pro-tumorigenic Effects of miR-31 Loss in Mesothelioma. *J. Biol. Chem.* **285**, 22809–22817 (2010).

202. Sato, N. *et al.* Gene Expression Profiling Identifies Genes Associated with Invasive Intraductal Papillary Mucinous Neoplasms of the Pancreas. *Am. J. Pathol.* **164**, 903–914 (2004).

203. Zhong, J. *et al.* Protein phosphatase PP6 is required for homology-directed repair of DNA double-strand breaks. *Cell Cycle* **10**, 1411–1419 (2011).

204. Wu, N. *et al.* MicroRNA-373, a new regulator of protein phosphatase 6, functions as an oncogene in hepatocellular carcinoma: MicroRNA-373 functions as an oncogene in HCC. *FEBS J.* **278**, 2044–2054 (2011).

205. Yan, S. *et al.* NF-κB-induced microRNA-31 promotes epidermal hyperplasia by repressing protein phosphatase 6 in psoriasis. *Nat. Commun.* **6**, (2015).

206. Voorhoeve, P. M. *et al.* A Genetic Screen Implicates miRNA-372 and miRNA-373 As Oncogenes in Testicular Germ Cell Tumors. *Cell* **124**, 1169–1181 (2006).

207. Ghasemi, M. *et al.* Upregulation of miR-371-373 cluster, a human embryonic stem cell specific microRNA cluster, in esophageal squamous cell carcinoma - J Can Res Ther. Available at: http://www.cancerjournal.net/article.asp?issn=0973-1482;year=2018;volume=14;issue=8;spage=132;epage=137;aulast=Ghasemi. (Accessed: 17th December 2018)

208. Ho Xuan, H. Investigation of the roles of circular RNA circZNF609 during colorectal cancer progression. (Regensburg, 2017).

209. Knippschild, U. *et al.* The casein kinase 1 family: participation in multiple cellular processes in eukaryotes. *Cell. Signal.* **17**, 675–689 (2005).

210. Wang, C. C., Tao, M., Wei, T. & Low, P. S. Identification of the Major Casein Kinase I Phosphorylation Sites on Erythrocyte Band 3. 7

211. Kosten, J. *et al.* Efficient modification of alpha-synuclein Serine 129 by protein kinase CK1 requires phosphorylation of Tyrosine 125 as a priming event. *ACS Chem. Neurosci.* (2014). doi:10.1021/cn5002254

212. MacDonald, B. T., Tamai, K. & He, X. Wnt/β-Catenin Signaling: Components, Mechanisms, and Diseases. *Dev. Cell* **17**, 9–26 (2009).

213. Komiya, Y. & Habas, R. Wnt signal transduction pathways. *Organogenesis* **4**, 68–75 (2008).

214. Filali, M., Li, S., Kim, H. W., Wadzinski, B. & Kamoun, M. Identification of a type 6 protein Ser/Thr phosphatase regulated by interleukin-2 stimulation. *J. Cell. Biochem.* **73**, 153–163 (1999).

215. Kajino, T. *et al.* Protein Phosphatase 6 Down-regulates TAK1 Kinase Activation in the IL-1 Signaling Pathway. *J. Biol. Chem.* **281**, 39891–39896 (2006).

216. Shankar, S. *et al.* An Essential Role for Argonaute 2 in EGFR-KRAS Signaling in Pancreatic Cancer Development. (2017). doi:10.1101/227264

217. Morita, S. *et al.* One Argonaute family member, Eif2c2 (Ago2), is essential for development and appears not to be involved in DNA methylation. *Genomics* **89**, 687–96 (2007).

218. Shekar, P. C., Naim, A., Sarathi, D. P. & Kumar, S. Argonaute-2-null embryonic stem cells are retarded in self-renewal and differentiation. *J. Biosci.* **36**, 649–657 (2011).

219. Cheloufi, S., Dos Santos, C. O., Chong, M. M. W. & Hannon, G. J. A dicer-independent miRNA biogenesis pathway that requires Ago catalysis. *Nature* **465**, 584–9 (2010).

220. Klum, S. M., Chandradoss, S. D., Schirle, N. T., Joo, C. & MacRae, I. J. Helix-7 in Argonaute2 shapes the microRNA seed region for rapid target recognition. *EMBO J.* **37**, 75–88 (2018).

221. Park, J. H. & Shin, C. Slicer-independent mechanism drives small-RNA strand separation during human RISC assembly. *Nucleic Acids Res.* **43**, 9418–9433 (2015).

222. Weinmann, L. *et al.* Importin 8 is a gene silencing factor that targets argonaute proteins to distinct mRNAs. *Cell* **136**, 496–507 (2009).

223. Hauptmann, J., Kater, L., Löffler, P., Merkl, R. & Meister, G. Generation of catalytic human Ago4 identifies structural elements important for RNA cleavage. *RNA* **20**, 1532–8 (2014).

224. Schraivogel, D. *et al.* Importin-beta facilitates nuclear import of human GW proteins and balances cytoplasmic gene silencing protein levels. *Nucleic Acids Res.* **43**, 7447–7461 (2015).

225. Carvalho, B. S. & Irizarry, R. A. A framework for oligonucleotide microarray preprocessing. *Bioinformatics* **26**, 2363–2367 (2010).